NTNU

Norwegian University of
Science and Technology

Experimental study of smouldering fires in wood pellets

Virginia Rebaque Valdes

Petroleum Geoscience and Engineering
Submission date: June 2017
Supervisor: Ivar Ståle Ertesvåg, EPT
Co-supervisor: Anne Elise Steen-Hansen, SP Fire Research AS
Ragni Fjellgaard Mikalsen, SP Fire Research AS

Norwegian University of Science and Technology
Department of Energy and Process Engineering

Acknowledgements

I want to thank my supervisor Ivar Ståle Ertesvåg at NTNU and supervisor Anne Steen-Hansen at RISE Fire Research AS, for the opportunity to do this thesis and for helping me with all the questions about my research. I would also thank Ragni Fjellgaard Mikalsen at RISE Fire Research AS, she consistently allowed this paper to be my own work, but steered me in the right direction whenever she thought I needed it.

Finally, I would like to thank my parents Luis Alberto and Pilar for giving me the opportunity to live this experience and for showing me how important it is to build your own future.

Trondheim, 2017

Virginia Rebaque Valdés

Abstract

Development of renewable energy sources for energy production has become increasingly significant in European energy markets. Energy consumption is almost completely due to petroleum, a non-renewable resource that is generating global warming because of the greenhouse effect. Due to this situation and the increase in demand and oil price, it is necessary to search for alternatives which may be used as fuel. One of the most viable alternatives is woody biomass, and specifically pellets.

Smouldering is a flameless form of combustion, sustained by the heat evolved when oxygen directly react to the surface of the fuel. Smouldering constitutes a serious fire hazard for two reasons: it typically yields a higher conversion of fuel to toxic compounds than flaming, and because it provides a pathway to flaming that can be initiated by weak heat sources. Many materials can sustain a smouldering reaction, among them wood pellets, which are becoming more widely used as an alternative to oil-fired central heating in residential and industrial buildings.

The purpose of this thesis was to study the smouldering behaviour by varying the airflow propagation. It has been used two different configurations: semi reverse and forward. These are defined according to the direction in which the smoulder reaction propagates relative to the oxidizer flow.

The project is based on experimental tests. The samples were placed in an insulated steel pipe above a heater, and heated from underneath. Temperature development, air flow measurements, smoke composition (CO, CO_2 and O_2) and mass loss were registered during the testing. The results showed that forward smouldering experienced a more intense combustion in comparison to semi reverse, undergoing the reaction at higher temperatures (~720ºC) in less time (~7 hours).

Three different types of smouldering were observed in the test samples: *Semi reverse smouldering*, *Forward smouldering Type 1* and *Forward smouldering Type 2*. The distinction was made based on the different smouldering temperature behaviour during the tests.

Table of contents

ACKNOWLEDGEMENTS I

ABSTRACT III

FIGURES AND TABLES V

1. INTRODUCTION 1

1.1 Previous own work 1

1.2 Problem 1

1.3 Hypotheses 2

1.4 Report structure 2

2. THEORETICAL BACKGROUND 3

2.1 World Energy situation 3

2.2 Biofuel and Biomass 6

2.3 Bioenergy's role in renewables 7

2.4 Pelletizing process 7

2.5 Pellet market 8

2.6 Smouldering combustion 11

2.7 Smouldering propagation 13

2.8 Smouldering gas emissions 16

2.9 Transition to Flaming 17

2.10 Smouldering combustion in biomass 18

3. METHOD 19

3.1 Materials 19

3.2 Test equipment 20

3.2.1 Test setup 20

3.2.2 Thermocouples 24

3.2.3 Bidirectional probe 26
3.2.4 Gas measurement unit 27
3.2.5 Data logging 32

3.3 Test procedure 34

4. RESULTS 35

4.1 Test scheme 35

4.2 Observed types of smouldering 36
4.2.1 Semi reverse smouldering behaviour 37
4.2.2 Forward smouldering behaviour Type 1 39
4.2.3 Forward smouldering behaviour Type 2 40

4.3 Flaming fire 41

4.4 Maximum temperatures and time readings on forward and semi reverse smouldering in the different stages 42

4.5 Total combustion time 51

4.6 Mass Loss and Mass Loss Rate 52

4.7 Airflow velocities 54

4.8 Gas measurements 56

4.9 Sorted residues in forward and semi reverse smouldering 59

4.10 Pictures of tested samples 60

5. DISCUSSION 63

5.1 Discussion of hypotheses 67

6. CONCLUSIONS 68

REFERENCES 69

APPENDICES 72

A) Semi reverse smouldering charts 72

B) Forward smouldering charts 85

Figures and tables

Figure 1: illustration of world energy consumption from 2012 to 2040 in quadrillion btu [2]. *3*
Figure 2: total world energy consumption 1990-2040 by energy source, including energy resources with clean power plant (cpp) policy in quadrillion btu [2]. *4*
Figure 3: oil reserves chart distribution worldwide in 2015 [4]. *5*
Figure 4: crude oil price chart (1861-2019) [2]. *5*
Figure 5: scheme of a typical overview of the biomass densification process, based on [7] chart. *7*
Figure 6: typical pellet mill design a) ring and die b) flat die, taken from [7]. *8*
Figure 7: european wood pellet production in 2015 [tonnes] [8]. *9*
Figure 8: european wood pellet consumption in 2015 [tonnes] [8]. *10*
Figure 9: forward propagation overview, adapted from [9]. *14*
Figure 10: reverse propagation overview, adapted from [9]. *14*
Figure 11: peak surface temperature for red oak and white pine in forward smouldering, graph taken from ohlemiller experiments [20]. *16*
Figure 12: picture of the pellets used in this study. *19*
Figure 13: picture of the heater (a), steel pipe (b) and insulation (c). *21*
Figure 14: picture of the aluminium plate used in this study. A) top side and b) bottom. For comparison the ruler is 30 cm long. *21*
Figure 15: test set up consisting of, from the bottom: scale, hotplate, aluminium plate, steel annulus and the insulated steel pipe. *22*
Figure 16: (a,b) close-up of the perforated steel annulus; (c) sketch illustrating how the perforated steel annulus enables air flow into the pipe. *23*
Figure 17: 3d scaled view of the setup. The dashed rectangle represents the thermocouple ladder inside the pipe, where the thermocouples are attached. *24*
Figure 18: picture of the thermocouple ladder. For comparison the ruler is 30 cm long. *25*
Figure 19: cross section of the pipe with a sketch of the thermocouple positions (the circles refers to each thermocouple). *25*
Figure 20: sketch of bidirectional probe, low-velocity flow design, adapted from [28]. *28*

Figure 21: a) sensors placed inside the unit; b) gas measurement unit; c) electronic circuit (right). *28*
Figure 22: a) carbon dioxide sensor; b) carbon monoxide sensor; c) oxygen sensor; d) solvent vapours detector. Taken from [30][31][32][33] *29*
Figure 23: gas unit calibration equipment scheme *30*
Figure 24: picture of the two units and the bidirectional probe after running a test *31*
Figure 25: a) co_2 readings from both units [ppm]; b) co [ppm] and c) o_2 [%]..... *32*
Figure 26:close-up picture of the gas measurement unit and bidirectional probe position with regards to the pipe. *34*
Figure 27: scheme of the smouldering temperature development periods. H corresponds to external heating period, bic: before intense combustion, mic: maximum intense combustion, aic: after intense combustion. *36*
Figure 28: chart showing a case of semi reverse smouldering behaviour, in temperature vs time graph. This example corresponds to the test vr1. ..... *37*
Figure 29: chart showing a case of forward smouldering behaviour type 1, in temperature vs time graph. This example corresponds to the test vf2. ..... *39*
Figure 30: chart showing a case of forward smouldering behaviour type 2, in temperature vs time graph. This example corresponds to the test vf5. ..... *40*
Figure 31: chart showing a case of flaming fire, in temperature versus time graph. This example corresponds to test vf3..... *41*
Figure 32: explanation of a box and whiskers diagram..... *42*
Figure 33: box and whiskers diagram of maximum temperature peak and time to maximum temperature for semi reverse tests during bic period. There is no forward smouldering data for this period as it was not developed.. The white rhombus shows the average value...... *45*
Figure 34: box and whiskers diagram of average temperatures and duration time on semi reverse tests during bic period. *45*
Figure 35: box and whiskers diagram of maximum temperature peak and time to maximum temperature for both semi reverse and forward tests during mic period. The white rhombus shows the average value. *46*
Figure 36: box and whiskers diagram of maximum temperature peak and timing to maximum temperature on both semi reverse and forward tests during aic period. The white rhombus shows the average value. *47*

Figure 37: box and whiskers diagram of average temperatures and duration time on both semi reverse and forward tests during aic period. *48*
Figure 38: box and whiskers diagram of maximum temperatures in each height for semi reverse tests. The white rhombus shows the average values. *50*
Figure 39: box and whiskers diagram of maximum temperatures on each height for forward tests. The white rhombus shows the average values. *50*
Figure 40: box and whiskers plot of total combustion time in semi reverse and forward propagation. The white rhombus shows the average values. *51*
Figure 41: mass loss rate [-dm/dt] vs time [h]. This example corresponds to the test vr1. ..... *52*
Figure 42: mass change (-%) vs time [h]. This chart correspond to test vr1 ..... *53*
Figure 43: mass loss box and whiskers diagram (-%) for semi reverse and forward propagation for the entire tests. *53*
Figure 44: airflow measurement [kg/s] versus temperature related to a semi reverse smouldering type. This chart corresponds to test vr1. ..... *54*
Figure 45: airflow measurement [kg/s] versus temperature in forward smouldering type 1. This chart corresponds to test vf2. ..... *55*
Figure 46: airflow measurement [kg/s] versus temperature in forward smouldering type 2. This chart corresponds to test vf5. ..... *55*
Figure 47: airflow measurement [kg/s] versus temperature in flaming fire. This chart corresponds to test vf3. ..... *56*
Figure 48: co and co_2 levels [ppm]. The grey line is referred to the co data obtained by the sensor, the black line corresponds to the moving average (6 time periods) and the blue line relates to the co_2 data. The vertical line indicates when the external heater was turned off. This example is from test vr1. ..... *57*
Figure 49: o_2 levels [%]. The vertical line indicates when the external heater was turned off. This example is from test vr1. ..... *58*
Figure 50: co/co_2 ratio for vr1 test. The grey line is the actual data; the black line refers to the moving average (6 time period). *58*
Figure 51: combustion efficiency (%) in vr1. The white rhombus refers to the average value. *59*
Figure 52: amount of char and ash residue left on forward and semi reverse smouldering *59*
Figure 53: semi reverse smouldering combustion: sample vr1 after test *60*

Figure 54: sorted residue vr1. A) ash (25.5 g); b) black/char (205.4 g). 60
Figure 55: forward smouldering combustion type 1: sample vf1 after test 61
Figure 56: sorted residue vf1. A) ash (20 g); b) black/char (127 g)..... 61
Figure 57: forward smouldering combustion type 2: sample vf4 after test 61
Figure 58: sorted residue vf4. A) ash (20,9 g); b) black/char (114,7 g)..... 62
Figure 59: forward smouldering combustion type 1: sample vf1 after test 62
Figure 60: sorted residue vf4. A) ash (17,5 g); b) black/char (78,4 g)..... 62

Figures a-1: vr1 test. Temperature development within the sample vs time (top graph), airflow measurement vs time (middle graph), mass change (%) vs time (bottom graph). 72
Figures a-2: vr1 test. Co_2 readings [ppm] vs time (top graph), co and co moving average (6 times period) vs time [ppm] (middle graph), co/co_2 ratio and moving average (6 times period) vs time (bottom graph). 75
Figures a-3: vr2 test. Temperature development within the sample vs time (top graph), airflow measurement vs time (middle graph), mass change (%) vs time (bottom graph). 72
Figures a-4: vr2 test. Co_2 readings [ppm] vs time (top graph), co and co moving average (6 times period) vs time [ppm] (middle graph), co/co_2 ratio and moving average (6 times period) vs time (bottom graph). 75
Figures a-5: vr3 test. Temperature development within the sample vs time (top graph), airflow measurement vs time (middle graph), mass change (%) vs time (bottom graph). 76
Figures a-6: vr3 test. Co_2 readings [ppm] vs time (top graph), co and co moving average (6 times period) vs time [ppm] (middle graph), co/co_2 ratio and moving average (6 times period) vs time (bottom graph). 77
Figures a-7: vr6 test. Temperature development within the sample vs time (top graph), airflow measurement vs time (middle graph), mass change (%) vs time (bottom graph). 78
Figures a-8: vr7 test. Temperature development within the sample vs time (top graph), airflow measurement vs time (middle graph), mass change (%) vs time (bottom graph). 79

Figures a-9: vr8 test. Temperature development within the sample vs time (top graph), airflow measurement vs time (middle graph), mass change (%) vs time (bottom graph). *80*
Figures a-10: vr9 test. Temperature development within the sample vs time (top graph), airflow measurement vs time (middle graph), mass change (%) vs time (bottom graph). *81*
Figures a-11: vr10 test. Temperature development within the sample vs time (top graph), airflow measurement vs time (middle graph), mass change (%) vs time (bottom graph). *82*
Figures a-12: vr11 test. Temperature development within the sample vs time (top graph), airflow measurement vs time (middle graph), mass change (%) vs time (bottom graph). *83*
Figures a-13: vr12 test. Temperature development within the sample vs time (top graph), airflow measurement vs time (middle graph), mass change (%) vs time (bottom graph). *84*

Figures b-1: vf1 test. Temperature development within the sample vs time (top graph), airflow measurement vs time (middle graph), mass change (%) vs time (bottom graph). *85*
Figures b-2: vf1 test. Co_2 readings [ppm] vs time (top graph), co and co moving average (6 times period) vs time [ppm] (middle graph), co/co_2 ratio and moving average (6 times period) vs time (bottom graph). *86*
Figures b-3: vf2 test. Temperature development within the sample vs time (top graph), airflow measurement vs time (middle graph), mass change (%) vs time (bottom graph). *87*
Figures b-4: vf2 test. Co_2 readings [ppm] vs time (top graph), co and co moving average (6 times period) vs time [ppm] (middle graph), co/co_2 ratio and moving average (6 times period) vs time (bottom graph). *88*
Figures b-5: vf3 test. Temperature development within the sample vs time (top graph), airflow measurement vs time (bottom graph),there is no mass change (%)chart due to defect in the equipment. *89*

Figures b-6: vf4 test. Temperature development within the sample vs time (top graph), airflow measurement vs time (middle graph), mass change (%) vs time (bottom graph). *90*
Figures b-7: vf5 test. Temperature development within the sample vs time (top graph), airflow measurement vs time (middle graph), mass change (%) vs time (bottom graph). *91*
Figures b-8: vf6 test. Temperature development within the sample vs time (top graph), airflow measurement vs time (middle graph), mass change (%) vs time (bottom graph). *92*
Figures b-9: vf7 test. Temperature development within the sample vs time (top graph), airflow measurement vs time (middle graph), mass change (%) vs time (bottom graph). *93*
Figures b-10: vf8 test. Temperature development within the sample vs time (top graph), airflow measurement vs time (middle graph), mass change (%) vs time (bottom graph). *94*
Figures b-11: vf9 test. Temperature development within the sample vs time (top graph), airflow measurement vs time (middle graph), mass change (%) vs time (bottom graph). *95*
Figures b-12: vf10 test. Temperature development within the sample vs time (top graph), airflow measurement vs time (middle graph), mass change (%) vs time (bottom graph). *96*
Figures b-13: vf11 test. Temperature development within the sample vs time (top graph), airflow measurement vs time (middle graph), mass change (%) vs time (bottom graph). *97*

Table 1: characteristics of the fire stages from [25]..... 17
Table 2: pellet properties. 20
Table 3: jumo b 70.1050.0 thermostat parameters. 22
Table 4: sensors characteristics used in the gas measurement unit based on information given by the supplier [30][31][32][33]. 28
Table 5: calibration mixture conform to iso/iec-17025. 29
Table 6: reference values and gas measurement unit relative error..... 30
Table 7: placement of the measurement points per channel. 33
Table 8: test name list, annulus thickness, heating time and smouldering type observed. 35
Table 9: maximum temperature [ºc], time to maximum temperature and duration period [h] referred to the external heating period (h) for both semi reverse and forward propagations. The temperatures in brackets refer to the average temperature during h for each test. 44
Table 10: maximum temperature [ºc], time to maximum temperature [h] and duration period [h] referred to the before intense combustion (bic) period for both semi reverse and forward propagations. The hyphen shows that those tests did not developed any bic period. The temperatures in brackets refer to the average temperature during bic for each test. 44
Table 11: maximum temperatures [ºc], time to maximum temperature [h] and duration period [h]related to the maximum intense combustion (mic) period for both semi reverse and forward configurations. The temperatures in brackets refer to the average temperature during mic for each test. 46
Table 12: maximum temperatures [ºc], time to maximum temperature [h] and total duration [h] related to the after intense combustion (aic) period for both semi reverse and forward configurations. The temperatures in brackets refer to the average temperature during aic for each test. 47
Table 13: maximum temperatures for each height in semi reverse tests..... 48
Table 14: maximum temperatures for each height in forward tests..... 49
Table 15: total combustion time in semi reverse and forward smouldering..... 51
Table 16: maximum co_2 and co values [ppm] during the after intense combustion period..... 58

1. Introduction

This master thesis is carried out with the *Emerging Risks from Smouldering Fires,* also known as the *EMRIS* project. EMRIS aims to improve the knowledge related to smouldering fire in different kind of materials, including pellets. In this project, smouldering combustion in woody combustibles (pellets) was studied and discussed.

1.1 Previous own work

Smouldering behaviour in wood pellets has been studied in the fall of 2016. [1] In those tests, it was possible to get in touch with the smouldering combustion pattern by varying the airflow and combustion time. It was established that with 6 hours heating, both forward and semi reverse air flow propagations underwent a self-sustained smouldering combustion, contrary to 4 hours heating, when only forward smouldering managed to maintain the reaction. Because of this, the heating period in this thesis will be 6 hours for the entire tests. The difference in the setup between forward and semi reverse configuration was the presence of a 1 mm thick steel annulus that allows the air entrance from below, obtaining forward air propagation.

Previous results showed three different types of smouldering which differs from one another in air flow configuration, maximum temperatures, mass loss rate and temperature development. As the obtained results were interesting and new, and due to the lack of investigation in pellets, going further into specific parts of this field and doing more testing would provide a better understanding of the process, clarifying some aspects that, due to time limit, were uncertain.

1.2 Problem

The goal of this thesis was to study the smouldering behaviour by varying the airflow propagation. This research could be of interest to ensure the safety in industrial storage units (silos) as smouldering combustion can be initiated with weak ignition sources, including self-heating. In this thesis two different configurations were studied: forward and semi reverse, 10 tests of each type have been carried out.

1.3 Hypotheses

Many factors may influence smouldering behaviour. There were formulated seven questions about factors related to airflow propagation that may influence smouldering. In this thesis, questions 1, 2, 3, 4 and 5 were assessed.

1. Is forward propagation two times more intense than reverse? If so, are the highest temperatures reached in half the time?
2. Is the total combustion time two times lesser than reverse propagation?
3. As forward smouldering is more intense, is the total mass loss significantly greater than reverse? Does the airflow readings in forward smouldering show more ups and downs in the air flow velocity than reverse?
4. Does the maximum temperature peak match the highest mass loss rate in time?
5. Is a higher air flow associated to greater amounts of CO_2 and lower CO?
6. Does the annulus thickness affect smouldering behaviour? Does a bigger gap provide a more intense reaction, with the possibly of, at some point, the transition to a flaming fire? Does a smaller gap have a closer behaviour to reverse smouldering?
7. Can different pellet compositions change the smouldering process?

1.4 Report structure

This project is based on experimental testing. A literature study was done as part of the report with the aim to give background information about smouldering. In Section 2, the theoretical background was described. Section 3 corresponds to the method, followed by the results, discussion and conclusions in Sections 4, 5 and 6 respectively.

2. Theoretical background

In this section, the currently energy situation along with the use, consumption and wood fuel market will be discussed (see Section 2.1-2.4). From Section 2.5 until Section 2.10 smouldering combustion, with its general characteristics and airflow propagations, will be discussed.

2.1 World Energy situation

In today's society, the energy availability and consumption are closely related to the welfare of a country. That is why rich countries show higher energy consumption than the poor ones [2].

However, this scenario is changing since in recent years the energy consumption has grown considerably due to the strong development of the emerging countries, as much in its economy and in its population [2].

According to the latest report from the International Energy Outlook [2] it is estimated that the world energy consumption will increase by 48% between 2012 and 2040. The largest increase in oil consumption will occur in countries outside the Organization for Economic Co-operation and Development (OECD) as it can be seen in Figure 1.

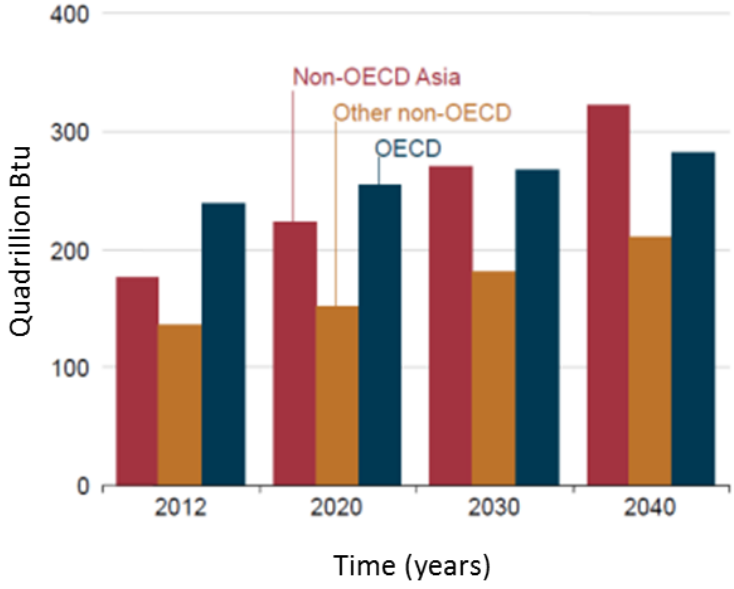

Figure 1: Illustration of World energy consumption from 2012 to 2040 in quadrillion Btu [2].

Analysing the global consumption by fuel type, it is illustrated in Figure 2 that renewable energy technologies are the world's fastest-growing energy source over the projection period [2]. Renewable energy consumption increases by an average of 2.6 % [3] per year between 2012 and 2040. This reflects not just the accelerating growth of wind and solar energy, but also a great expansion of bioenergy [3]. The use of renewable energy has many potential benefits, including the reduction of greenhouse gas emissions, the diversification of energy supplies and a reduced dependency on fossil fuel markets (in particular, oil and gas).

Even though consumption of non-fossil fuels is expected to grow faster than consumption of fossil fuels, fossil fuels will account for 78% of energy use in 2040 [2].

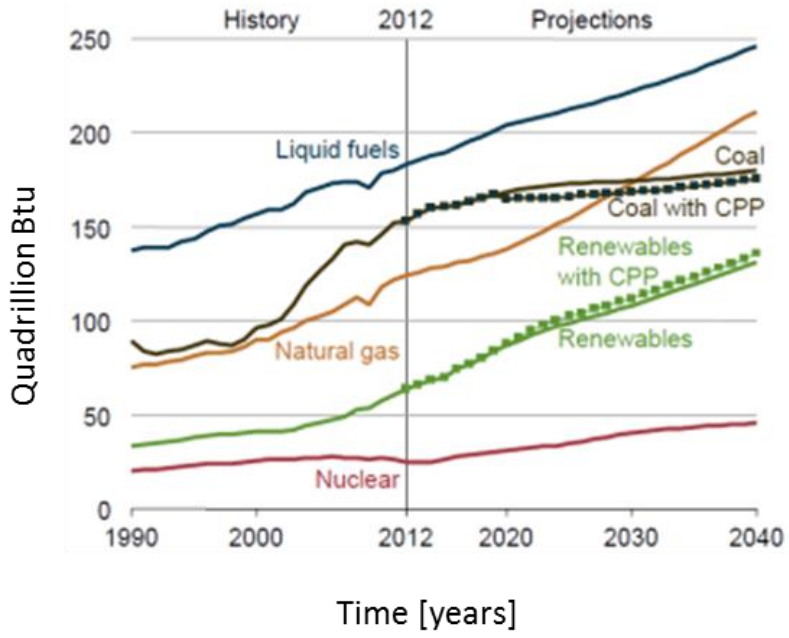

Figure 2: Total world energy consumption 1990-2040 by energy source, including energy resources with Clean Power Plant (CPP) policy in quadrillion Btu [2].

Concerning worldwide oil reserves, the largest reserves in 2015 are located in the Middle East and North America, as it is depict in Figure 3 [4].

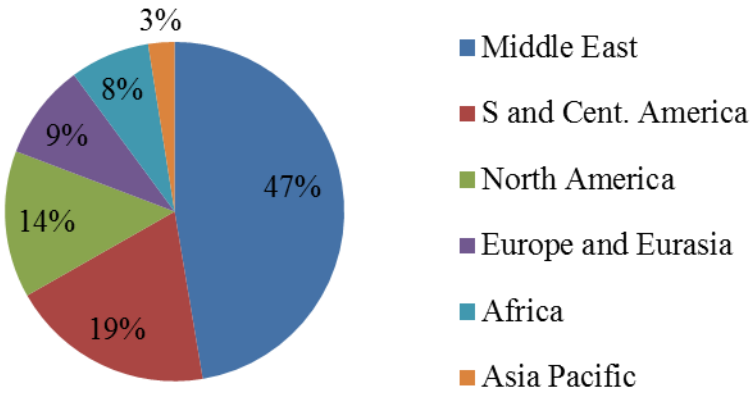

Figure 3: Oil reserves chart distribution worldwide in 2015 [4].

Figure 4 shows the variation over the years in oil price, in the two oil crises during the 1970's and the gulf crisis of 1990, a disruption of crude oil supply was triggered by the 4th Middle East War, the Iran Revolution, and the Kuwait invasion. After that, crude oil prices in the 1990's didn't exceed 30 $ per bbl. However, after it went down to 10$ per bbl in 1998, the price started to go up around the Iraq crisis in 2003 [3].

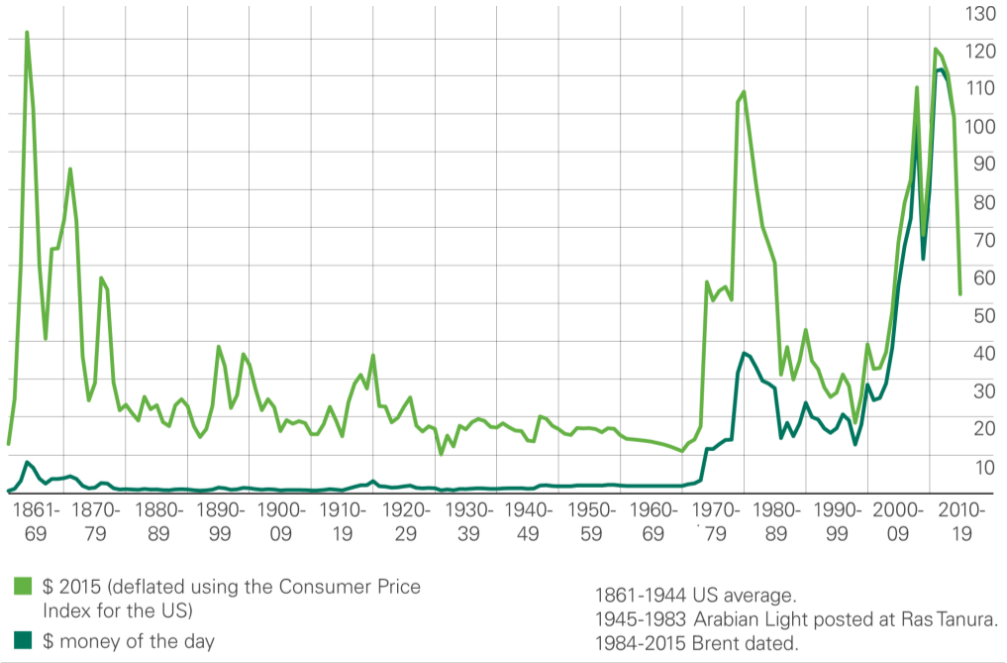

Figure 4: Crude Oil price chart (1861-2019) [2].

With the present situation of increasing energy demand, rising energy prices, and political reinforcement of countermeasures for global warming, renewable energy sources have a vital role to play in ensuring the energy availability in the future [3].

2.2 Biofuel and Biomass

Biomass and biofuel come from the same source; the main distinction is that biomass is used to produce biofuel.

Biomass is organic matter derived from living, or recently living organisms [5]. It is a stored source of energy initially collected by plants during the photosynthesis process, whereby carbon dioxide is captured and converted to plant materials mainly in the form of cellulose, hemi-cellulose and lignin. As an energy source, biomass can either be used directly via combustion to produce heat, or indirectly after converting it to various forms of biofuel [5].

Biofuels are primarily used as fuel for automobiles, thermal and power generation [6]. A distinction is made between primary and secondary biofuels [6]. In the case of primary biofuels, such as fuelwood, wood chips and pellets, organic materials are used in an unprocessed form, primarily for heating, cooking or electricity production. Secondary biofuels result from processing of biomass and include liquid biofuels such as ethanol and biodiesel, which can be used in vehicles and industrial processes.

Biomass technologies are under constant improvement; with the right type of policies and cost effective and efficient technologies it can be available for heat and electricity production.
One of the major factors limiting the utilization of biomass for heat and power production is its low bulk density, resulting in inefficient and cost-intensive handling properties [6]. The distances between biomass production sites, such as forest and agricultural land to industrial and residential areas, where the energy is needed, are often long and require significant logistics for transportation and storage. The bulk density of biomass is about 40 to 150 kg/m^3 for grasses and about 150 to 200 kg/m^3 [7] for commercial woodchips. Pelletization of biomass increases the biomass bulk density to about 700 kg/m^3; apart from the density increase, pelletization offers several other benefits, such as homogeneous shape and structure that is advantageous for automated feeding into boiler system [7].

2.3 Bioenergy's role in renewables

Bioenergy is the energy derived from biofuels; it covers approximately 10% [6] of the total energy demand. Bioenergy is mainly used in residential buildings (80%), to a lesser extent in industry (18%), while liquid biofuels for transport still play a limited role (2%) [6]. Bioenergy is the only renewable energy source that is able to provide green fuel for the three energy applications: heating and cooling, power generation and transport applications.

Renewables are becoming a key priority for European Union policy, in buildings specifically. Bioenergy is currently the leading renewable in heating and cooling (88%) representing 16% of European gross final consumption of energy [6]. With regards to power generation, bioenergy represents 5% of the overall EU generation [6].

2.4 Pelletizing process

The compaction of biomass into pellets is an old process that has been known for more than 130 years [7]. Pelletizing processes consist of multiple steps which include raw material pre-treatment, pelletization and post-treatment. The Pre-treatment steps generally consist of size reduction, drying and conditioning. After pelletization, the pellets are sent into a pellet cooler for further handling or storage and later sieved to remove the small particles. In Figure 5 it can be seen the biomass densification process.

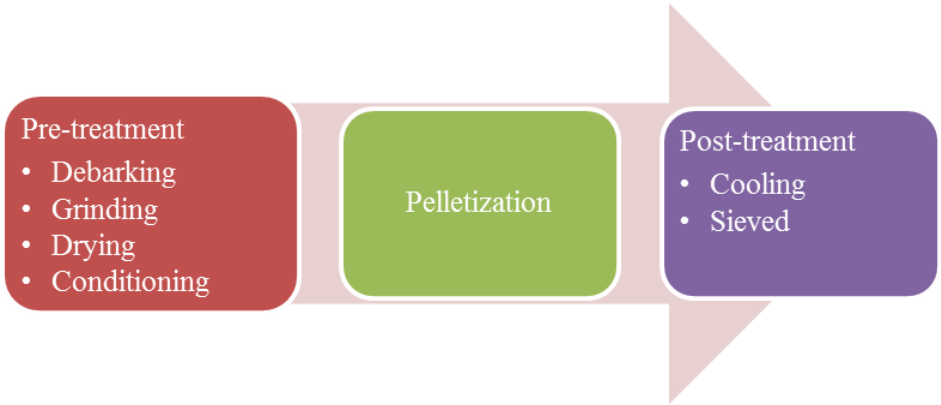

Figure 5: Scheme of a typical overview of the biomass densification process, based on [7] chart.

Pellets are produced in a mill that generally consist of a die with cylindered press channels and rollers that force the biomass to flow into and through the channels. Due to the friction between the steel surface and the biomass in the press channel, a high back pressure is built-up and heat is generated. Either the die or the rollers can be rotating as illustrated in Figure 6, and due to that movement, the biomass in the mill is squeezed between roller and die and forced to flow into the press channels [7].

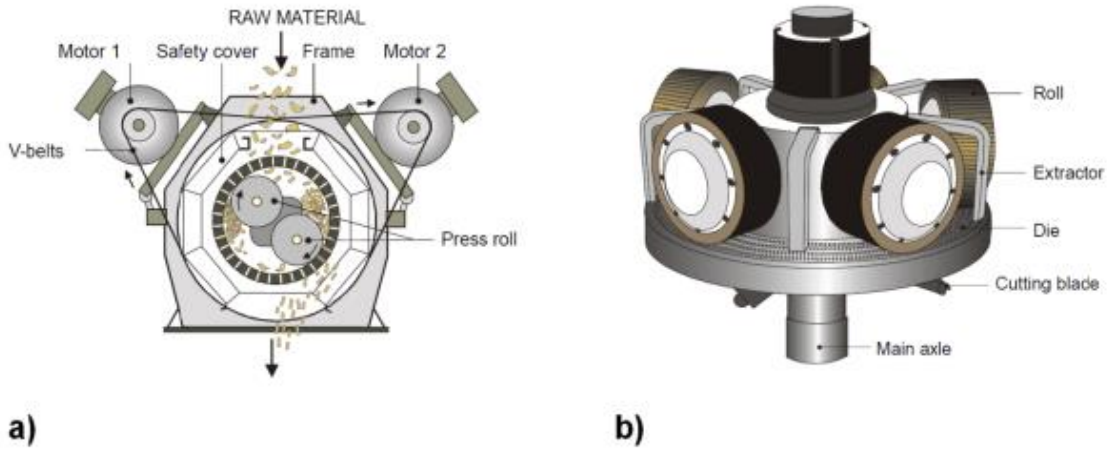

Figure 6: Typical pellet mill design a) ring and die b) flat die, taken from [7].

2.5 Pellet market

Wood pellets are the most common product on the international biomass market. Global wood pellet production has shown an exponential growth. The European Union produced 14.1 million tonnes of pellets covering 70 % of its demand [8]. Therefore, the majority of wood pellet demand is covered by its own domestic production.

As shown in Figure 7, Germany is the biggest producer among the 28 Member States (EU-28) that conform the European Union with 2 million tonnes, followed by Sweden, Latvia, Estonia and Austria.

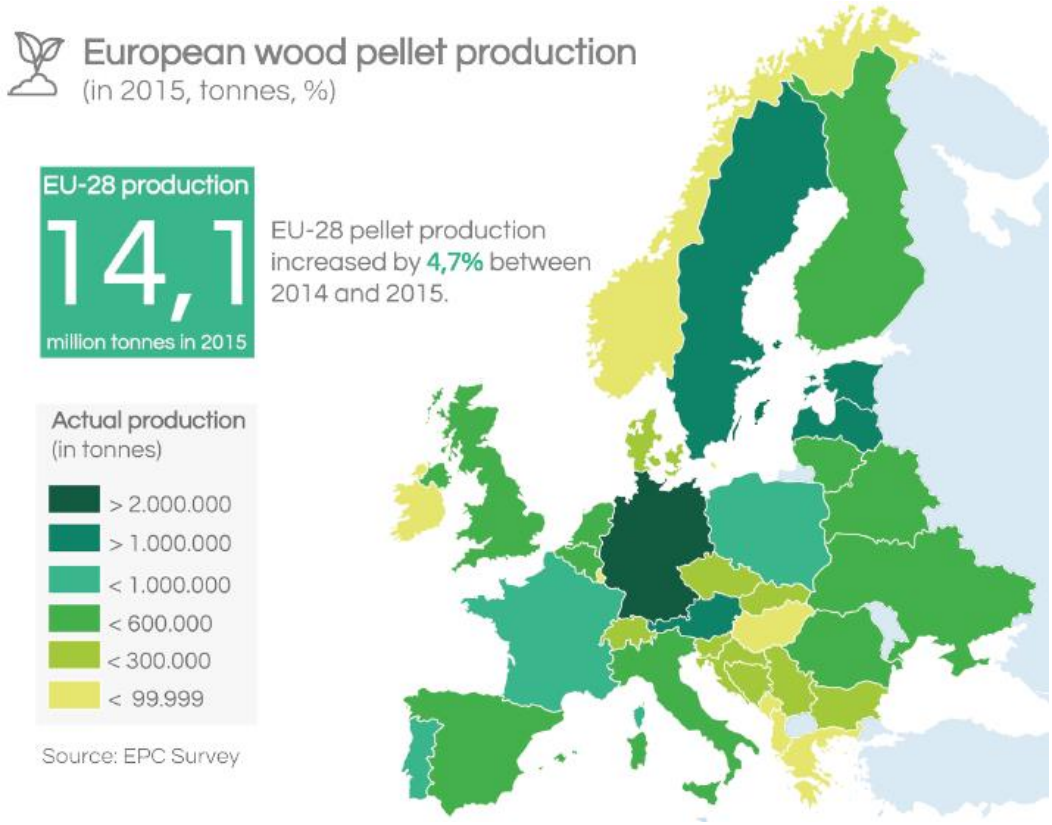

Figure 7: European wood pellet production in 2015 [tonnes] [8].

In Europe, 20.2 million tonnes of wood pellets were consumed in 2015. The predominant use was for heat production, which can be divided into three markets [8].

- Residential heating (42.2 %)
- Commercial heating (15.7 %)
- Heat generated from combined heat and power (6 %)

The remaining 36.1 % of wood pellets was used for power production, as shown in Figure 8.

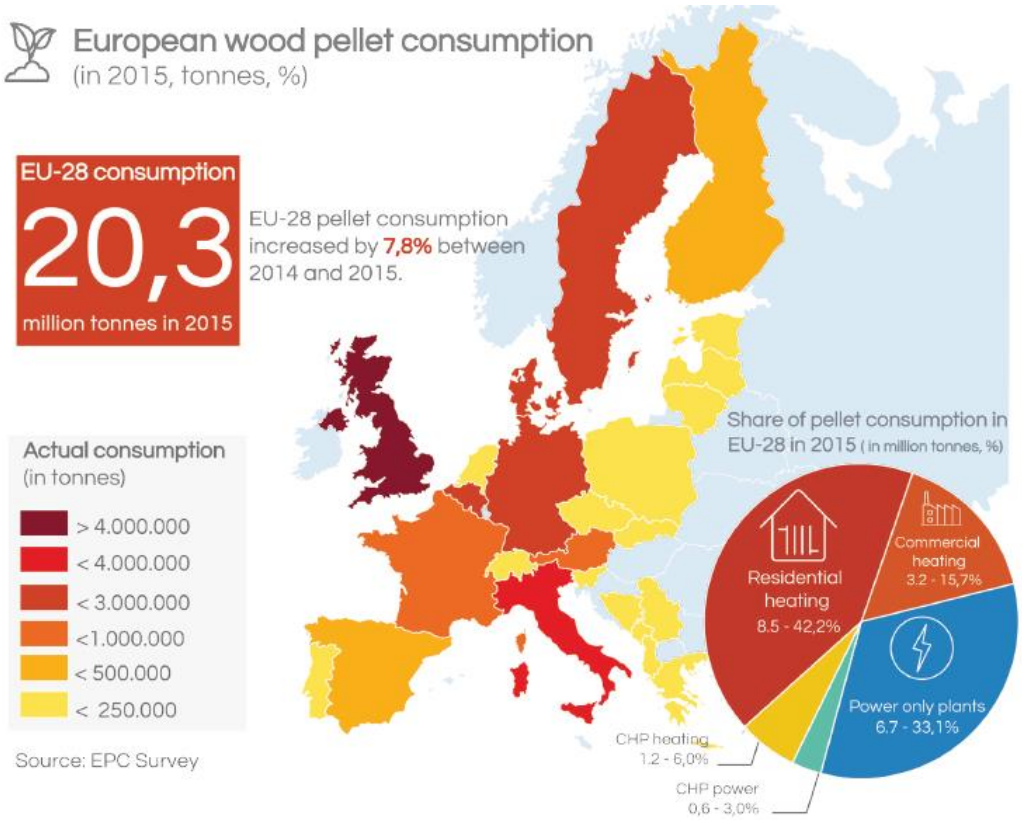

Figure 8: European wood pellet consumption in 2015 [tonnes] [8].

Italy was the biggest consumer of pellets using 3.1 million tonnes in 2015 for heat production. Among the top 5 pellet consuming countries, the use of wood pellet varies: In Italy, Germany and France the majority of wood pellet use goes to residential heating market. In Denmark, most of them are used in combined heat and power plants for heating and power production, and in Sweden to heating installations for commercial purposes [8].

Commercial heating is usually seen as the most potential one. Unfortunately, there is a lack of awareness about the use of pellets in these sectors such as industry or services (hotels, swimming pools or public buildings) [8].

With the current emphasis on biomass usage as a green fuel for energy plants, there is a need for understanding the requirements for storing biomass.
Biomass is not an easy material to handle, it appears in a lot of species, forms and sizes, it consolidates and packs easily, has a wide range of moisture contents, basic and bulk densities and calorific values. Biomass can also freeze and catch fire easily and is self-combustible.

It cannot be underestimated that heat can build-up within woody biomass storage piles to the point of spontaneous-combustion, which can result in huge inventory losses and potential damage to structures and equipment. Fires will smoulder deep inside a pile for a long time and if the pile is opened up it can flare up into open flames due to the oxygen exposure.

2.6 Smouldering combustion

Smouldering is a non-flaming combustion mode, deriving its heat from heterogeneous reactions occurring on the surface of a solid fuel when heated in an oxidizer environment [9]. The combustion process is generally oxygen deficient, and the propagating reaction leaves behind a char that contains a significant amount of unburned fuel.

Smouldering is of interest both as a fundamental combustion problem and as a practical fire hazard, for instance in industrial storage units. Statistics show that about 75% of unwanted fires in dwellings can be expected to undergo smouldering in their initial stage, followed only later by flaming [9]. Smouldering is also the ruling combustion phenomena in wildfires of natural deposits of peat and coal, which are the largest and longest burning fires on Earth. These fires contribute to global greenhouse gas emissions, destroying ecosystems and causing the waste of natural resources [9].

Many materials can sustain a smouldering reaction including: coal, cotton, tobacco, dust, paper, peat, duff and hummus, paper, wood, board of organic fibres, synthetic foams and charring polymers including polyurethane foam [9].
Summing up the main smouldering researches in different raw materials, U.E. Jensen [18] studied the smouldering propagation in building insulation materials; Rein et al., [11] in polyurethane foam; B.C.Hagen studied the transition from smouldering to flaming fire in cotton [20], and T.J. Ohlemiller the smouldering combustion on solid wood [15].

Smouldering must not be confused with flaming combustion. The main difference between smouldering and flaming is that, in smouldering, the oxidation reaction and the heat release occur on the solid surface of the fuel and, in flaming, these occur in the gas phase surrounding the fuel. There is also a difference in the range of temperatures; maximum temperatures in smouldering combustion are typically found around 500-700°C, while flaming combustion has values around 1500-1800°C [12-15]. Because of its lower temperature, smouldering is an incomplete oxidation reaction that emits a mixture of toxic gases at a higher yield than flaming fires; smouldering favours CO_2 to CO ratios around unity (in contrast to ratios around 10 for flaming combustion), so CO is an important toxic factor to take into account [9].

Smouldering chemistry can be understood as a two-step process: the pyrolysis of fuel and char oxidation. Both reactions produce ash, a mineral-rich residue of insignificant reactivity that is left after the fire, and char, a carbon-rich porous material with a high surface-to-volume ratio and a high heat of reaction [9].

The first step is pyrolysis, in other words, the endothermic chemical decomposition of a solid material due to heating, involving the irreversible and simultaneous change of chemical composition and physical phase. [9]

$$Fuel\ (solid) + Heat \rightarrow Pyrolyzate(gas) + Char(solid) + Ash(solid) \quad (1)$$

After pyrolysis it is developed the char oxidation, which is the principal heat source in most self-sustained smoulder propagation processes.

$$Char(solid) + O_2(gas) \rightarrow Heat + CO_2 + H_2O + other\ gases + Ash(solid) \quad (2)$$

There is also hold a gas-phase oxidation that leads to flaming combustion.

$$Pyrolyzate(gas) + O_2(gas) \rightarrow Heat + CO_2 + H_2O + other\ gases \quad (3)$$

Equations (1) and (2) can be extended to include the direct oxidation of the fuel [9].

$$Fuel(solid) + O_2 \rightarrow Heat + CO_2 + H_2O + other\ gases + Char(solid) + Ash(solid) \quad (4)$$

Depending on the ambient oxygen concentrations and partial pressure, smouldering can be steady and self-sustained, or transient and followed by flaming or extinction. Lower oxygen values and partial pressures are associated with transient smouldering followed

by extinction; while higher values ends up with flaming and flame spreading over the raw material.
A smouldering fire can be very difficult to extinguish such us on heaps of coal, which in some cases require large amounts of water. As volumetric cooling of a fuel bed is a very slow process, the extinguishing process is much longer for smouldering than for flaming (months versus hours) [9].

Hadden and Rein [16] investigated three water suppression methods (pipe, shower and spray) on a small-scale coal bed. They proved that the most efficient in terms of total water required is the shower.
Furthermore, Tuomisaari et al. [17] tested some extinguishing agents (liquids: water, water with additives; gases: N2, CO2, Ar and Halon) on a small bed of smouldering wood chips. The result was that gaseous CO2, injected from the bottom, was found to be the most effective.

In the case of pellet silo fires, the traditional extinguishing agents will not have the desired effect since water will flow down in channels within the bulk material without necessarily extinguishing the seat of the fire; furthermore, if the silo is opened without proper control, oxygen may be supplied so that the smouldering fire can change into an open fire.

2.7 Smouldering propagation

Once smouldering ignition occurs, the smoulder reaction advances gradually through the material. There are three main indications that show if the material ignited or not: a significant rise of temperature above the external heating source, a meaningful mass loss and a colour change in the material.

Smouldering spread is controlled by two factors: oxygen availability to the smouldering front and the heat loss from it. When external heating is prolonged in time, an assisted propagation is possible; once the external heat supply ceases the smouldering reaction will be either self-sustained or extinct.

When studying smouldering propagation through the interior of combustible materials it is common to classify it into two different configurations: reverse and forward, as illustrated in Figures 9 and 10. These are defined according to the direction in which the smouldering reaction propagates relative to the oxygen flow; in reverse smoulder, the reaction front propagates in the opposite direction to the oxidizer flow, and in forward smoulder, the front propagates in the same direction.

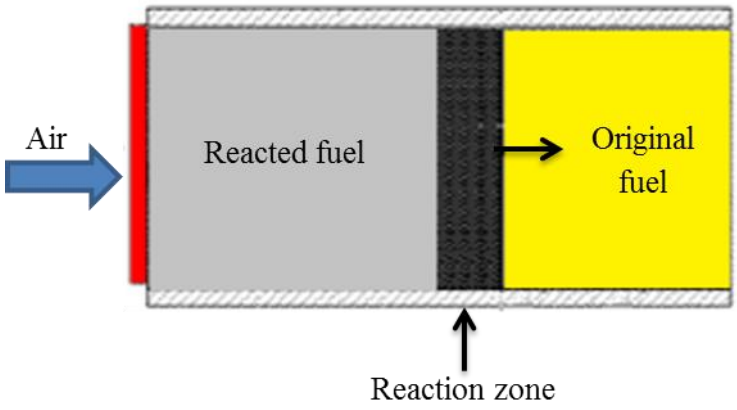

Figure 9: Forward propagation overview, adapted from [9].

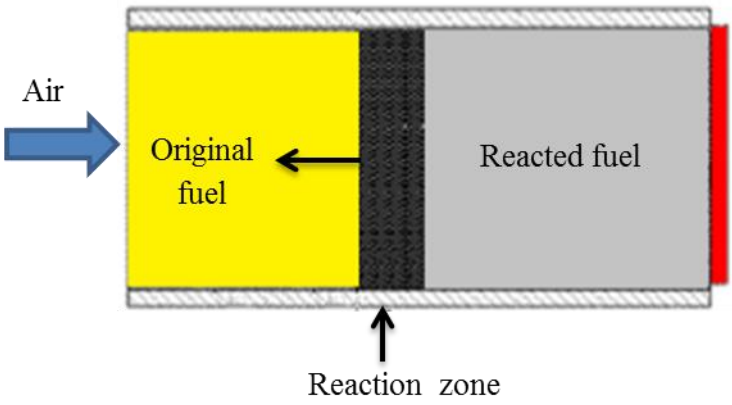

Figure 10: Reverse propagation overview, adapted from [9].

In forward propagation, the fresh oxygen flow through the char, reacts at the smoulder zone and then the oxidizer depleted flow goes through the original fuel. Convective transport is in the direction of the original fuel ahead, preheating it before the smouldering zone arrives.

In reverse propagation, the fresh oxidizer flows through the original fuel and reacts at the smouldering zone; convective transport is in the direction of the char behind the front, reducing the preheating of the fuel [11].

When a bed of fuel is ignited locally, the spread will include horizontal and vertical spread. Each front will be dominated by forward or reverse propagation depending on the roles of buoyancy, wind and diffusion. The spread can be presented in two different configurations: downwards and upwards through the fuel bed.

If initiation occurs on the top surface of the fuel bed, the fire will spread laterally and downward. Downward spread is dominated by forward smouldering, and creates a growing layer of ash that only decreases if wind carries the particles away. The horizontal spread is enhanced by a direct supply of atmospheric oxygen, and the rate is significantly greater than downward spread where oxygen transfer is limited by the layer of ash and char [9].
If initiation occurs deep within a layer of fuel and the nearest free surface is on the top, the fire will slowly spread upwards dominated by reverse smouldering. The reaction front usually spreads without fully consuming the char left behind.

From Rein experiments [11] it was concluded that the smouldering peak temperature in reverse propagation was around 400 ºC with a propagation velocity of 0.12 mm/s [11] while in forward propagation the temperature was 430 °C with the double propagation velocity than the reverse case [11].

On the other hand, T.J. Ohlemiller [20] studied the smouldering spread in forward smouldering, reverse and a mix of the two. Increasing the smouldering spread rate with increased air supply is consistent with the behaviour of forward smouldering in other configurations. The increased air flow accelerates the transfer oxygen rate to the wood char surface, hence the char oxidation rate, the local heat release rate and thus the local temperature. Figure 11 shows that the char surface temperature does indeed increase substantially with increased air flow rate.

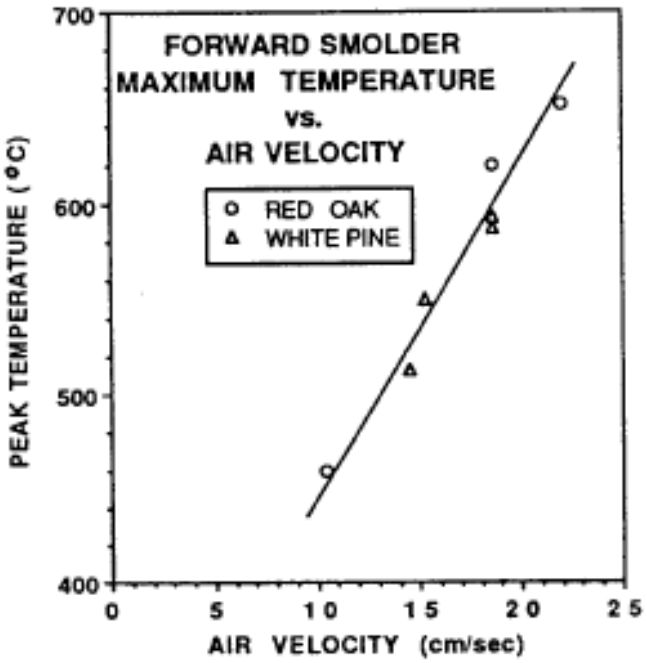

Figure 11: Peak surface temperature for red oak and white pine in forward smouldering, graph taken from Ohlemiller experiments [20].

2.8 Smouldering gas emissions

Smoke is the mixture of tiny solid, liquid and gas particles emitted when a material undergoes combustion. Smoke poisoning is considered the primary cause of death in victims of indoor fires [24]. Its composition depends on the nature of the burning fuel and combustion conditions; smoke also contains flammable compounds so that if the oxygen is increased, these compounds can ignite either thorough open flames or by their own temperature. Smouldering combustion results in the production of a large amount of hydrocarbons, both aliphatic and aromatic [24].

Gas emissions related to smouldering fires are different in comparison to flaming fires, both in terms of emission rate and chemistry. As smouldering is an incomplete combustion, it releases species and quantities that differ from the ones in stoichiometric and complete combustion, as shown in Table 1 [25]. The combustion efficiency described in Table 1 refers to how efficiently the fuel is being burned in the combustion process.

Table 1: Characteristics of the fire stages from [25].

Fire type	Max. Temp (ºC)		Oxygen volume %		CO/CO_2 (v/v)	$\frac{100x(CO_2)}{(CO_2+CO)}$ % efficiency
	Fuel surface	Upper layer	Entrained	Exhausted		
Self-sustaining (smouldering)	450 to 800	25 to 85	20	0,2	0,1 to 1	50 to 90
Well-ventilated flaming	350 to 650	50 to 500	≈ 20	0,2	< 0,05	> 95

The presence of pyrolyzate in Equation 1 contributes to a complex gaseous mixture, which includes volatile organic compounds (VOC), polyaromatic hydrocarbons (PAH), other hydrocarbons and particulate matter.

While the yield of toxic species is bigger in smouldering than in flaming fires [9], the production rate, which is proportional to the spread rate, is much lower. This means that in a confined space, a smouldering fire of long duration can lead to a lethal dose of toxicity, especially CO.

2.9 Transition to Flaming

The transition from smouldering to flaming is a spontaneous gas-phase ignition supported by the smoulder reaction which acts both as the source of gaseous fuel, the pyrolyzate produced in Equation (1), and the source of the heat required to initiate the flame in Equation (3) [10].

The transition occurs within the depth of the char left by the smoulder front [9], where both critical conditions of flammability of the pyrolyzate mixture and the net excess of heat released by char oxidation are met. The heat driving the transition is released mostly by the secondary char oxidation in Equation (3), which is more exothermic and takes places at higher temperatures than char oxidation [9].

The transition to flaming has only been observed in forward propagation. [9] Ohlemiller [25] argued that this is because in forward mode, the hot gases of combustion preheat the fuel ahead and thereby enhancing the combustion; while in reverse mode, the cool air reduces preheating. However, upward propagation inside a pile of fuel, which is

mostly in reverse mode, can lead to the transition to flaming once the reaction breaks through to the free surface and finds a supply of oxygen [9].

2.10 Smouldering combustion in biomass

Smouldering fires burn two types of biomass: thick fuels, like tree branches or logs, and organic soil, like peat [20]. Peat soils are made by the natural accumulation of biomass and are the largest reserves of terrestrial organic carbon; due to this fuel accumulation, once ignited, smouldering peat fires burn for very long periods of time despite extensive rains, weather changes or fire-fighting attempts.

Possible ignition events can be natural (lightning, self-heating, volcanic eruption) or anthropogenic (land management, accidental ignition, arson).

Because water content of wildland fuels like peat can vary naturally over a wide range of values, and because water represents a significant energy sink, moisture content is the single most important property governing the ignition and spread of smouldering wildfires. [9] The second most important property is the mineral content. There is a decreasing relationship between the mineral content and the critical moisture content: higher mineral loads mean soil can only ignite at lower moistures [9]. Any soil which composition is more than 80 % mineral cannot be ignited [9].

Smouldering wildfires can be classified in shallow or deep fronts. Shallow fires have a good supply of atmospheric oxygen, but are exposed to large convective heat losses, propagating laterally and downwards along the organic layers of the ground. By contrast, deep fires have a poorer atmospheric oxygen supply but are better insulated from heat losses.

In this thesis, the studied biomass were pellets; the reason for choosing this fuel was because there were no studies about smouldering for this material, and also because as they are becoming more widely used as an alternative to oil-fired central heating in residential and industrial buildings in Europe, it is very important to study its properties to guarantee the safety by avoiding any possible flame or explosion [11].

3. Method

3.1 Materials

Norwegian wood made 50-80 % of spruce and 20-50 % of pine was used in all the experiments as illustrated in Figure 12.

Figure 12: Picture of the pellets used in this study.

The pellets were stored at a low temperature in the factory for 3 months after production, and sent to the laboratory. In the laboratory they were stored in a freezer until its use, to preserve their freshness.

The values shown in Table 2 were measured and given by the pellets producer. The moisture content of the sample was 7.4 %, the technique used to determine this percentage is based on the ASTM E 871 [26], in this method the pellets were dried at 105 ºC, repeating this drying process three times with a 24 hours interval, after that the sample experienced a mass change lower than 0.1 % of the total mass. The sample was taken out of the furnace and weighed immediately; this weight is the one used as dry mass. The difference between the sample mass when it was wet and dry is what is given as moisture content.

Bulk density was defined as the weight per unit volume of material. For its measure, a funnel was suspended above the measuring cylinder and filled with the sample; the excess material on top of the measuring cylinder was scraped off with a straight edge. The sample and the cylinder were then weighed so that Bulk Density was determined.

Table 2: Pellet properties.

Material properties	Pellets
Type of material	Wood (including bark) 50-80 % pine 20-50 % spruce
Country of origin	Norway
Pellet diameter (mm)	8
Unit density (kg/m3)	1157
Bulk density (kg/m3)	736
Porosity (%)	36.4
Moisture content (%)	7.4

3.2 Test equipment

3.2.1 Test setup

The test setup was formed by an insulated steel pipe heated by a hotplate. In all the experiments the test equipment was positioned within a vent hood, the fan was turned on and kept at the same level for all the tests during the entire test. The test setup equipment could be divided into different parts:

- A scale in the bottom, type *Systec IT1000*, measures the weight before, during and after the test to calculate the amount of sample that had been consumed. The scale consisted on a kern weighing platform KFP 30V20M IP65, and Systech it 1000 m/420 MAMP weighing terminal, as illustrated in Figure 13A. It has a measurement range of 200g-30kg with accuracy of 1 gram.
- On top of the scale (see Figure 13A) a *Wilfa* cooking electric hotplate of 2000 W was placed.
- Over the hotplate a 2.8 cm thick aluminium plate with a width and depth of 28x28 cm was put. The aluminium plate has milled channels on its top and bottom surface for placing the thermocouples. The thermocouples measured the temperature on its surface and under hotplate, as shown in Figure 14.
- On top of the aluminium plate the steel pipe is placed (see Figure 13B). The steel pipe was 33 cm high with an inner diameter of 15 cm. The insulation around the pipe is 60 mm mineral wool with a density of 140 kg/m^3 as shown in Figure 13C.

- A bidirectional probe is placed on top of the steel pipe, as vertical as possible. This probe uses the pressure difference to measure flow velocity. As it is used for fire research, the tubing is made by metal to prevent melting as well as the pressure transducers.

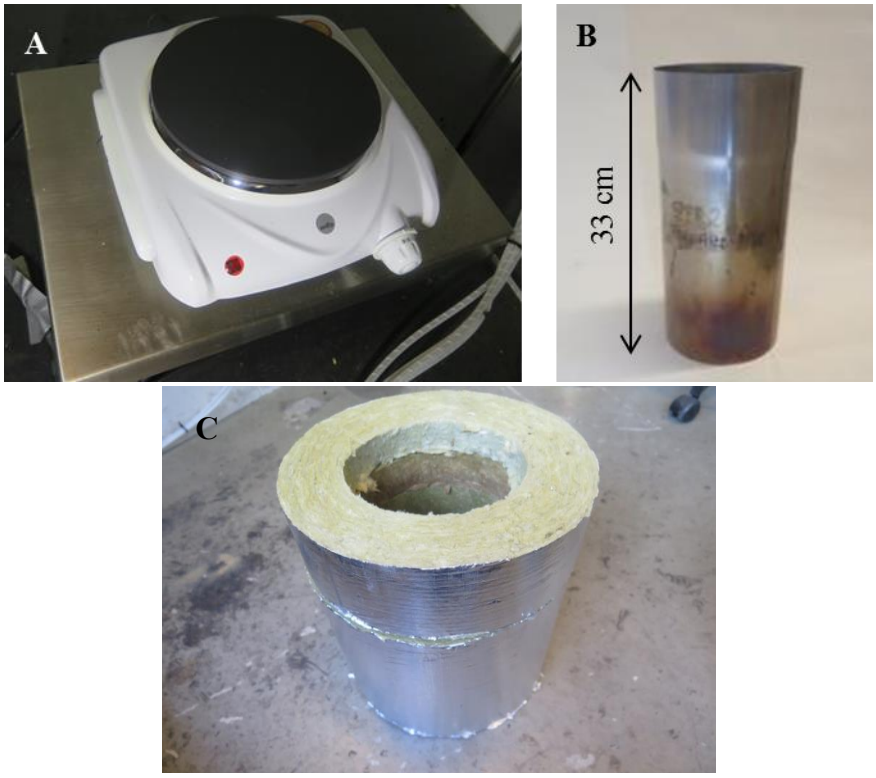

Figure 13: Picture of the heater (A), steel pipe (B) and insulation (C).

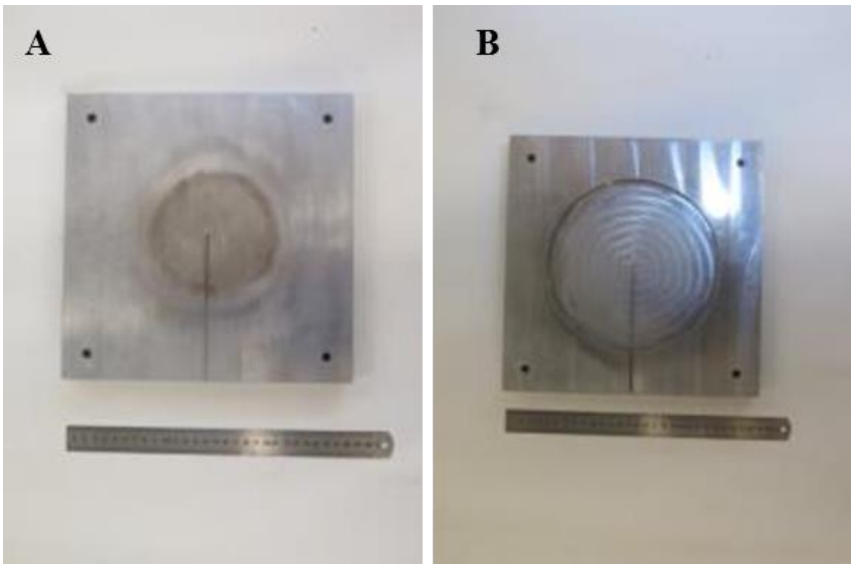

Figure 14: Picture of the aluminium plate used in this study. A) top side and B) bottom. For comparison the ruler is 30 cm long.

When the heater was tuned on, it was controlled by a JUMO B 70.1050.0 thermostat. In all the experiments the temperature was settled as the maximum one that the heater could reach (around 350 ºC).The different parameters were set up, as shown in Table 3.

Table 3: JUMO B 70.1050.0 Thermostat parameters.

Parameter	Meaning	Value
Set point	Target value of control action (temperature value)	370 ºC
Hysteresis	Time-based dependence of a system's output on present and past inputs	0.2
Low set point limit	Set point can be set up to this low limit	200 ºC
High setup limit	Set point can be set up to this high limit	380 ºC
Controller type	Cold: cooling controller Hot: heating controller	Hot

The thermostat controls the heater based on the temperature readings from the thermocouples placed in the milled channel on the bottom side of the aluminium plate. The thermostat will keep the heat on until the thermocouple under the aluminium plate reaches a given set point temperature.

With all this setup the semi reverse flow was obtained (see Figure 15), to obtain a forward propagation a 0.1 cm steel annulus was placed over the aluminium plate. The annulus had holes of 0.3 cm diameter (see Figure 16B) which enable the airflow into the pipe.

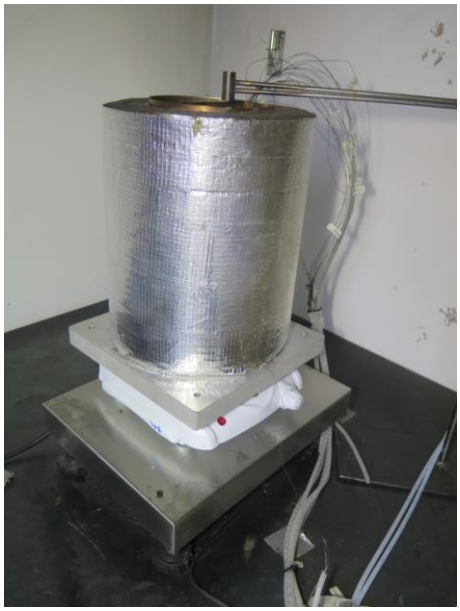

Figure 15: Test set up consisting of, from the bottom: scale, hotplate, aluminium plate, steel annulus and the insulated steel pipe.

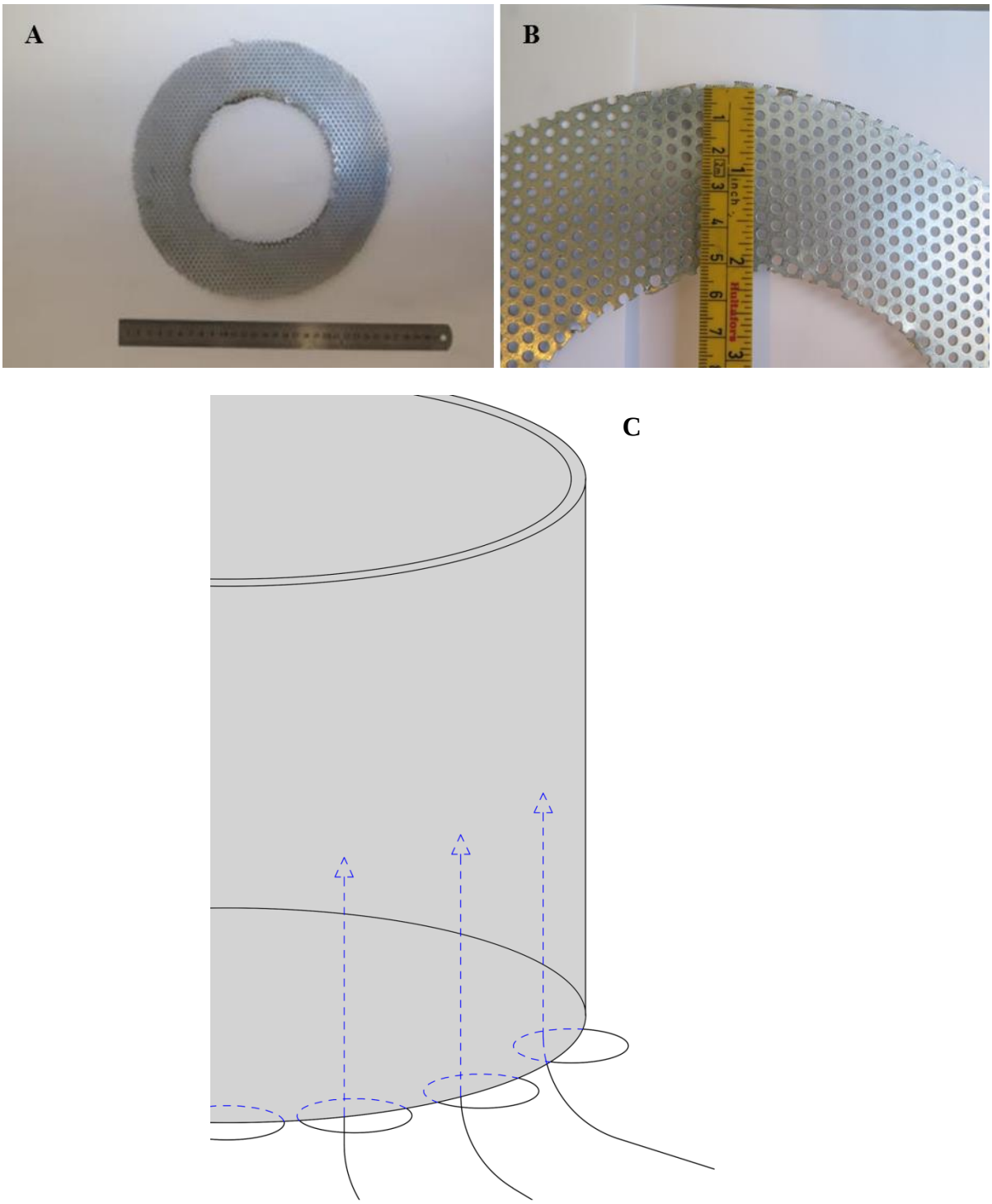

Figure 16: (A,B) Close-up of the perforated steel annulus; (C) sketch illustrating how the perforated steel annulus enables air flow into the pipe.

A 3D scaled view of the setup was sketched in Google SketchUp as shown in Figure 17. The test setup was located indoor, with an air temperature of 19-24 ºC during all experiments.

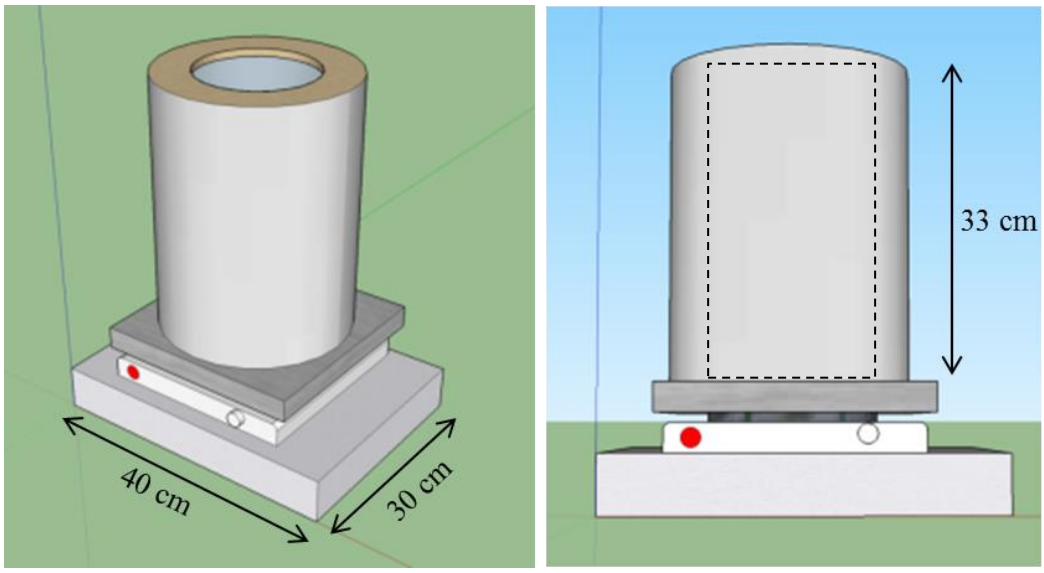

Figure 17: 3D Scaled view of the Setup. The dashed rectangle represents the thermocouple ladder inside the pipe, where the thermocouples are attached.

3.2.2 Thermocouples

A thermocouple is an electrical device that measures the temperature.

During the tests, a stainless thermocouple ladder was placed inside the pipe, as illustrated in Figure 18. It was possible to measure the sample temperatures at 2, 4, 6, 8, 10, 12, 14 and 33 cm height as depicted in Figure 19. On each level there were three thermocouples that read the temperatures on the left, centre and right side inside the pipe, with a horizontal separation of 3.75 cm among them. As it was explained in Section 3.2.1, there were also a thermocouple underneath the aluminium plate and another one on its top.

Figure 18: Picture of the thermocouple ladder. For comparison the ruler is 30 cm long.

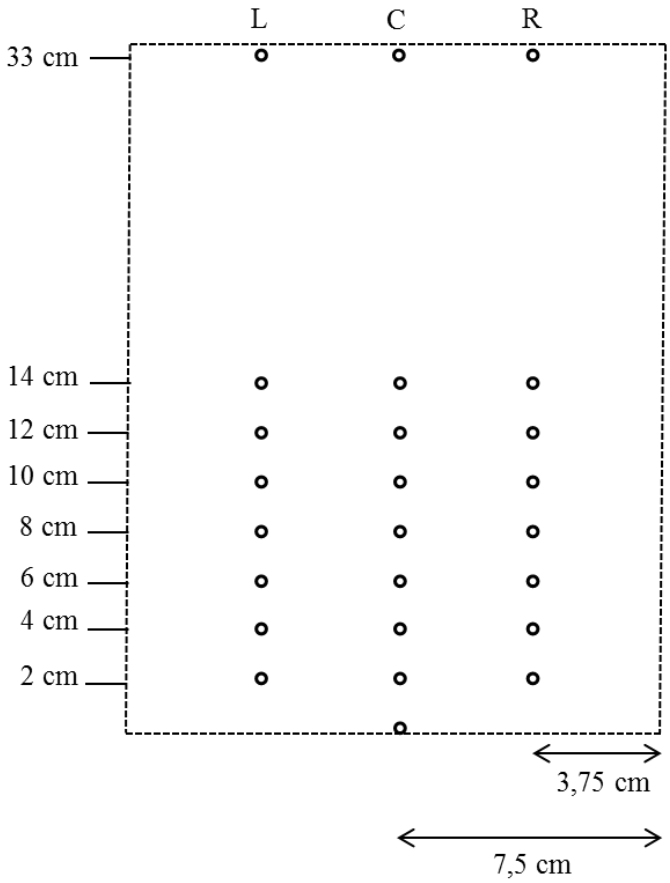

Figure 19: Cross section of the pipe with a sketch of the thermocouple positions (the circles refers to each thermocouple).

The reason why the thermocouples were fixed into a ladder was for making sure that they will stay in that position in all the tests that had being run.

The thermocouples were checked every 3 experiments to make sure that they were working properly without being damaged during the testing.

Type K (chromel-alumel) thermocouples were used during the experiments. This type is the most popular type of thermocouples [27] as it is inexpensive, accurate (+/- 2.2º C) , they are well suited to oxidizing atmospheres and can manage a wide range of temperatures (-200ºC to 1350ºC).

3.2.3 Bidirectional probe

The flow was measured by a bidirectional probe located at the centre line of the pipe. The probe consists of a stainless steel cylinder, 44 mm long and with an inner diameter of 20 mm as Figure 20 illustrates. The cylinder has a massive wall in the centre, dividing it into two chambers. The pressure difference between the two chambers is measured by a pressure transducer with an accuracy of ±5 Pa and a suitable range of measurement between 0 and 2000 Pa.

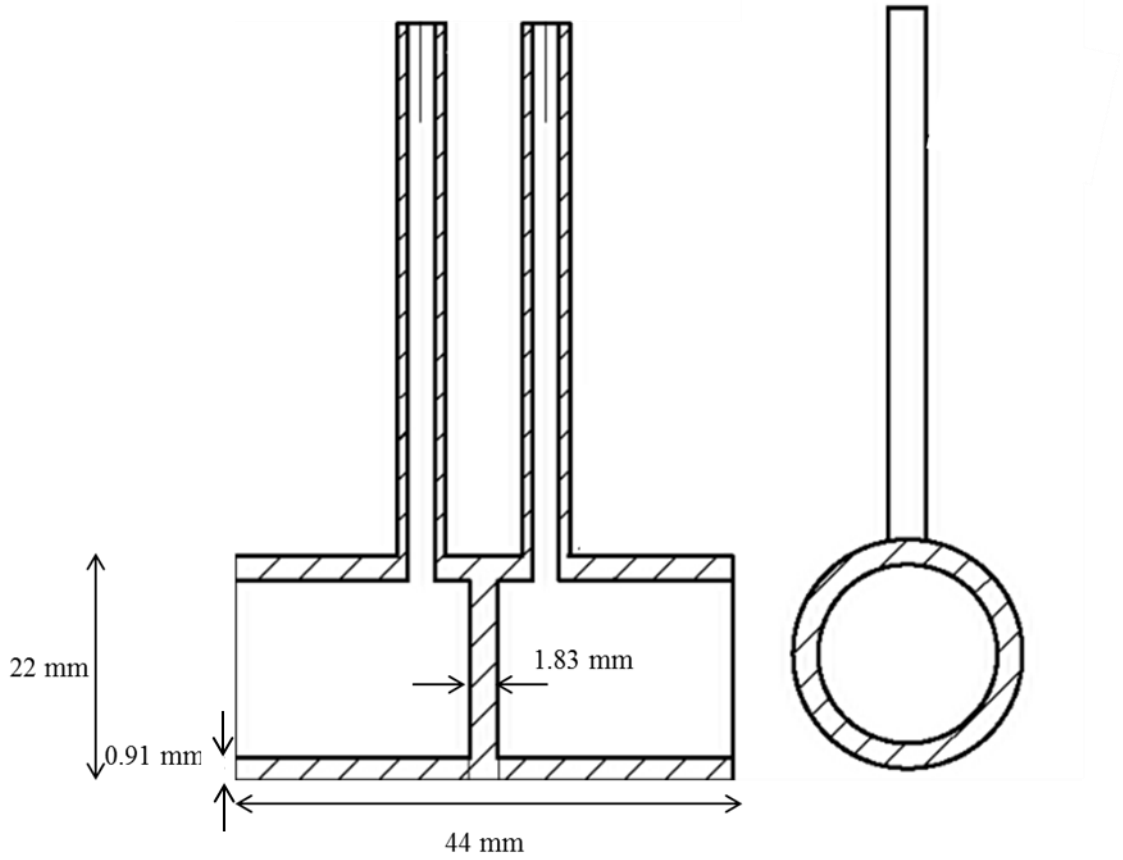

Figure 20: Sketch of Bidirectional probe, low-velocity flow design, adapted from [28]

Gas temperature in the vicinity of the probe is measured by the 33 cm height thermocouple. This thermocouple did not disturb the flow pattern around the bidirectional probe as well as it did not interfere on the thermocouple measurements.

The readings were given in Pascal. To get the data in kg/s the following formulas were used.

$$\rho = \frac{P_{amb}}{R_{gas}T_{33cm}}$$

$$V_{air} = A_{air}\rho v = A_{air}\sqrt{2\rho\Delta P}$$

Where:

V_{air}: air flow rate [kg/s]

A_{air} : Area of air flowing upwards [0.018 m^2]

T_{33cm}: Temperature at 33 cm height [K]

ΔP: Pressure difference [Pa]

P_{amb} : Ambient pressure [101325 Pa] [30]

ρ: Air density, temperature dependent [kg/ m^3]

R_{gas}: gas Specific gas constant, dry air [287.06 J/kgK] [30]

3.2.4 Gas measurement unit

As illustrated in Figure 21 and 22, the unit was formed by 4 sensors that measured carbon dioxide (CO_2), carbon monoxide (CO), oxygen (O_2) and volatile organic compounds (VOC). A thermocouple was placed inside the gas unit to extract the smoke temperature values. All the sensors and the thermocouple were connected to an electronic circuit which stores and extracts the data. The sensor data shown in Table 4 was provided by the supplier.

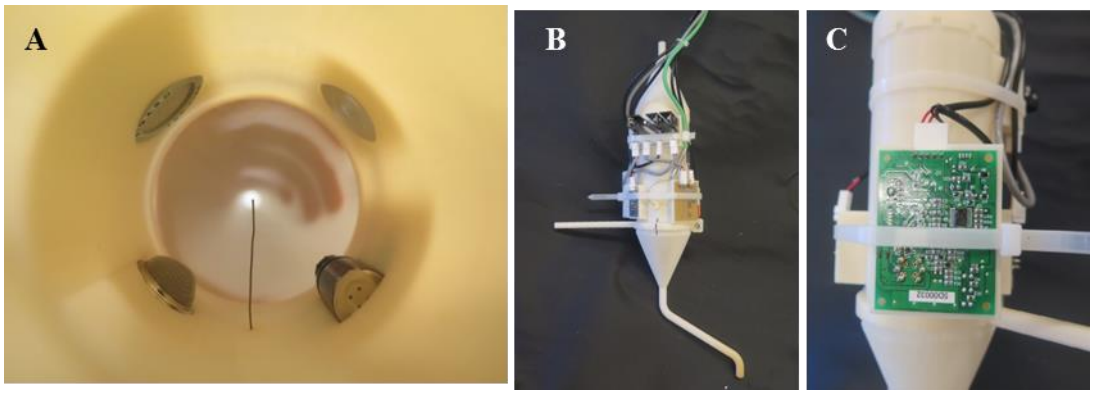

Figure 21: A) Sensors placed inside the unit; B) gas measurement unit; C) electronic circuit (right).

Table 4: Sensors characteristics used in the gas measurement unit based on information given by the supplier [30][31][32][33].

Sensor name	Detection range	Sensor (principle)	Accuracy	Operational temperature
CDM4160 - Pre-calibrated module for carbon dioxide	400 to 9000 ppm	Solid state electrolyte	Approx. ± 20%	-10 to 50 ºC
TGS 5342 - Carbon Monoxide detector	0 to ~ 10000 ppm	Electrolyte	± 5%	-5 ºC to 55ºC
Oxygen Sensor SK-25F	0~30% O_2	Galvanic cell type	± 1%	20˚±1˚C
TGS 823 - Organic Solvent Vapors detector*	300 ppm	Tin dioxide (SnO_2) semiconductor	-	20°±2°C

** The results from this unit are not going to be used, as there was no reference gas for its calibration*

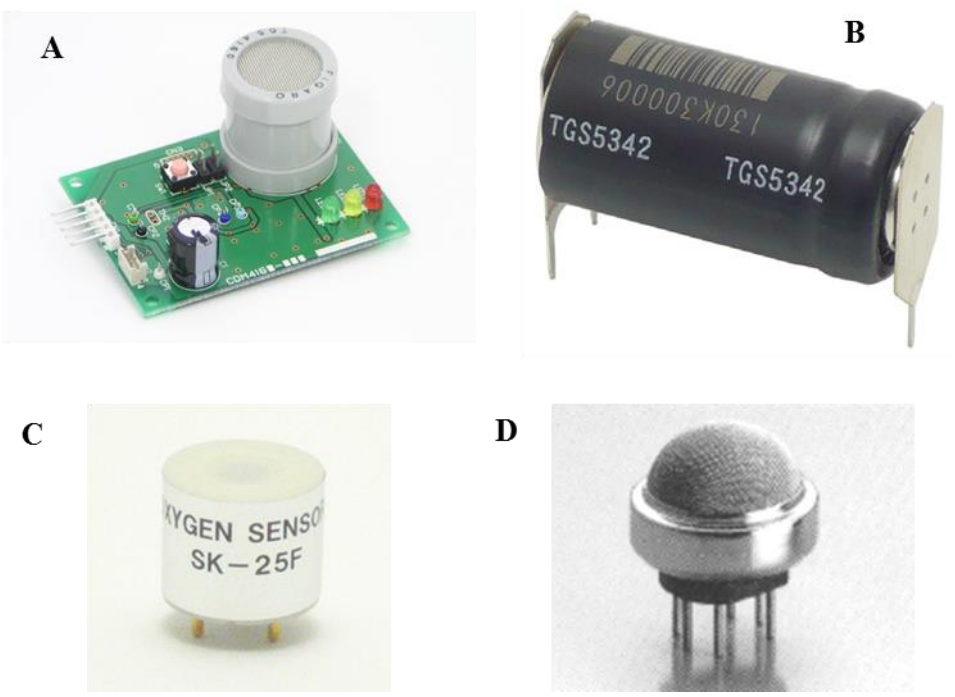

Figure 22: A) Carbon dioxide sensor; B) carbon monoxide sensor; C) Oxygen sensor; D) Solvent Vapours detector. Taken from [30][31][32][33]

For the experiments it was important to see how accurate the gas measurement unit was; for that purpose the sensor readings were measured using a gas cylinder with known conditions and gas compositions (see Table 5).

The gas measurement unit was sealed in a box with a hole on its side that enables the gas entrance, as described in Figure 23. Afterwards, the gas from the gas cylinder was introduced inside the box with two gas detectors during 8 minutes; when the values from both detectors and sensors were stable the gas flow was interrupted and the box was opened, letting the gas go directly to the atmosphere.
In Table 6 is shown the CO_2 and CO readings compared to the reference values.

Table 5: Calibration mixture conform to ISO/IEC-17025.

Gas	% mol	Pressure
Carbon dioxide	0.2504 ± 0.0025	
Carbon monoxide	7.580 ± 0.038	150 bar
Nitrogen	Balance	

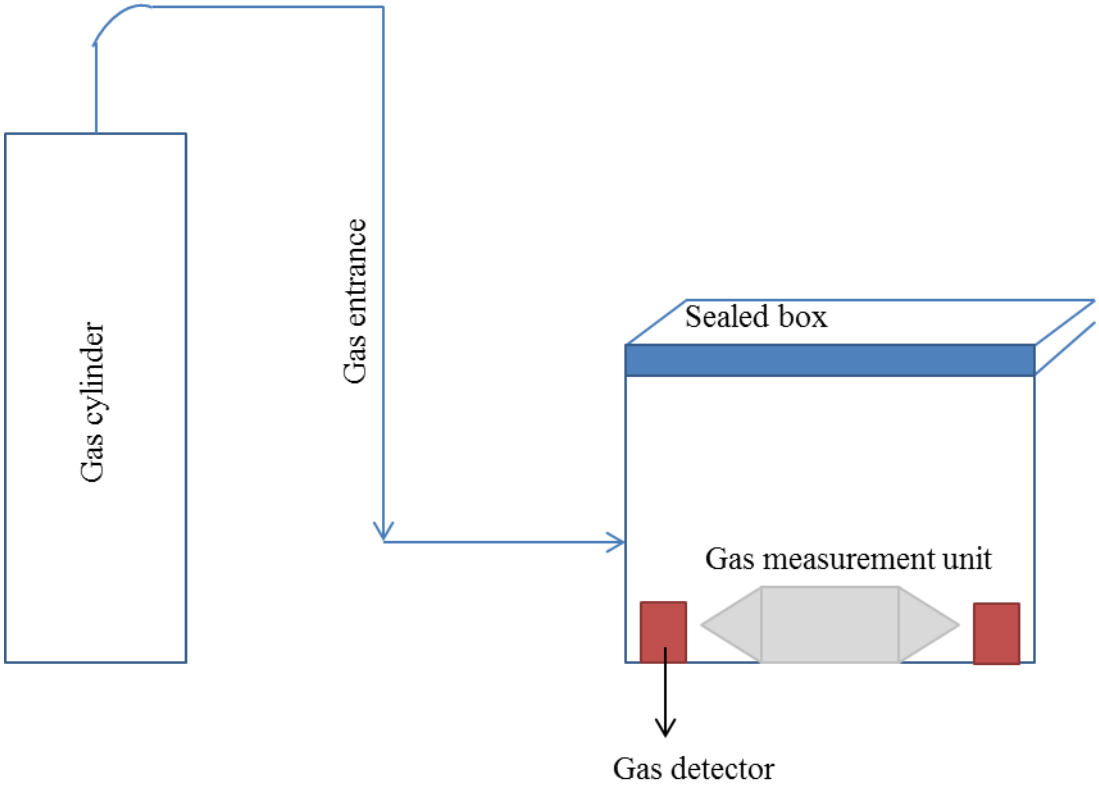

Figure 23: Gas unit calibration equipment scheme

Table 6: Reference values and gas measurement unit relative error.

	Reference value	**Gas Unit**	**Relative error (%)**
CO_2	75800 ppm	98652.2 ppm	23.2
CO	2504 ppm	1810.9 ppm	38.3

Two gas measurement units were available for the experiments, the chosen one was the unit with the smallest deviation, which in this case corresponds to Unit 2. A test with both units was carried out at the same time, as Figure 24 illustrates. To start the testing the pellets were heated with a torch till a flame was obtained; once the flame was extinguished the logging was started to get the smoke composition.

Figure 24: Picture of the two units and the bidirectional probe after running a test

As it is seen in Figures 25A, 25B and 25C both units followed the same trend during the self-sustained smouldering process. It must be taken into account that Unit 1 reached higher values in comparison to Unit 2 due to it was more exposed to the smoke column.

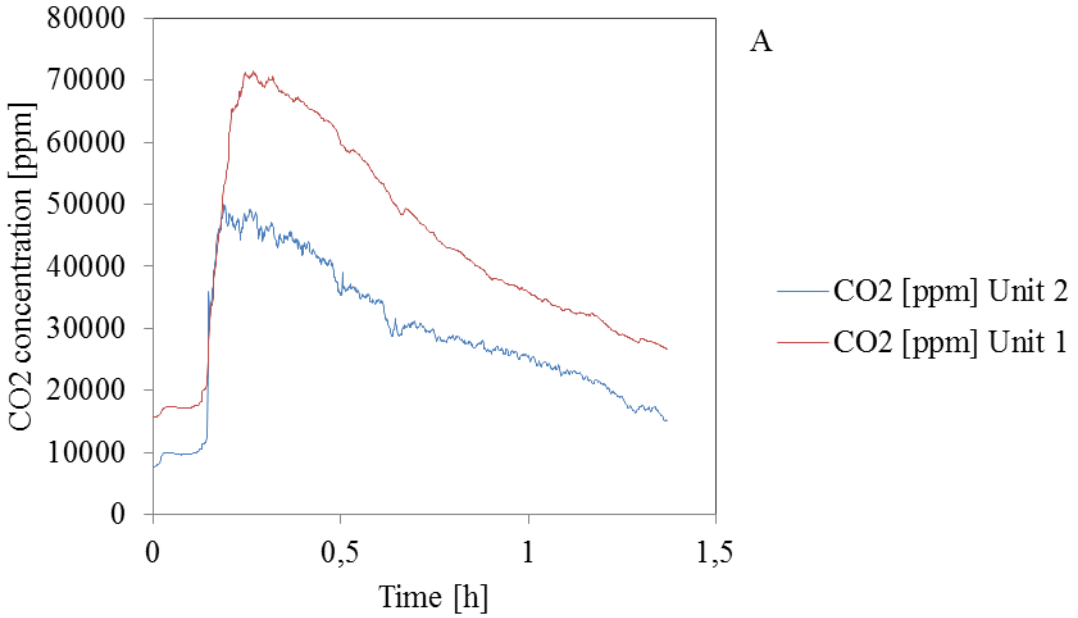

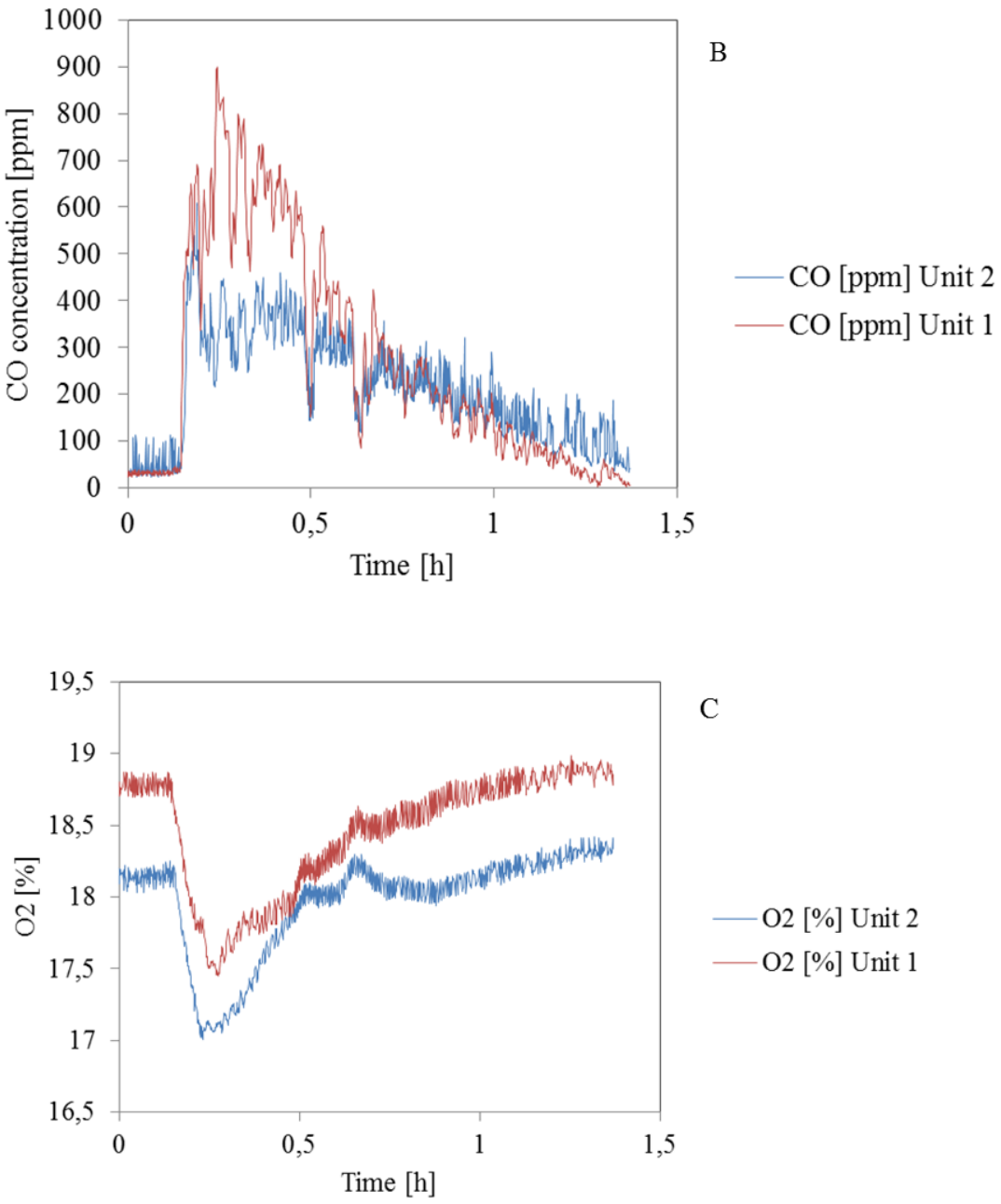

Figure 25: A) CO_2 readings from both units [ppm]; B) CO [ppm] and C) O_2 [%].

3.2.5 Data logging

The thermocouples were connected to a *KEYSIGHT 34972A LXI* logger. A laptop with the registered number *NBL2874* and the software *Agilent BenchLink Data Logger 3* was used to register the data every 5 seconds.

Table 7 shows the 32 logging channels that were used during the experiments.

Table 7: Placement of the measurement points per channel.

Channel	Naming	Placement/measurement point
101	UnderAl	In a milled channel underneath the aluminium plate
102	0cmC	In a milled channel on the top of the aluminium plate
103	2cmL	2 cm above the aluminium plate - left
104	2cmC	2 cm above the aluminium plate – centre
105	2cmR	2 cm above the aluminium plate – right
106	4cmL	4 cm above the aluminium plate - left
107	4cmC	4 cm above the aluminium plate – centre
108	4cmR	4 cm above the aluminium plate – right
109	6cmL	6 cm above the aluminium plate - left
110	6cmC	6 cm above the aluminium plate – centre
111	6cmR	6 cm above the aluminium plate - right
112	8cmL	8 cm above the aluminium plate - left
113	8cmC	8 cm above the aluminium plate – centre
114	8cmR	8 cm above the aluminium plate – right
115	10cmL	10 cm above the aluminium plate - left
116	10cmC	10 cm above the aluminium plate – centre
118	10cmR	10 cm above the aluminium plate - right
201	12cmL	12 cm above the aluminium plate - left
202	12cmC	12 cm above the aluminium plate – centre
203	12cmR	12 cm above the aluminium plate – right
204	14cmL	14 cm above the aluminium plate – left
205	14cmC	14 cm above the aluminium plate – centre
206	14cmR	14 cm above the aluminium plate – right
207	33cmC	33 cm above the aluminium plate – centre
120	Thermostat	Thermostat
121	Mass	Mass
213	VOC	Volatile Organic Compounds (VOC)
214	CO_2	CO_2 concentration
215	CO	CO concentration
216	O_2	O_2 concentration
217	Gas Temperature	Gas Temperature at the gas unit height
220	Airflow	Airflow measurement

3.3 Test procedure

The pellets were taken out of the freezer within 3 days to make sure that they were unfrozen without losing their properties. Before each test, a sample of 1249.4 grams was weighed; this amount is based on the volume and bulk density of the pellets. With this amount ~ 10 cm sample height was reached within the pipe. Based on initial experiments, it was demonstrated that with less height the heat losses were too high so the results would be unreproducible, and with a bigger height the development of the test would take a lot of time. The thermocouple ladder was lowered into the steel pipe, and then the pellets were placed inside. Once the gas measurement unit and the bidirectional probe were placed perpendicular to the pipe, as Figure 26 illustrates, the logging was started.

Figure 26:Close-up picture of the gas measurement unit and bidirectional probe position with regards to the pipe.

All the tests were run with the same thermostat settings, and these were checked before each test. The total mass on the scale was read before the test started, and the software was set to log data. Mass, temperature, gas composition and air flow were logged for two minutes before the hotplate was turned on at maximum effect during 6 hours. Once the thermocouples reached ambient temperature the logging was stopped.

When the test was finished the remaining sample was carefully removed from the steel pipe and stored. The test equipment (steel pipe and aluminium plate) were washed after each test using a basic detergent.

After a few days the residue was sorted and weighed, sorting it into two different residues: char and ash.

4. Results

The same type of pellet has been tested in all the experiments. The goal was to study the smouldering behaviour by varying the airflow. Two configurations have been used: forward and semi reverse. In this thesis it is referred to a semi reverse propagation instead of reverse because the air entered and exited at the top of the pipe, while the combustion propagated from bottom up, giving a semi reverse airflow system.

The results showed three variations of smouldering combustion, named as: *Semi reverse Smouldering behaviour*, *Forward Smouldering behaviour Type 1* and *Forward Smouldering behaviour Type 2*.

Twenty smouldering tests have been carried out (10 forward and 10 semi reverse).

4.1 Test scheme

Table 8 shows the test list that has been carried out with its corresponding air flow propagation, heating time and smouldering type observed.

Table 8: Test name list, annulus thickness, heating time and smouldering type observed.

Airflow	Test name	Annulus thickness	Heating time	Smouldering type observed
Semi reverse*	VR1, VR2, VR3 , VR6, VR7, VR8, VR9, VR10, VR11, VR12	No annulus	6 h	Semi reverse
Forward	VF1, VF2, VF3**, VF4, VF5, VF6, VF7, VF8, VF9, VF10, VF11	1 mm	6 h	Forward type 1 and 2

* VR4 and VR5 were excluded due to defect equipment.

**VF3 test developed flame combustion.

The gas measurement unit broke during VF3 test as it could not endure an extended exposure to high temperatures; made of plastic, the unit melted in the middle of the test resulting in flaming combustion. Gas composition was measured in 5 tests: VR1, VR2, VR3, VF1 and VF2.

4.2 Observed types of smouldering

In this section, the different smouldering types will be discussed. The tests were divided into four zones for their study: heating period (H), before intense combustion (BIC), maximum intense combustion (MIC) and after intense combustion (AIC); as illustrated in Figure 27.

The heating period (H) was defined as the 6 hours of external heating; the before intense combustion period (BIC) starts after the external heating until one hour before the maximum temperature peak; the most intense combustion (MIC) correspond to the time period where the maximum temperature was obtained, its length covers one hour before and after this maximum peak; AIC covers the time period after the most intense combustion zone until the test was stopped.

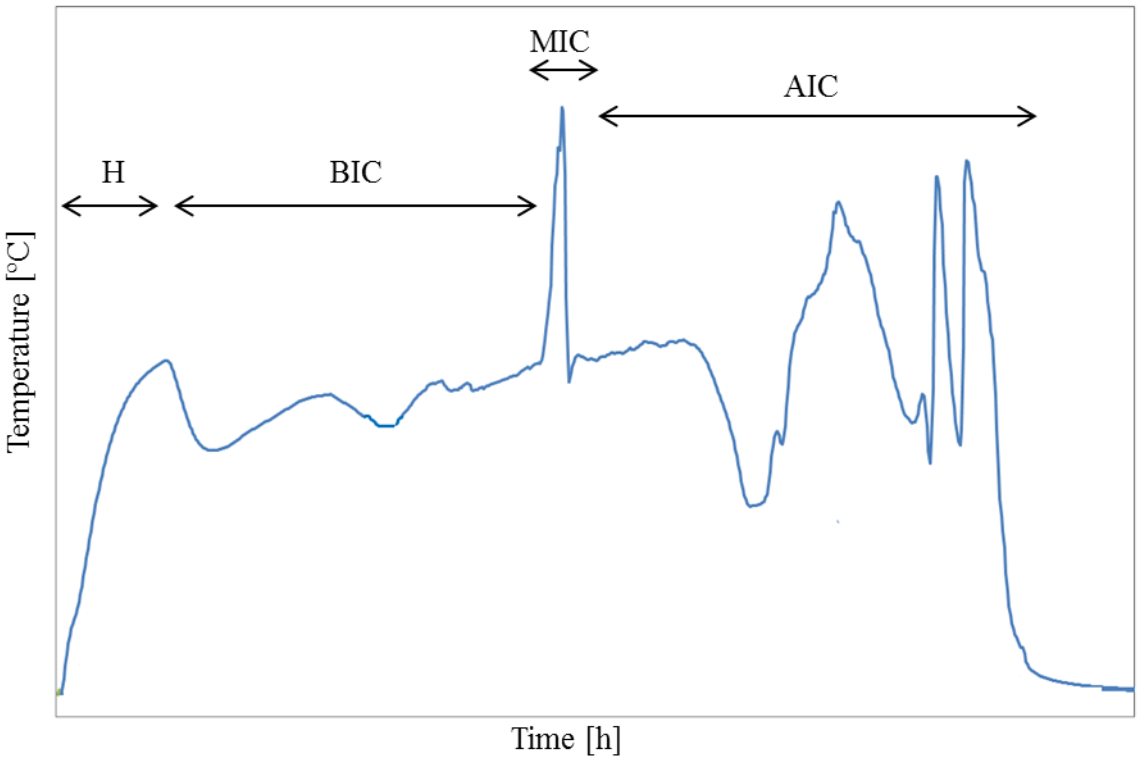

Figure 27: Scheme of the smouldering temperature development periods. H corresponds to external heating period, BIC: before intense combustion, MIC: maximum intense combustion, AIC: after intense combustion.

The charts of all tests can be found in Appendices A and B.

4.2.1 Semi reverse smouldering behaviour

Semi reverse temperature development will be described here, using Figure 28 as an example.

All the graphs written with centimetres placements and the under aluminium plate are temperature measurements, and the letters L, C and R refers to the thermocouple placement either on the left, centre or right side of the steel pipe (see Figure 19 in Section 3.2.2).

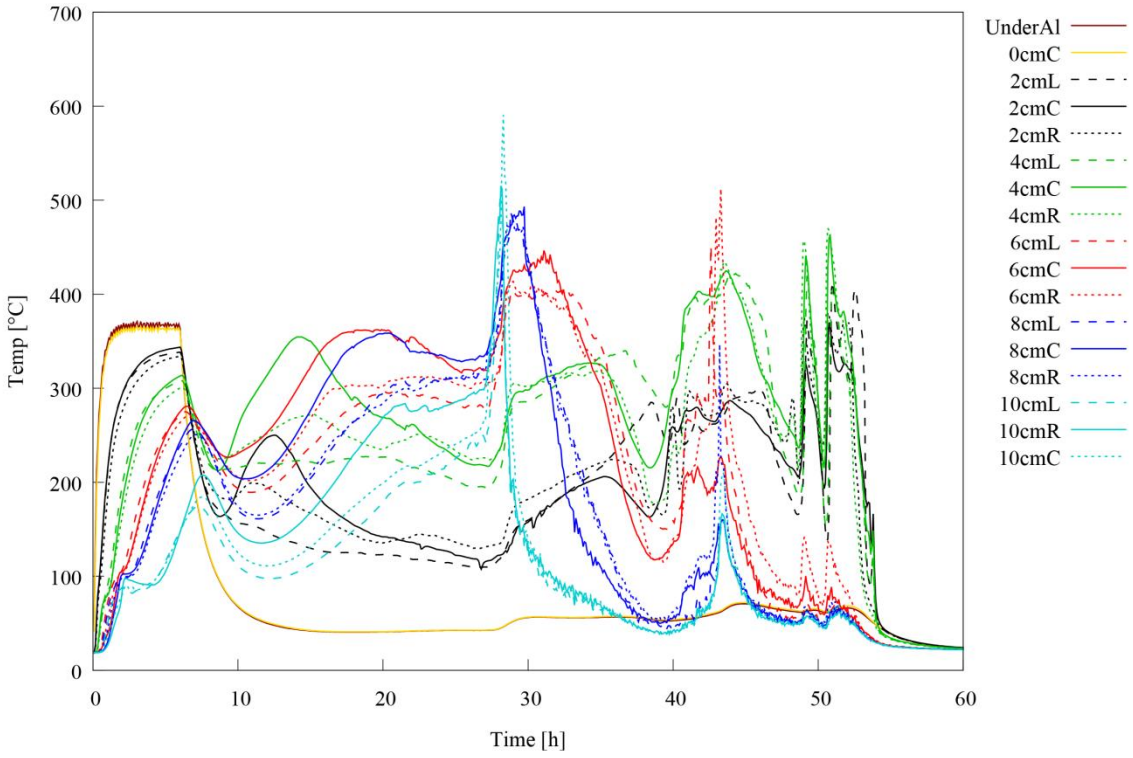

Figure 28: Chart showing a case of semi reverse smouldering behaviour, in temperature vs time graph. This example corresponds to the test VR1.

During the external heating period (H) the maximum temperatures were reached at the bottom of the pipe, approaching 371ºC at 0 cm placement; followed by 2, 4, 6, 8 and 10 cm height. The three thermocouple placements (L, C and R) showed a slightly different heating increase as the pellet distribution within the pipe was not uniform; in any case, the same trend was followed for each height.

The sample cooled down during the first 2 hours of the before intense combustion (BIC) period. This was followed by a turnaround zone that maintains an approximately constant temperature for 19 hours in this test, and 19.3 ± 3.1 hours for all the tests in this category. It can be seen that the temperature distribution inside the sample is not uniform; however, the shapes of the curves are somewhat similar. With the temperatures approaching 250 ºC in all the thermocouples with the exception of the 2 cm position, which cooled down together with the 0 cm and UnderAl placements. The maximum temperature in this period was registered in the thermocouples located in the middle of the pipe at 4, 6 and 8 cm height where the sample was closer to the air supply. The maximum temperature reached was 363ºC in this test, and an average of 412ºC for all the tests in this category.

The maximum intense combustion period (MIC) is the region where the maximum temperature peak in the whole combustion process is reached; in this test the maximum temperature reaches 590.8 ºC after 28.3 hours, while for all the tests in this category was 574 ºC ± 45 ºC after ~ 28.6 hours.

During the after intense combustion (AIC) period the thermocouples readings showed some ups and downs as the reaction was going forward at 6, 4 and 2 cm placements. This fluctuating period lasted for 25.8 hours in this case and 32.2 ± 6.3 hours for all the tests in this category; the maximum temperature peak reached was 512ºC in this example and an average of 500ºC for all the tests in this category. Once the thermocouples reached ambient temperature the logging was stopped.

4.2.2 Forward smouldering behaviour Type 1

Two out of ten forward experiments developed a *Forward smouldering Type 1*; Figure 29 is an example of this type of smouldering.

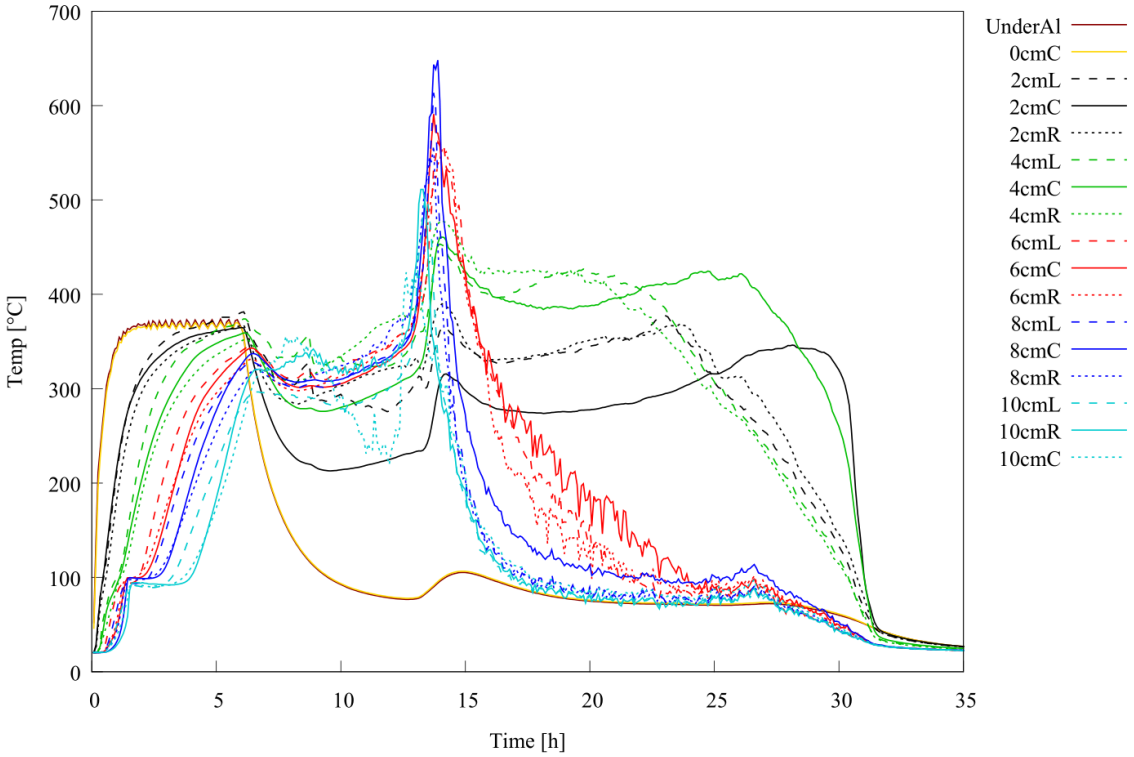

Figure 29: Chart showing a case of forward smouldering behaviour Type 1, in temperature vs time graph. This example corresponds to the Test VF2.

As shown in Figure 29, during the H period a more pronounced plateau on the temperature readings was observed on the thermocouples located at the upper part of the sample, between the first and the fourth hour of external heating.

During the BIC period the sample cooled down 60 ºC and immediately afterwards it underwent a steady temperature period for 5 hours. The maximum temperatures were reached at approximately 300 ºC in this particular case and 250 ºC in VF1.

In the MIC zone the temperature readings increased resulting in a maximum temperature peak of 644 ºC after 14 hours in this case and 585 ºC after 23 hours in VF1.

During the last stage of the process (AIC period), the sample cooled down for 16 hours developing a slight smouldering combustion on the thermocouples located at the bottom of the pipe.

4.2.3 Forward smouldering behaviour Type 2

Eight out of ten tests correspond to this smouldering type. Figure 30 is an example of how the second type of forward smouldering looks like.

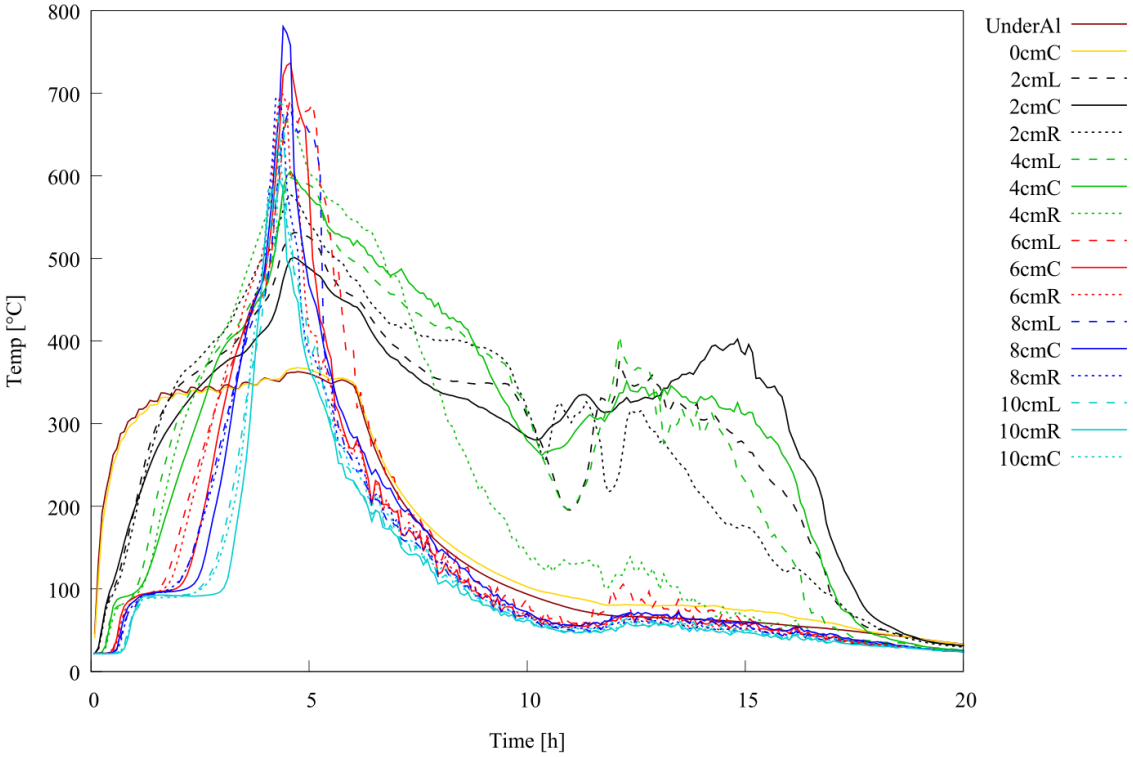

Figure 30: Chart showing a case of Forward smouldering behaviour Type 2, in temperature vs time graph. This example corresponds to the Test VF5.

Unlike the previous two cases, during the H period the sample reached higher temperatures than the ones provided by the heater. It can be seen that the temperatures started to increase at the bottom of the pipe to later spread to the upper layers of the sample.

In this smouldering type there is no BIC period, undergoing the MIC with the correspondent maximum temperature peak before the external heating period was finished. The highest temperature reached in this particular test was 781 ºC after 4,4 hours, while for all the tests in this category was 745,2 ± 44,3 ºC in ~5.2 hours. The MIC period was followed by a less intense AIC smouldering combustion during 16 hours on the thermocouples placed at 2 and 4 cm.

Comparing forward smouldering type 1 and type 2 it was observed that Type 2 had a total combustion time of 20 hours, approximately 1/3 less than Type 1.

4.3 Flaming fire

One of the tests underwent a flaming fire while a forward smouldering test was running.

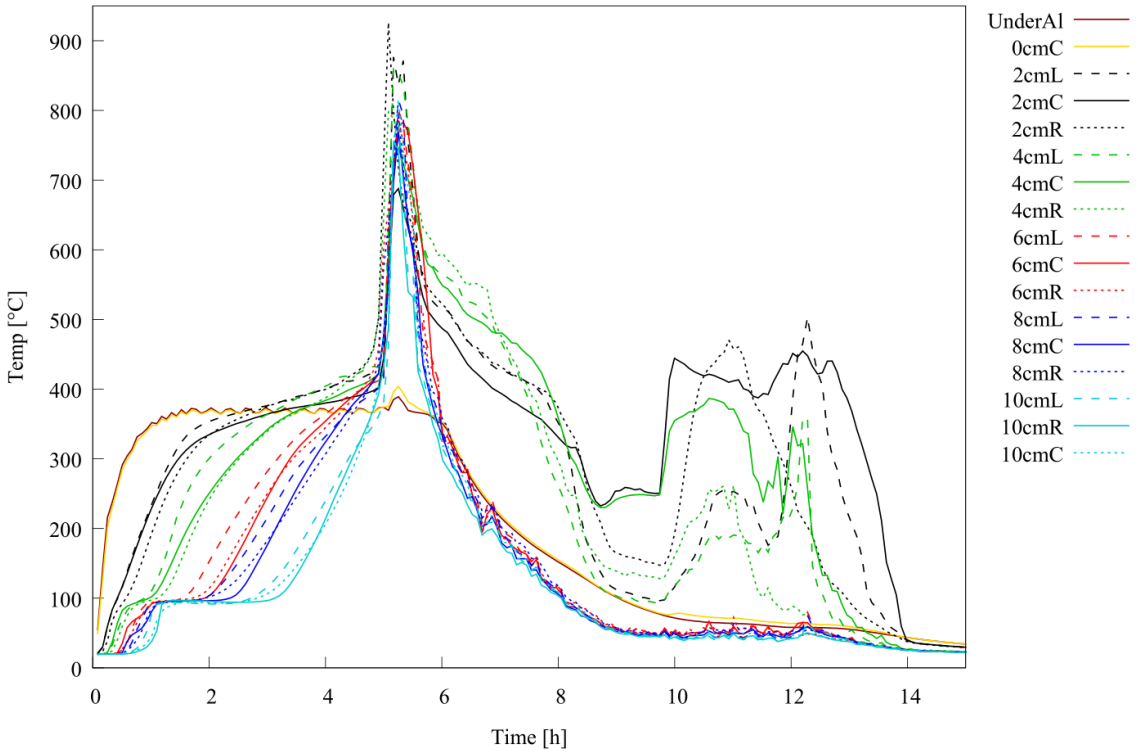

Figure 31: Chart showing a case of flaming fire, in temperature versus time graph. This example corresponds to test VF3.

Unlike smouldering cases, in flaming fires the combustion process took place on the gas phase surrounding the fuel; this could be observed on the 33 cm thermocouple readings. At that height the thermocouple readings reached a temperature of 720 ºC, while in the test that underwent smouldering combustion this value dropped to 120ºC. In addition, the maximum temperature peak is way higher (926 ºC) than the ones obtained in smouldering processes (~750ºC).

After the maximum temperature peak an 8 hour slight smouldering combustion was developed on the thermocouples placed at the bottom of the sample.

4.4 Maximum temperatures and time readings on forward and semi reverse smouldering in the different stages

As it was explained in Section 4.2, the smouldering process was divided into four main stages:

- External heating period (H)
- Before intense combustion (BIC)
- Maximum intense combustion (MIM)
- After intense combustion (AIC)

Maximum and average temperatures, time to maximum temperatures and total duration period were studied for each stage, as shown in Tables 9, 10, 11 and 12.

To achieve a better understanding of the findings, the results in Tables 9, 10, 11 and 12 were presented in a Box and Whiskers diagrams made in Microsoft Excel 2010. Box diagrams are used to show overall patterns of response for a group, providing a useful way to visualize the range and other characteristics of responses as shown in Figure 32.

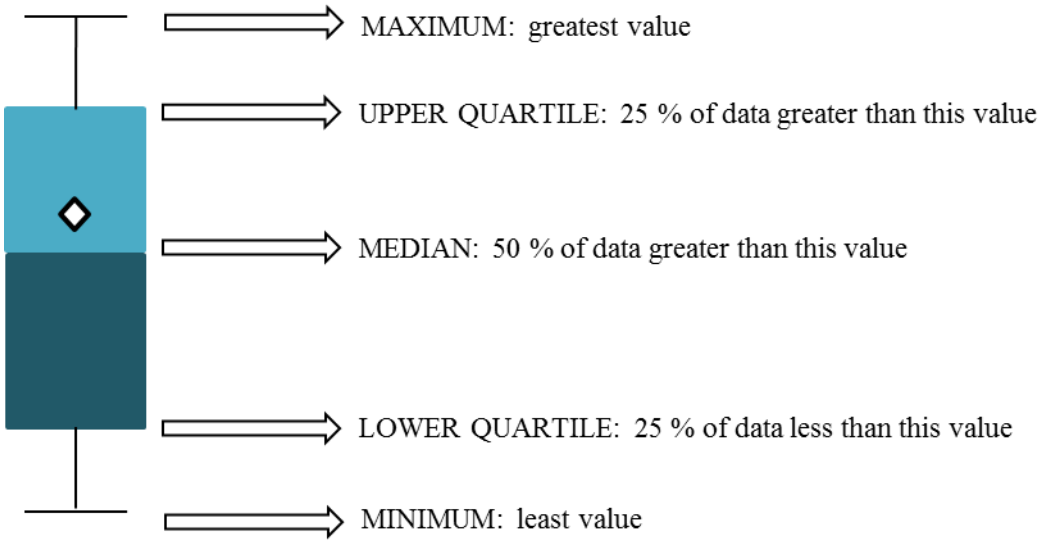

Figure 32: Explanation of a box and whiskers diagram.

The diagram can be divided in four parts as illustrated in Figure 40:

- Median: Half the scores are greater than or equal to this value and half are less.
- Upper quartile: Seventy-five percent of the scores fall below the upper quartile.
- Lower quartile: Twenty-five percent of scores fall below the lower quartile.
- Whiskers: The upper and lower whiskers represent scores outside the middle 50%. Whiskers often stretch over a wider range of scores than the middle quartile groups.
- The rhombus represents the average of overall values. It is normally not included in a box and whiskers diagram, but in this Thesis it will be included to get more information.

The wideness of the box refers to the cluster of the results, if there is a wide box and long whiskers means that the data is not very clustered; in contrast, if the box is small and the whiskers are short, the data does indeed cluster. If the box is small and the whiskers are long means that the data clusters but there are got some "outliers" that might be necessary to investigate further.

Figures 33, 35 and 36 show the maximum temperature peak and time to maximum temperature for the different stages. Figure 33 shows that during the BIC period most of the semi reverse experiments had their maximum temperature peak at 380-400 ºC in 20-28 hours; as there is no BIC in most of the forward tests, the box and whiskers study was only made for the semi reverse cases. Figure 35 shows that during the Mic period, the maximum temperature peaks reached were 550-560 ºC in 27-30 hours for the semi reverse smouldering tests, in contrast to forward smouldering where the peak reached was around 700-750 ºC in approximately 5 hours.
Comparing the AIC period in forward and semi reverse propagation, it is seen in Figure 36 that semi reverse tests reached its highest value around 500 ºC in ~ 40 hours while forward smouldering reached ~450 ºC in approximately 10 hours.

The duration period during the external heating period (H) and the maximum combustion period (MIC) was constant for all the experiments, as it was settled that the heater was going to be turned on for 6 hours and the MIC period will cover 2 hours. However, the time length for the BIC and AIC periods were not constant as shown in Figures 34 and 37. It was observed that the BIC average temperature for semi reverse

tests was 190-205 ºC taking ~22 hours. Looking at the AIC readings, the results showed that the average temperatures during both semi reverse and forward smouldering were very similar (around 150 ºC), the difference between them lies in the total duration period; Figure 37 shows that the after intense combustion period in semi reverse smouldering took more time (approximately 30 hours) than forward smouldering, which lasted 15 hours.

Table 9: Maximum temperature [ºC], time to maximum temperature and duration period [h] referred to the external heating period (H) for both semi reverse and forward propagations. The temperatures in brackets refer to the average temperature during H for each test.

External heating period (H)							
Semi reverse				Forward			
Test name	**$T_{max}(T_{avg})$[ºC]**	**Time to t_{max}[h]**	**Duration period [h]**	**Test name**	**$T_{max}(T_{avg})$[ºC]**	**Time to t_{max} [h]**	**Duration period [h]**
VR1	371 (190.2)	6	6	VF1	426.2 (132.2)	0.16	6
VR2	369.7 (192.5)	6	6	VF2	380.9 (217.8)	6	6
VR3	373.1 (199.9)	5.6	6	VF3			6
VR6	358.6 (177.1)	5.3	6	VF4			6
VR7	334.2 (172.1)	4.4	6	VF5	The maximum temperature peak was reached before the external heating period was finished, so that these values coincide with the ones in Table 11.		6
VR8	342 (167.6)	5.33	6	VF6			6
VR9	332.1 (168.2)	5	6	VF7			6
VR10	330.8 (168.4)	4.6	6	VF8			6
VR11	333.9 (164.7)	5.2	6	VF9			6
VR12	341 (168.8)	4.9	6	VF10			6
				VF11			6

Table 10: Maximum temperature [ºC], time to maximum temperature [h] and duration period [h] referred to the before intense combustion (BIC) period for both semi reverse and forward propagations. The hyphen shows that those tests did not developed any BIC period. The temperatures in brackets refer to the average temperature during BIC for each test.

Before intense combustion (BIC)							
Semi reverse				Forward			
Test name	**$T_{max}(T_{avg})$[ºC]**	**Time to t_{max}[h]**	**Duration period [h]**	**Test name**	**$T_{max}(T_{avg})$[ºC]**	**Time to t_{max}[h]**	**Duration period [h]**
VR1	363.1 (207.9)	19.9	21.3	VF1	515.1 (227)	21.5	15.6
VR2	371.8 (204.7)	25.2	19.1	VF2	423.3 (290.7)	12.6	6.7
VR3	509.2 (213.8)	25.9	21	VF3	-	-	-
VR6	541.8 (192.3)	28.6	22.7	VF4	-	-	-
VR7	383.5 (183.1)	27.7	21.8	VF5	-	-	-
VR8	379.5 (186.8)	18.7	25.3	VF6	-	-	-
VR9	392.8 (184.7)	28.12	22.6	VF7	-	-	-
VR10	402.1 (200)	19.2	18.8	VF8	-	-	-
VR11	389.3 (199.1)	18.7	20.9	VF9	-	-	-
VR12	391.2 (203.3)	28.8	22.9	VF10	-	-	-
				VF11	-	-	-

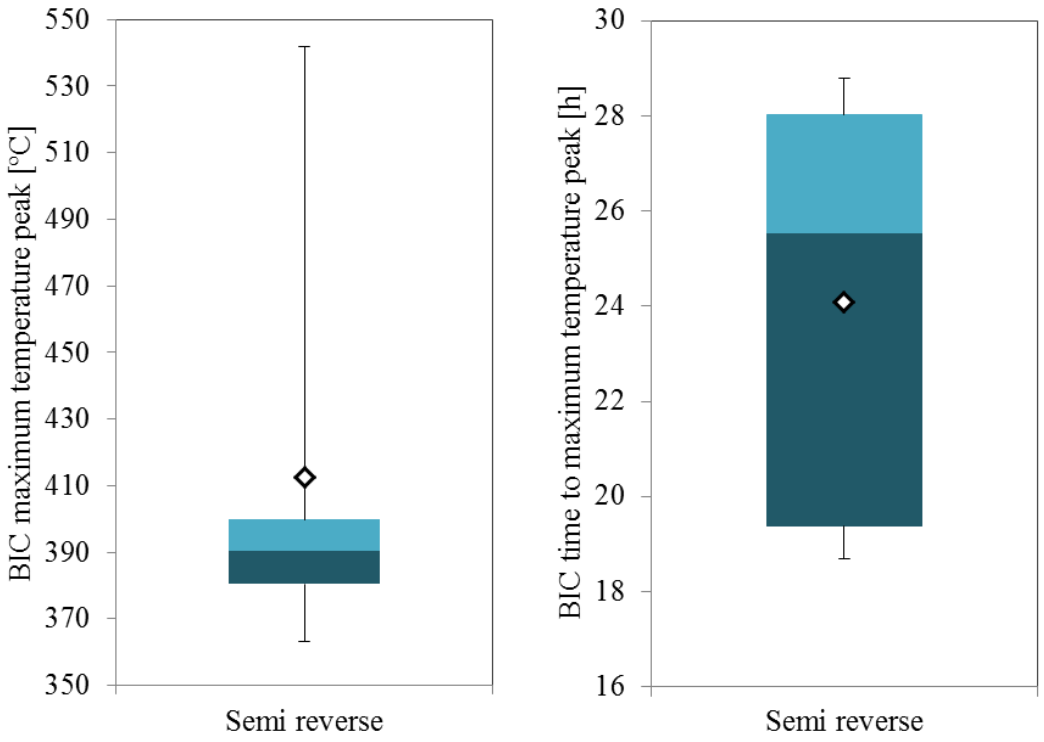

Figure 33: Box and whiskers diagram of maximum temperature peak and time to maximum temperature for semi reverse tests during BIC period. There is no forward smouldering data for this period as it was not developed.. The white rhombus shows the average value.

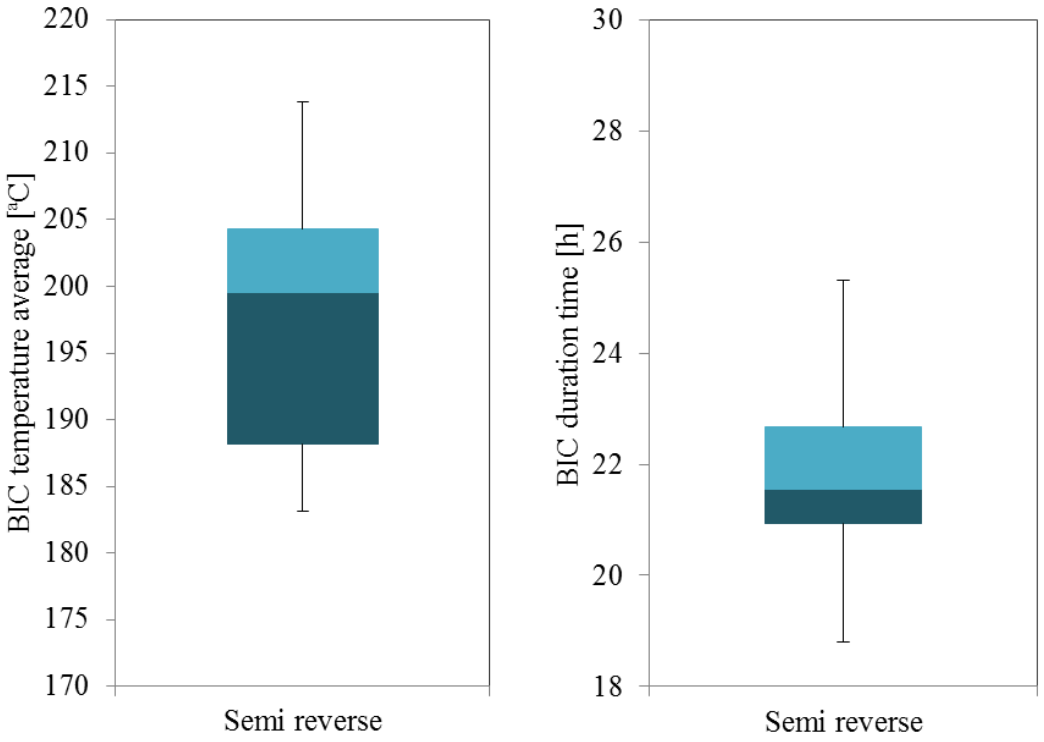

Figure 34: Box and whiskers diagram of average temperatures and duration time on semi reverse tests during BIC period.

Table 11: Maximum temperatures [ºC], time to maximum temperature [h] and duration period [h]related to the maximum intense combustion (MIC) period for both semi reverse and forward configurations. The temperatures in brackets refer to the average temperature during MIC for each test.

Maximum intense combustion (MIC)							
Semi reverse				Forward			
Test name	**$T_{max}(T_{avg})$[ºC]**	**Time to t_{max}[h]**	**Duration period [h]**	**Test name**	**$T_{max}(T_{avg})$[ºC]**	**Time to t_{max}[h]**	**Duration period [h]**
VR1	590.8 (275.4)	28.3	2	VF1	584.9 (308.3)	22.6	2
VR2	578.3 (288.1)	26.1	2	VF2	648.2 (359.3)	13.7	2
VR3	559.3 (253.3)	28.0	2	VF3	926.0 (473.1)	5.1	2
VR6	551.2 (276.3)	29.7	2	VF4	735.1 (461.2)	5.3	2
VR7	553.4 (269.3)	28.8	2	VF5	780.6 (437.4)	4.4	2
VR8	573.1 (268.1)	32.3	2	VF6	692.0 (453.1)	5.5	2
VR9	545.1 (268.4)	29.6	2	VF7	764.1 (460.5)	5.9	2
VR10	603,4 (278)	25.8	2	VF8	760.0 (461.7)	5.2	2
VR11	634.5 (287.7)	27.9	2	VF9	765.1 (473.1)	4.4	2
VR12	546.4 (268.5)	29.9	2	VF10	752.0 (464.4)	5.1	2
			2	VF11	712.8 (462.7)	5.5	2

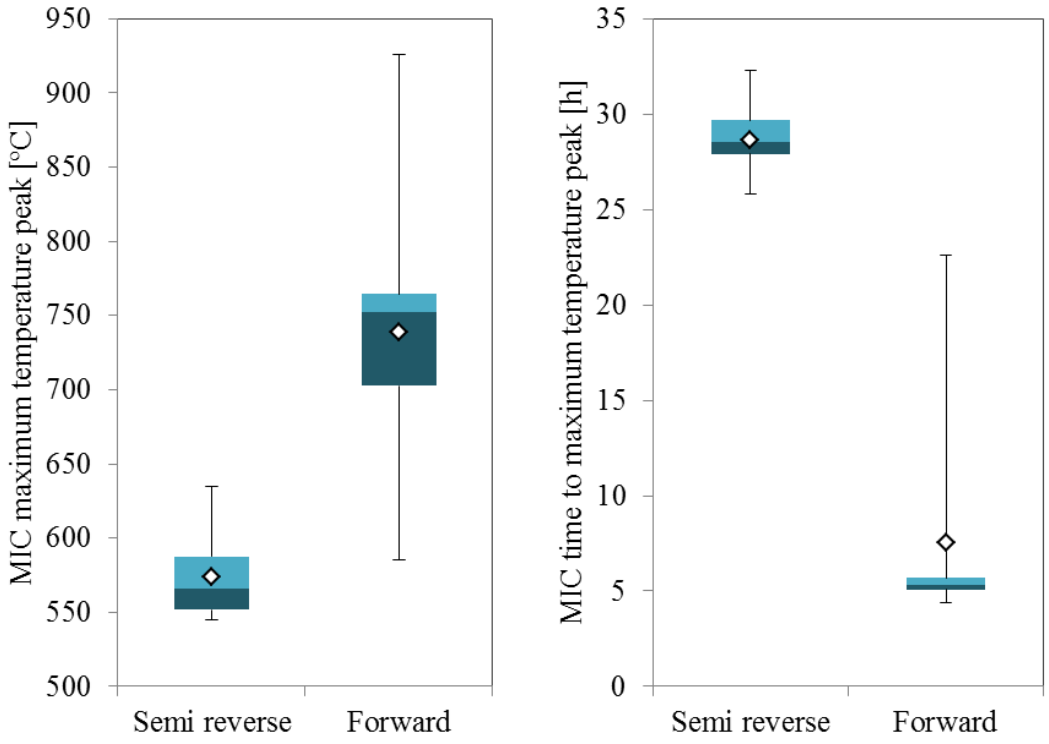

Figure 35: Box and whiskers diagram of maximum temperature peak and time to maximum temperature for both semi reverse and forward tests during MIC period. The white rhombus shows the average value.

Table 12: Maximum temperatures [ºC], time to maximum temperature [h] and total duration [h] related to the after intense combustion (AIC) period for both semi reverse and forward configurations. The temperatures in brackets refer to the average temperature during AIC for each test.

After intense combustion (AIC)							
Semi reverse				**Forward**			
Test name	**$T_{max}(T_{avg})$[ºC]**	**Time to t_{max}[h]**	**Duration period [h]**	**Test name**	**$T_{max}(T_{avg})$[ºC]**	**Time to t_{max}[h]**	**Duration period [h]**
VR1	512 (170)	43.3	30.7	VF1	469.2 (159.2)	26.2	15.7
VR2	466.1 (169.2)	30.9	27.9	VF2	475.4 (169.7)	15.9	16.5
VR3	500.6 (137.5)	40.7	32.7	VF3	503.5 (152.7)	12.3	7.8
VR6	459.5 (143.8)	32.2	31.4	VF4	423.2 (160.4)	9.1	13.7
VR7	485.9 (143.4)	30.1	34	VF5	483.8 (141)	6.9	12.8
VR8	557.6 (150)	48	29.2	VF6	472.2 (157.5)	9.5	15.1
VR9	502.1 (143)	54.1	37.3	VF7	459.8 (157.9)	9.1	13.6
VR10	511.8 (147.2)	55.7	33.8	VF8	434.3 (146.3)	10	17.3
VR11	491.5 (161.6)	29.1	24.9	VF9	419.4 (137.8)	16.9	16.9
VR12	500.7 (136.3)	47.8	33.5	VF10	498.5 (166.6)	8.4	13.6
				VF11	400.7 (149.3)	13.4	16

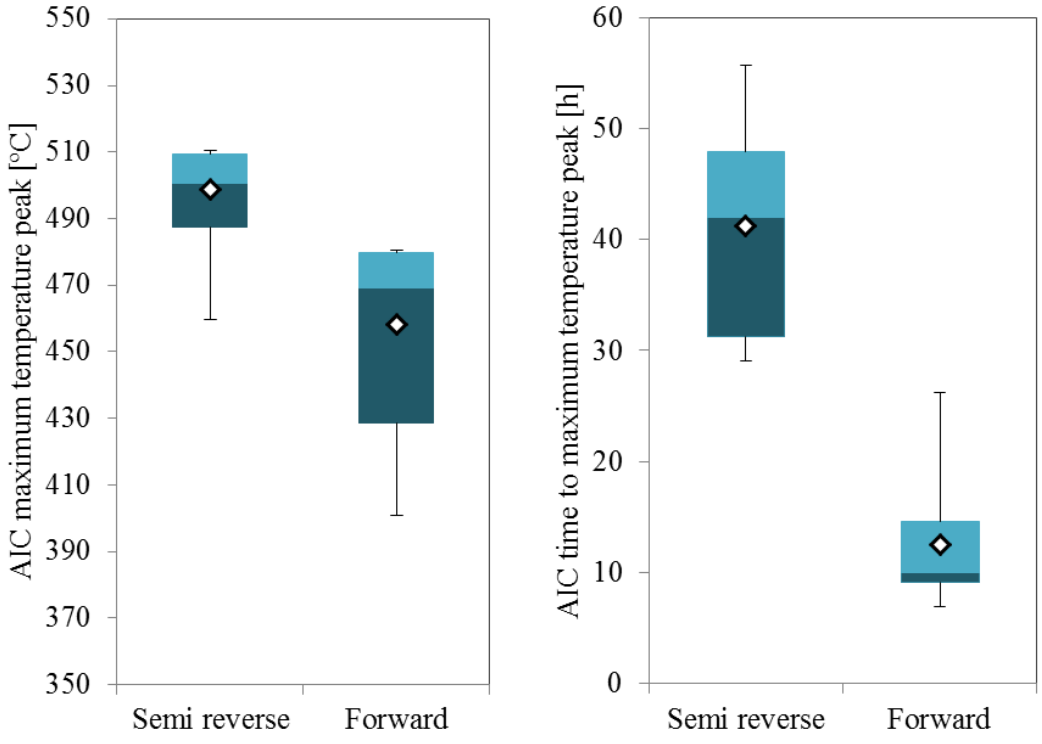

Figure 36: Box and whiskers diagram of maximum temperature peak and timing to maximum temperature on both semi reverse and forward tests during AIC period. The white rhombus shows the average value.

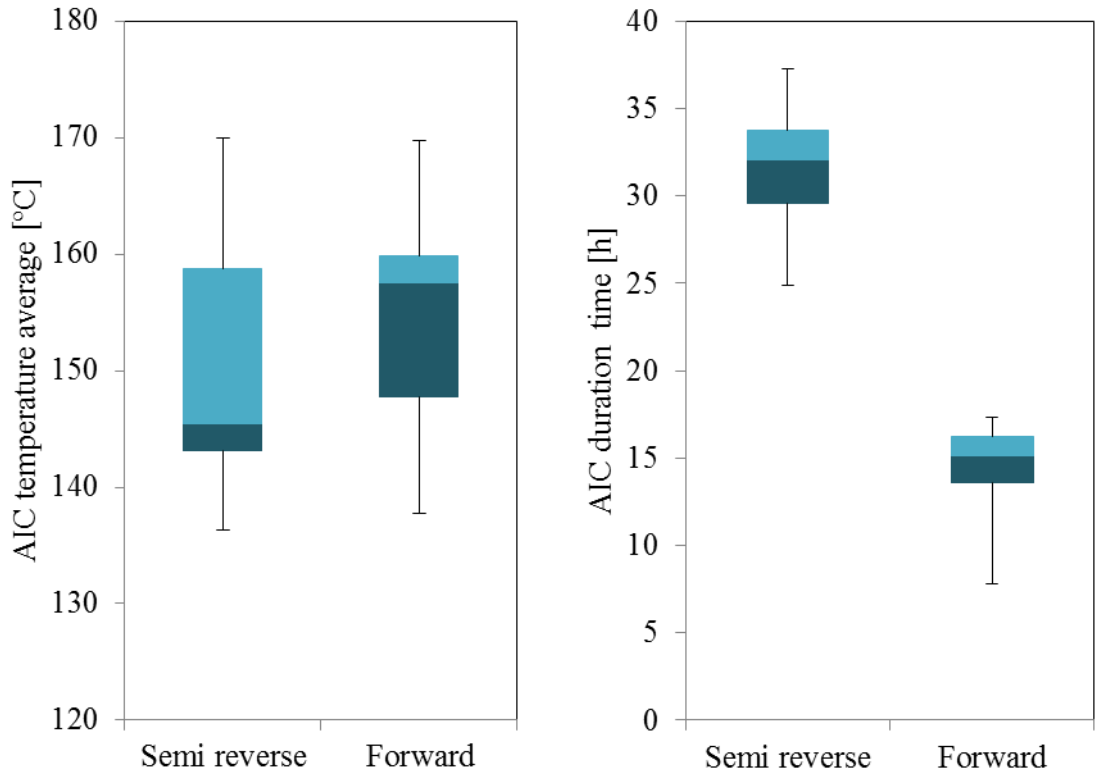

Figure 37: Box and whiskers diagram of average temperatures and duration time on both semi reverse and forward tests during AIC period.

Tables 13 and 14 show the maximum temperatures in the whole combustion process for each height. The average between the three thermocouples placements (left, centre and right) on each height were calculated for all 10 semi reverse and forward tests.

Table 13: Maximum temperatures for each height in semi reverse tests.

Semi reverse										
Height	**Maximum temperatures [ºC]**									
	VR1	**VR2**	**VR3**	**VR6**	**VR7**	**VR8**	**VR9**	**VR10**	**VR11**	**VR12**
UnderAl	371,0	369,8	373,1	358,6	334,2	342,0	332,1	330,8	333,9	341,0
0cm	365,8	366,1	370,6	351,0	330,9	333,3	324,9	325,6	328,5	325,2
2cm	413,5	433,0	436,5	351,4	429,7	422,5	461,1	438,1	441,8	420,6
4cm	469,9	461,9	442,7	418,3	457,0	470,2	502,1	511,8	441,8	487,6
6cm	512,0	460,9	500,6	459,5	464,7	557,6	458,4	484,2	498,0	500,7
8cm	493,2	515,3	559,3	551,2	540,5	550,7	545,1	550,4	587,2	546,5
10cm	590,8	578,3	509,2	541,9	553,4	573,1	540,9	603,4	634,5	521,4
12cm	289,9	269,1	274,1	252,6	284,5	242,8	267,4	264,1	277,4	236,7

Table 14: Maximum temperatures for each height in forward tests.

Forward											
Height	**Maximum temperatures [ºC]**										
	VF1	**VF2**	**VF3**	**VF4**	**VF5**	**VF6**	**VF7**	**VF8**	**VF9**	**VF10**	**VF11**
UnderAl	426,2	373,7	389,2	344,4	362,8	352,3	348,6	352,8	353,7	355,5	355,5
0cm	330,9	370,4	404,0	333,3	367,8	357,0	360,3	357,0	353,9	353,0	381,4
2cm	395,6	389,9	926,0	519,3	577,2	492,6	513,8	507,6	528,4	530,0	511,2
4cm	469,2	478,5	860,7	602,1	665,3	556,9	576,4	612,0	635,3	620,2	618,4
6cm	528,2	591,0	800,7	703,5	736,7	680,2	689,0	733,1	707,7	734,3	700,6
8cm	584,9	648,2	816,0	735,1	780,6	692,0	764,1	760,0	765,1	752,0	712,8
10cm	411,6	511,2	815,5	689,3	689,8	613,3	662,2	586,0	639,2	727,3	617,3
12cm	248,7	321,8	822,7	596,6	544,2	411,7	450,9	489,4	456,1	612,2	413,4

Working with the box and whiskers diagrams it can be seen in Figures 38 and 39 that semi reverse results were more clustered in comparison to forward propagation.

The temperatures in semi reverse and forward smouldering differ considerably; forward propagation reached higher temperatures at all heights in comparison to semi reverse. The maximum temperatures in semi reverse propagation were located at 10 cm height, in comparison to forward tests where the highest values were reached at 8 cm. It is needed to take into account that the maximum values in the Forward box and whiskers diagram correspond to the flaming test.

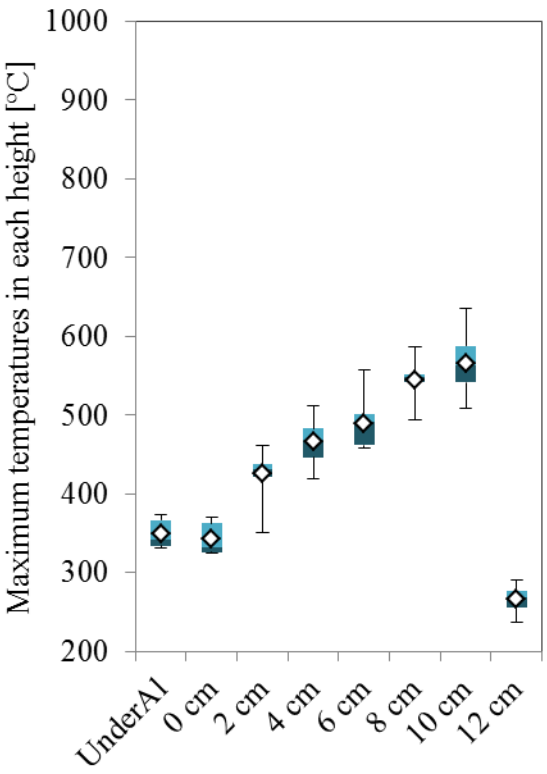

Figure 38: Box and whiskers diagram of maximum temperatures in each height for semi reverse tests. The white rhombus shows the average values.

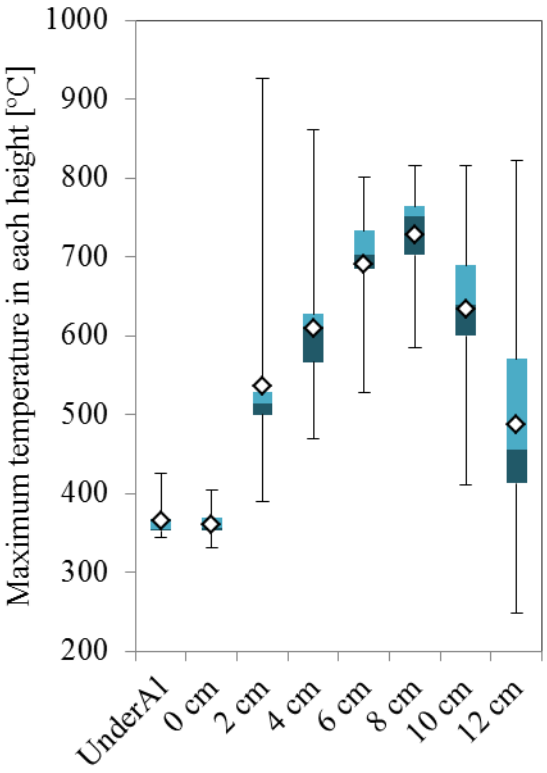

Figure 39: Box and whiskers diagram of maximum temperatures on each height for forward tests. The white rhombus shows the average values.

4.5 Total combustion time

Total combustion time was defined as the total duration of the smouldering process. Table 15 and Figure 40 show the total combustion time for semi reverse and forward smouldering. It is seen that semi reverse took around 60 hours to complete the whole process while forward smouldering lasted for approximately 20 hours.

Table 15: Total combustion time in semi reverse and forward smouldering.

Semi reverse		Forward	
Tests	**Combustion time (h)**	**Tests**	**Combustion time (h)**
VR1	54,1	VF1	39,3
VR2	56,7	VF2	31,2
VR3	62,7	VF3	13,9
VR6	62,1	VF4	20,0
VR7	63,8	VF5	18,2
VR8	62,5	VF6	21,6
VR9	67,9	VF7	20,5
VR10	60,6	VF8	23,5
VR11	53,8	VF9	22,3
VR12	64,4	VF10	19,7
		VF11	22,5

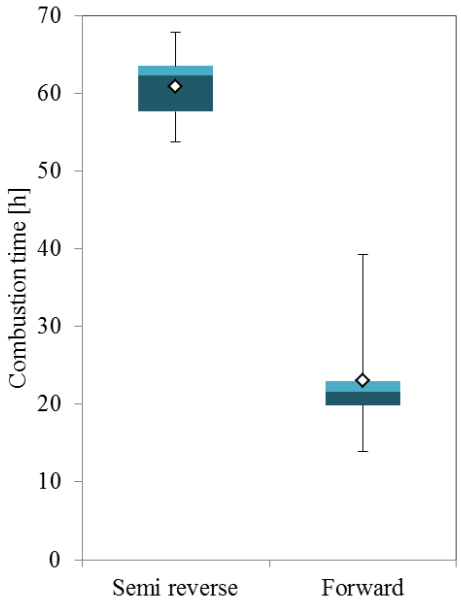

Figure 40: Box and whiskers plot of total combustion time in semi reverse and forward propagation. The white rhombus shows the average values.

4.6 Mass Loss and Mass Loss Rate

Mass loss rate was studied in all the tests to see when and how the total mass was consumed by the heat.

Figure 41 illustrates the mass loss rate in VR1; the fluctuating zone during the first six hours was due to the electromagnetic interference of the scale with the heater. After the 6 hours heating, the fluctuation continued in a minor amount, indicating a source of error in the tests.

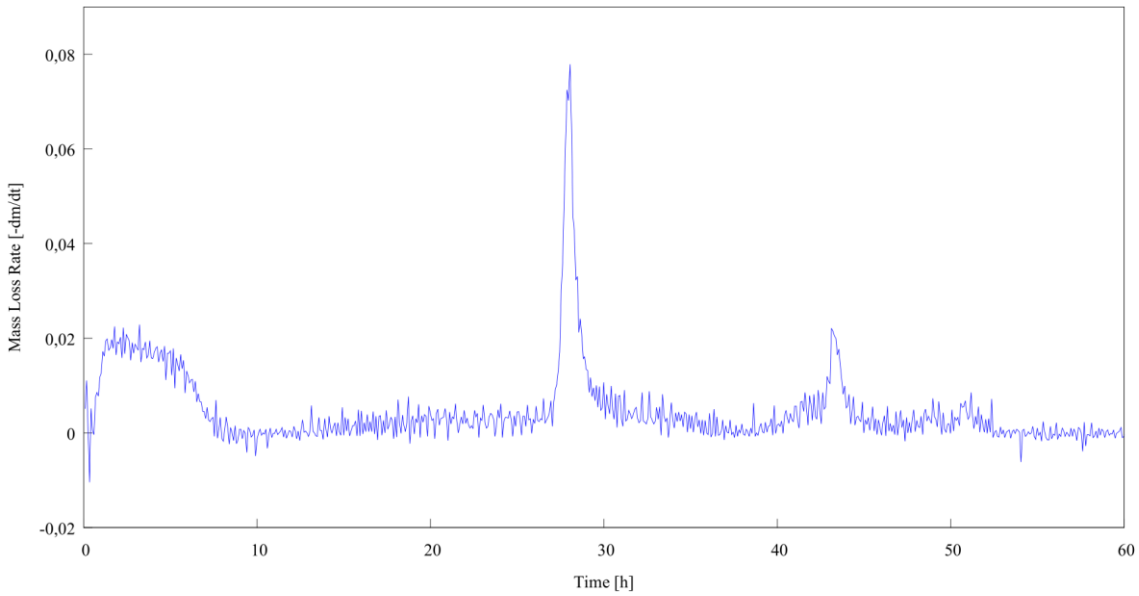

Figure 41: Mass loss rate [-dm/dt] vs time [h]. This example corresponds to the test VR1.

Mass loss is presented in Figure 42; the steepest zone corresponds to the maximum temperature peak, losing in that period of time 20 % of its mass. Afterwards the sample kept losing mass but in a smoother range.

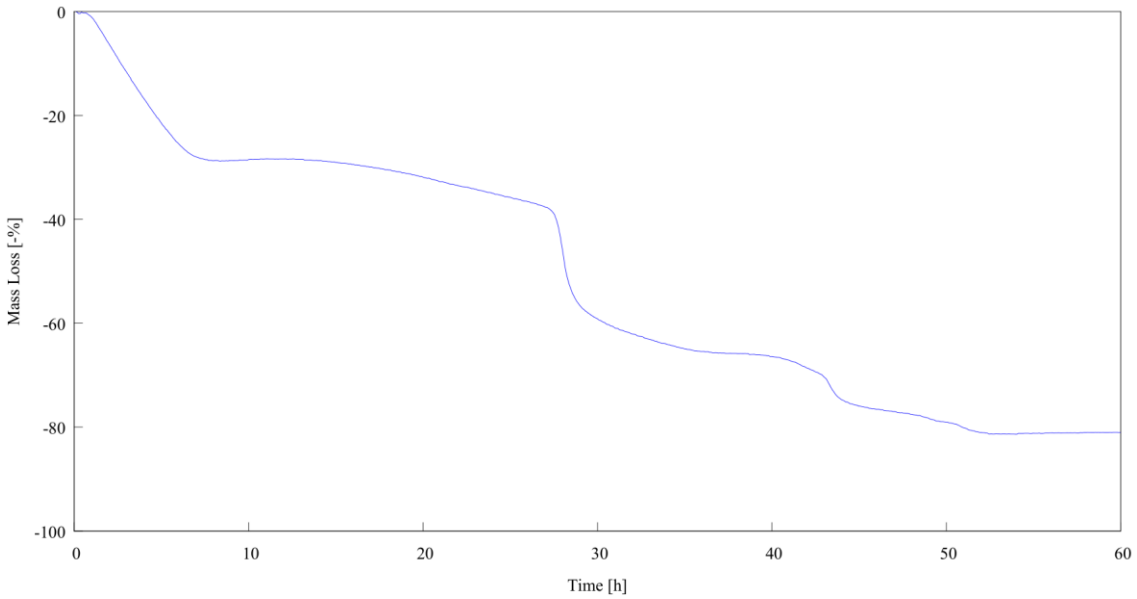

Figure 42: Mass change (-%) vs time [h]. This chart correspond to test VR1

A box and whiskers diagram was done in order to compare the mass loss in semi reverse and forward propagation. Figure 43 shows that forward propagation experienced a higher mass loss (~ -91%) in comparison to reverse (~ -85%).

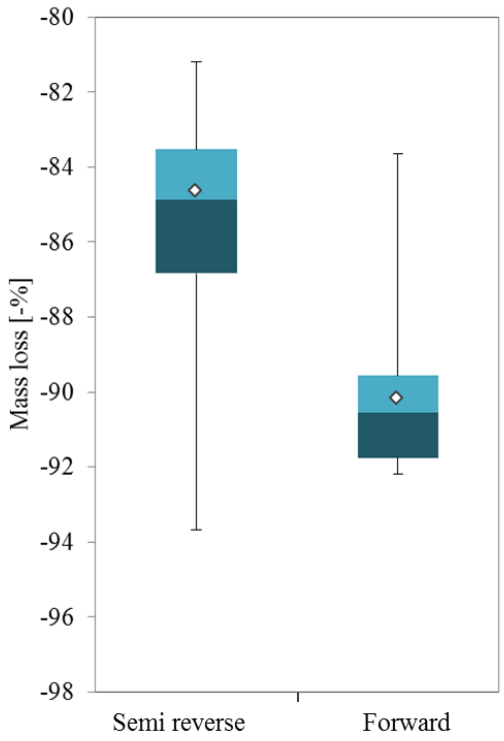

Figure 43: Mass loss Box and whiskers diagram (-%) for semi reverse and forward propagation for the entire tests.

4.7 Airflow velocities

Figures 44, 45, 46 and 47 shows the airflow development, in kg/s, of the three different smouldering types defined in Section 4.2 and the flaming case explained in Section 4.3.

The zero level was not reached in the airflow charts due to an accuracy error in the equipment; as in the mass loss rate calculation, the fluctuating zone during the first six hours was due to the electromagnetic interference between the bidirectional probe and the heater.

The maximum ups and downs match the most intense combustion zones in the entire tests, showing more fluctuations during the MIC and AIC periods.

The period when the temperatures were more or less constant, that is, during the BIC period, the airflow readings showed also an approximately constant behaviour. The greatest fluctuations were read in the flaming combustion test, where during the MIC period the airflow value dropped 0.02 kg/s.

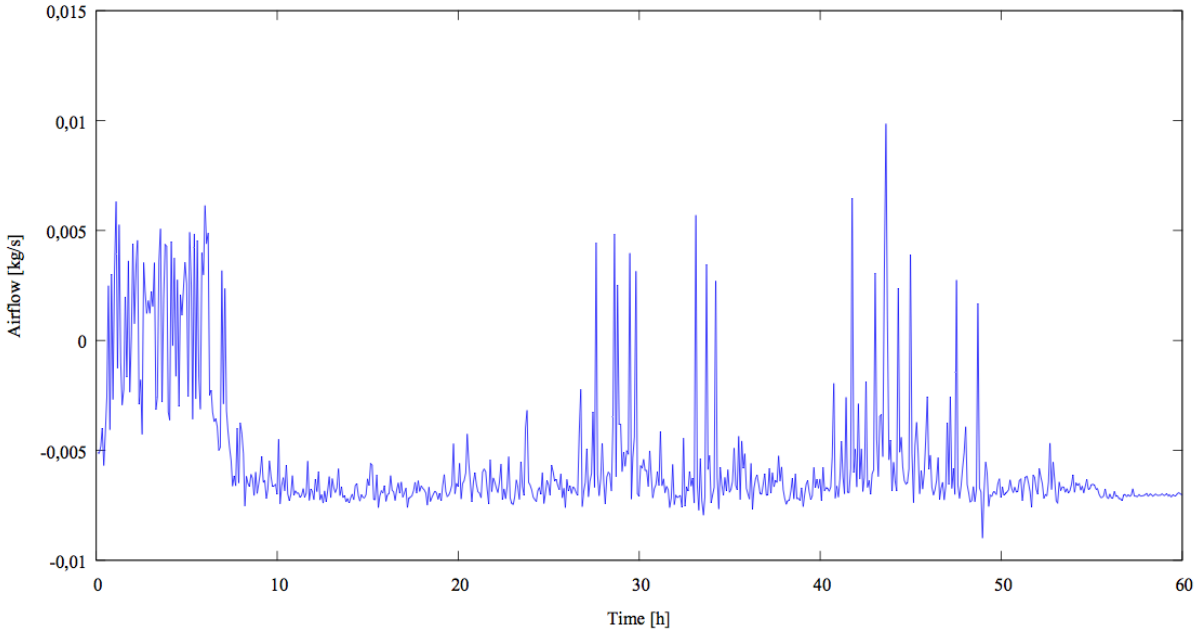

Figure 44: Airflow measurement [kg/s] versus temperature related to a Semi Reverse smouldering type. This chart corresponds to test VR1.

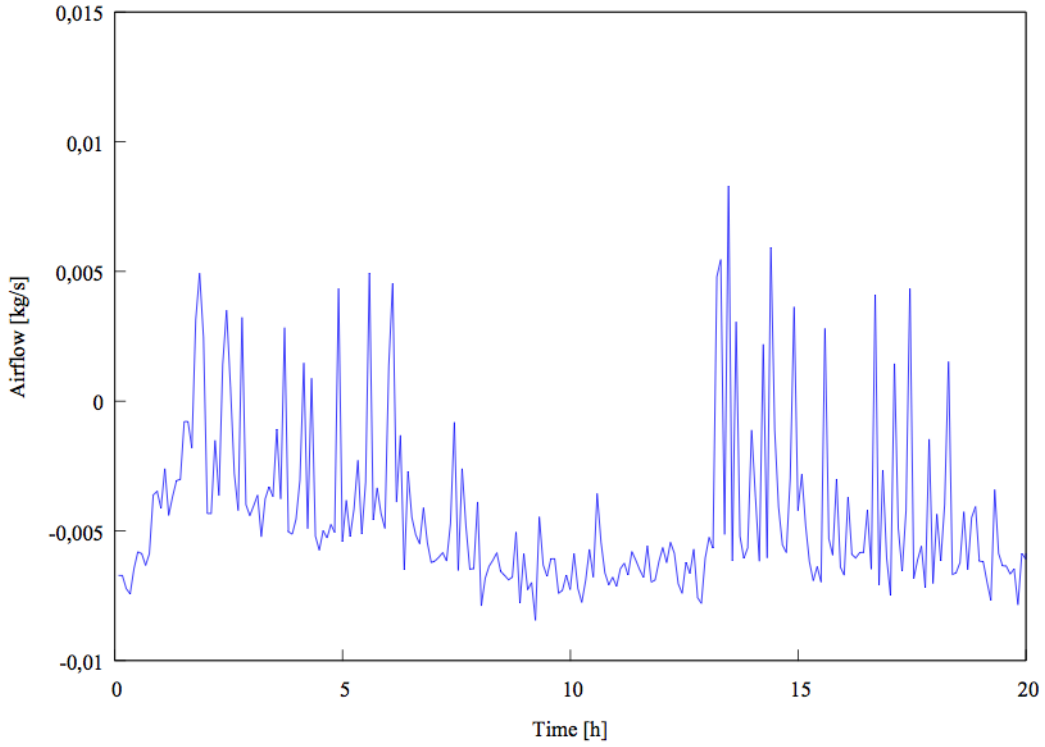

Figure 45: Airflow measurement [kg/s] versus temperature in forward smouldering Type 1. This chart corresponds to test VF2.

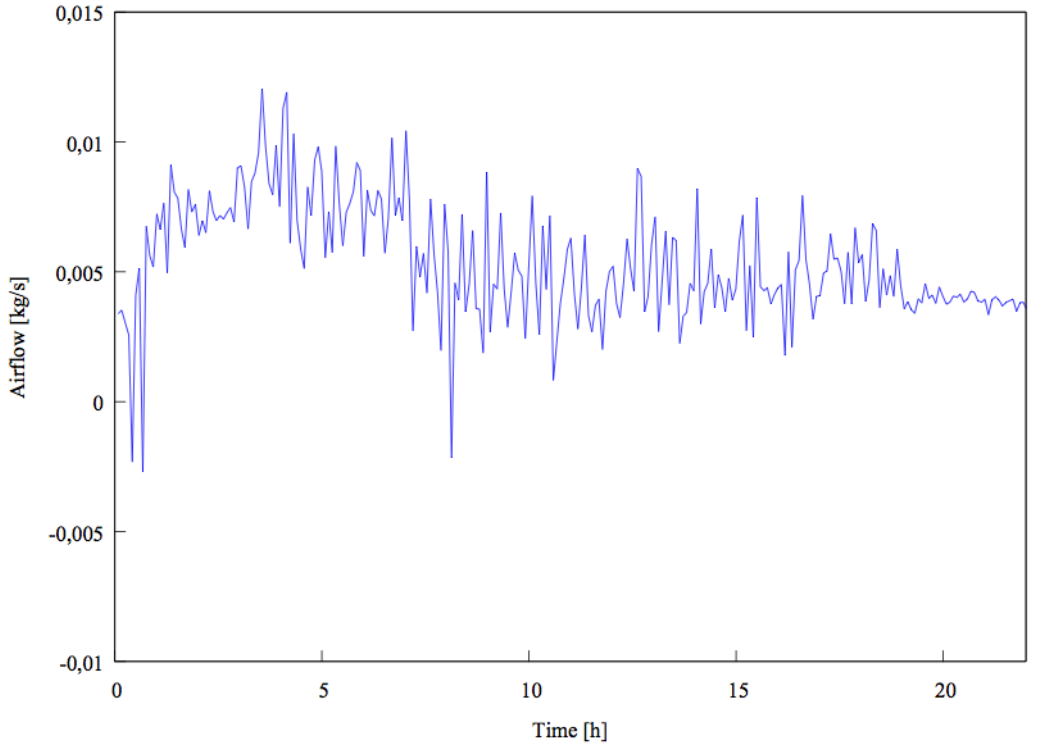

Figure 46: Airflow measurement [kg/s] versus temperature in Forward smouldering Type 2. This chart corresponds to test VF5.

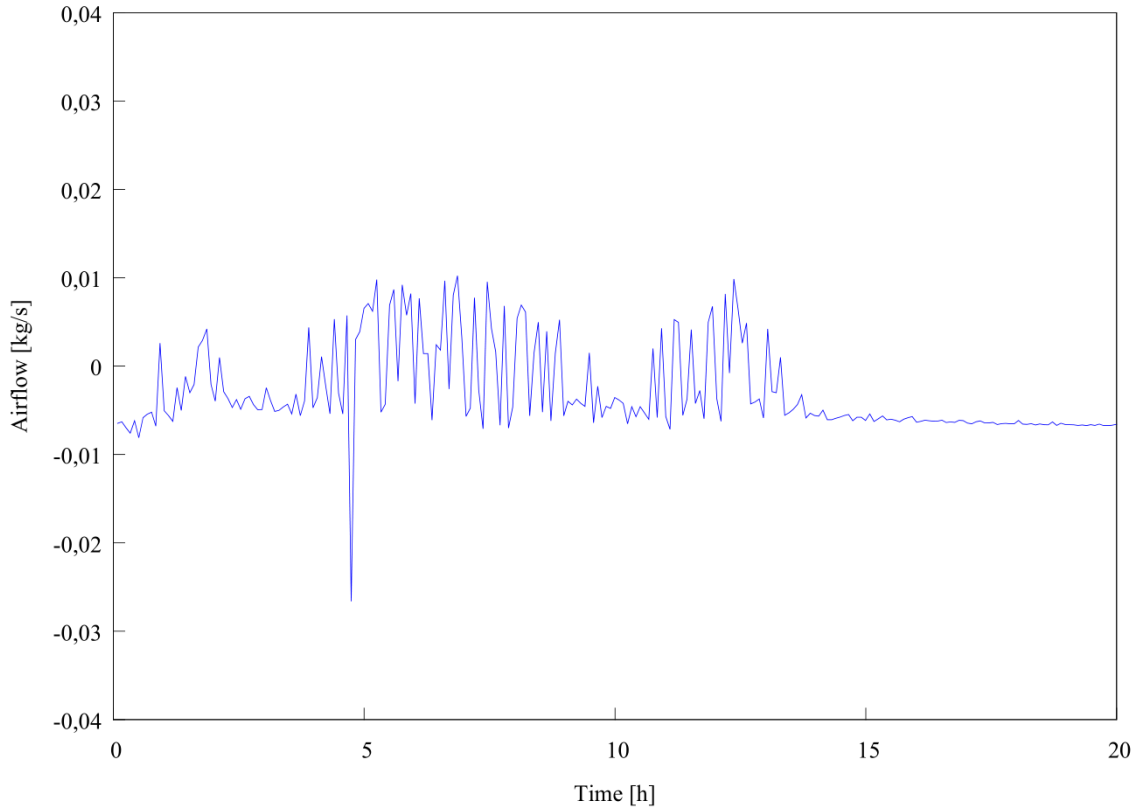

Figure 47: Airflow measurement [kg/s] versus temperature in flaming fire. This chart corresponds to test VF3.

4.8 Gas measurements

The gas measurement unit measured four different chemical compounds: volatile organic compounds (VOCs), carbon dioxide (CO_2), carbon monoxide (CO) and oxygen (O_2). The data from the VOC sensor is not going to be studied as there was no reference gas to use for its calibration. Even though there were no reference values for the oxygen, it was used to compare its readings with the CO_2 ones.

The smoke was measured in five tests: three semi reverse and two forward. The CO and CO_2 were given in ppm and the O_2 levels in percentage.

Figure 48 corresponds to a semi reverse test. CO and CO_2 levels were measured during the whole combustion process. CO values underwent some fluctuations due to a sort of

error of the sensor, so a moving average of six time periods was calculated to read the findings more easily. The vertical line indicates when the external heater was turned off.

The gas concentrations (CO and CO_2) increased exponentially during the external heating period and, once the heater was turned off, the concentrations dropped till they remained more or less constant from 7 to 27 hours; CO_2 and CO concentrations at this time were ~49100 ppm and 500 ppm respectively. A rapid increase led to a maximum concentration peak around 28 hours, reaching 87452 ppm of CO_2 and 704.5 ppm of CO. After the maximum peak, the smouldering process kept going forward and 3 concentration peaks showed up. These peaks (see Table 16) matches the three temperature peaks during the after intense smouldering combustion period, time when char oxidation was taking place.

Figure 49 shows that oxygen decreased while the reaction was going forward due to oxygen consumption during pyrolysis and oxidation processes. The maximum drops took place when CO and CO_2 levels reached their maximum.

CO/CO_2 ratio and combustion efficiency (%) were calculated for the entire tests, as it shown in Figures 50 and 51.

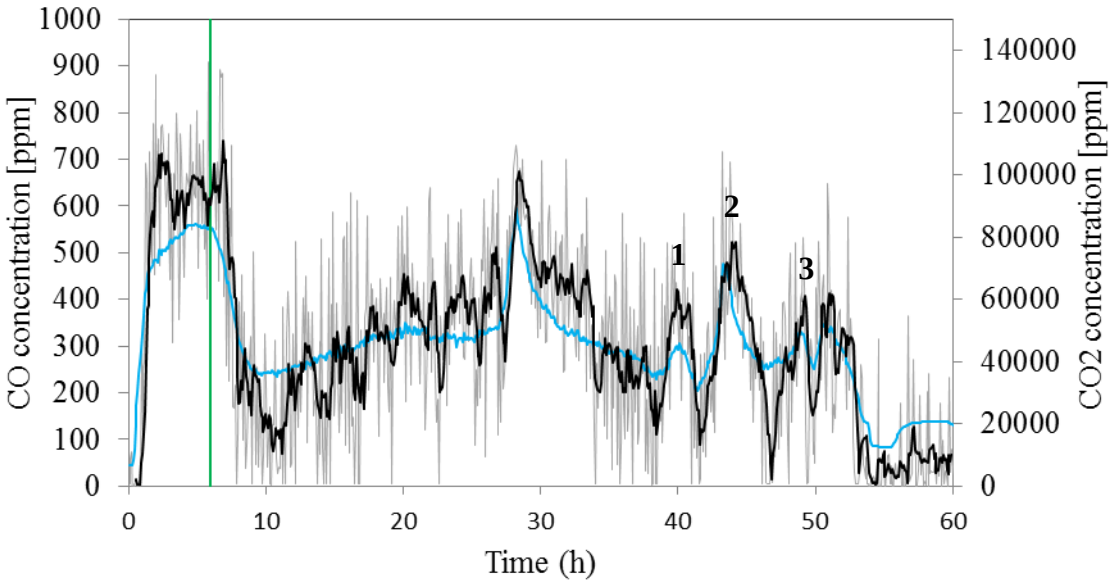

Figure 48: CO and CO_2 levels [ppm]. The grey line is referred to the CO data obtained by the sensor, the black line corresponds to the moving average (6 time periods) and the blue line relates to the CO_2 data. The vertical line indicates when the external heater was turned off. This example is from test VR1.

Table 16: Maximum CO_2 and CO values [ppm] during the after intense combustion period.

Peaks	CO_2 [ppm]	CO [ppm]
1	45853.3	381
2	71376.1	521.5
3	50121	400.7

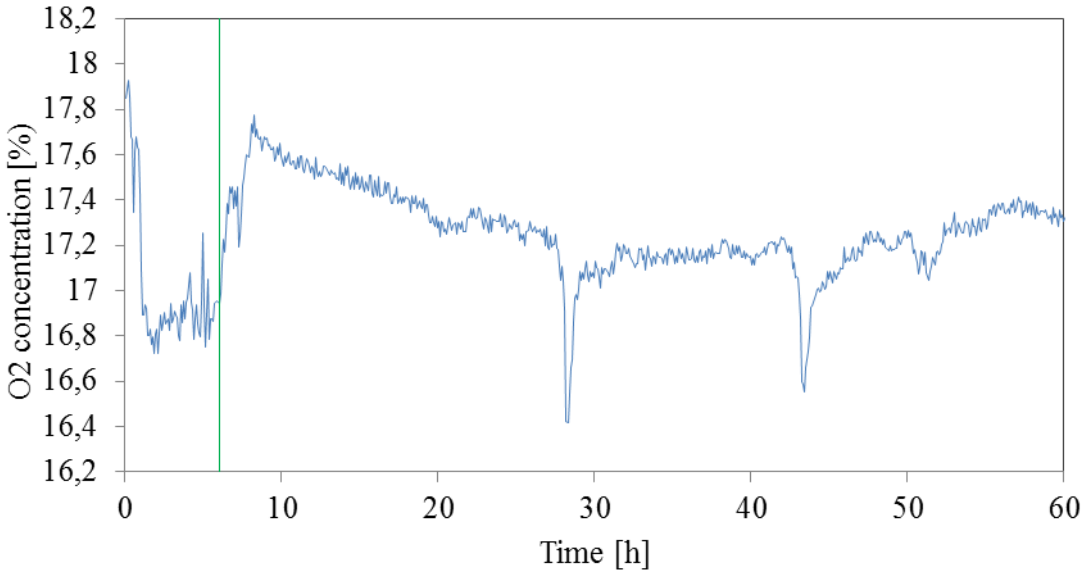

Figure 49: O_2 levels [%]. The vertical line indicates when the external heater was turned off. This example is from test VR1.

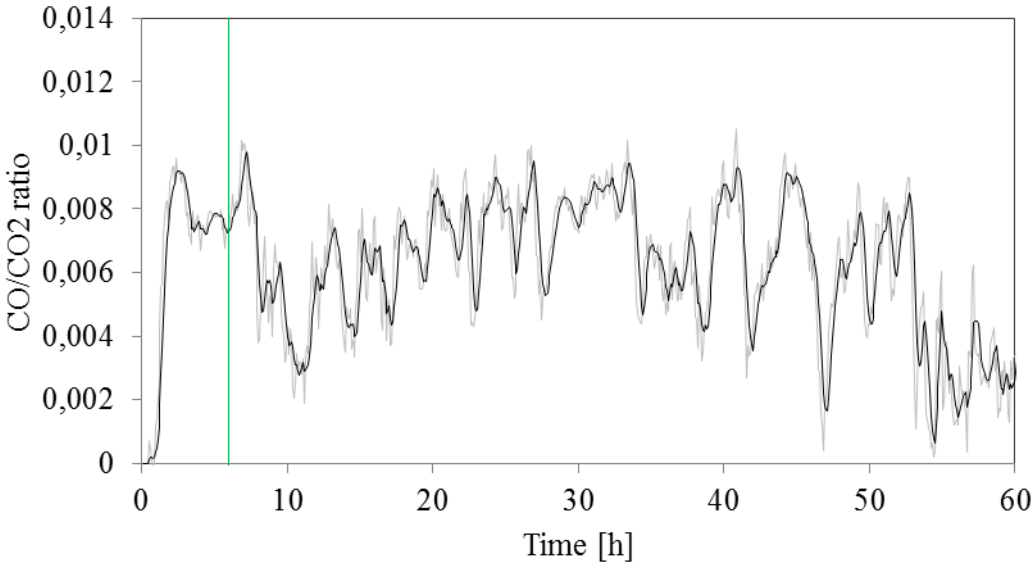

Figure 50: CO/CO_2 ratio for VR1 test. The grey line is the actual data; the black line refers to the moving average (6 time period).

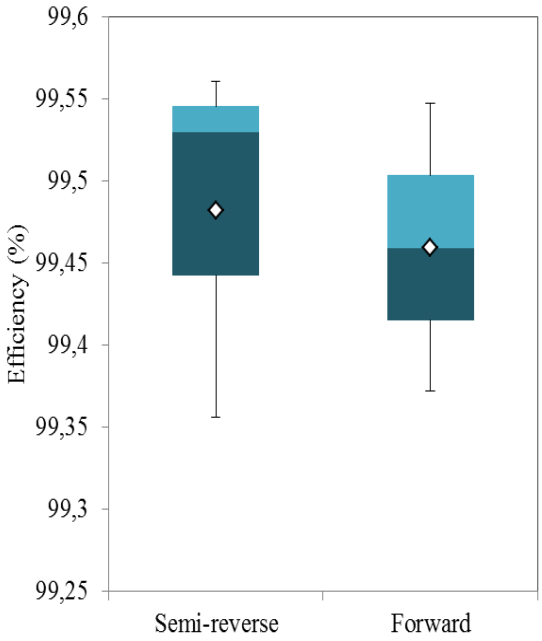

Figure 51: Combustion Efficiency (%) in VR1. The white rhombus refers to the average value.

4.9 Sorted residues in forward and semi reverse smouldering

After each test the residue was stored for at least 3 days, and then separated and weighed into ash and black (char). As Figure 52 illustrates, forward smouldering had more ash and less char comparing to semi reverse.

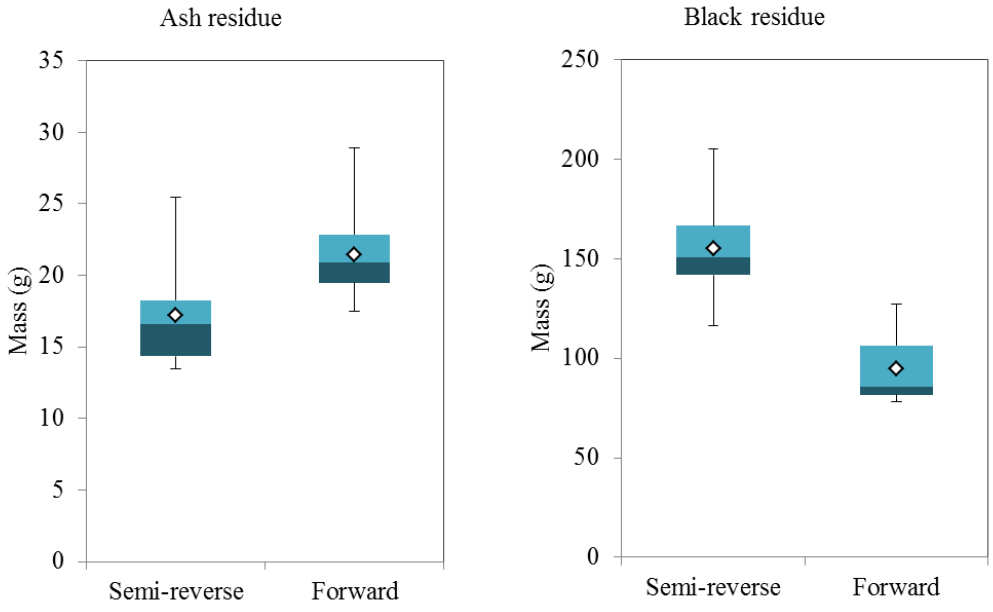

Figure 52: Amount of char and ash residue left on forward and semi reverse smouldering

4.10 Pictures of tested samples

In this section photos will illustrate the different smouldering types described in 4.2 and the flaming case in 4.3.

White ash and char were obtained after the *semi reverse* tests, as shown in Figure 53. The char residue maintained the original pellet form, not being smashed. The height of the stacked residue was approximately 3 cm. In semi reverse smouldering approximately 11% of the total residue was ash, with an 89 % of char as Figure 54 illustrates.

Figure 53: Semi reverse Smouldering combustion: Sample VR1 after test

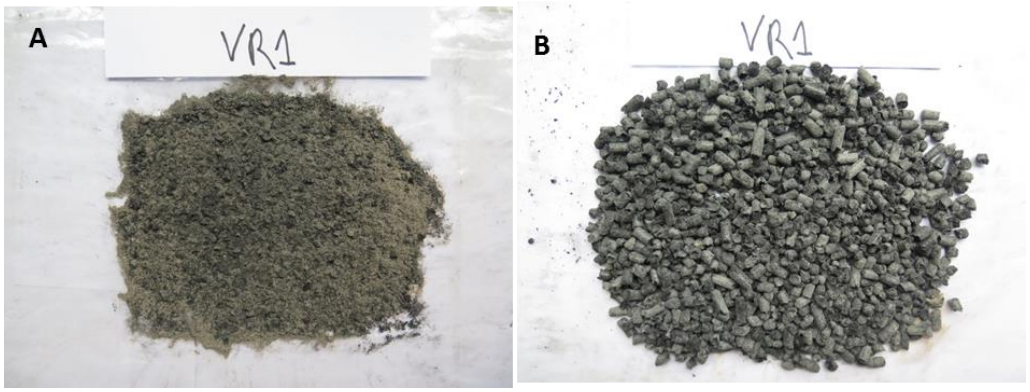

Figure 54: Sorted residue VR1. A) Ash (25.5 g); B) Black/char (205.4 g).

Forward smouldering behaviour type 1 looked similar comparing to *semi reverse smouldering behaviour*, as shown in Figure 55 and 56; the main difference between them was the different amounts of ash and char in the stack residue, having approximately 15 % of ash and 85 % of char in the forward case.

Figure 55: Forward smouldering combustion type 1: Sample VF1 after test

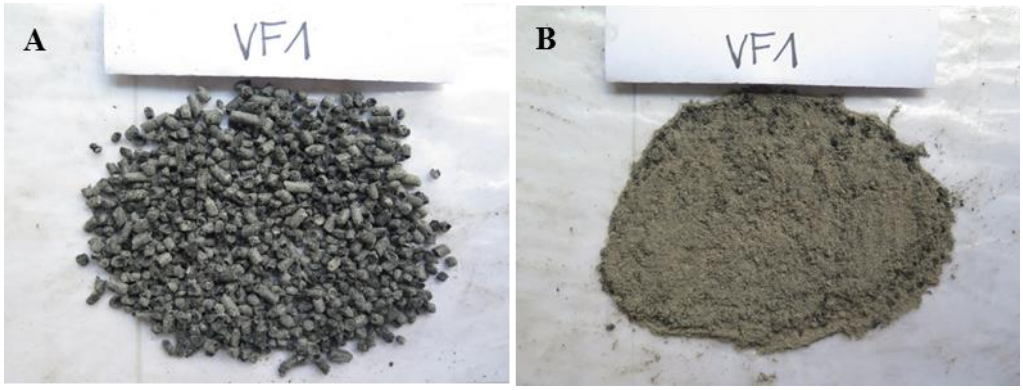

Figure 56: Sorted residue VF1. A) Ash (20 g); B) Black/char (127 g)

In *forward smouldering behaviour type 2* the ash residue looked different in comparison to the other two cases. It was more spread along the pipe surface and also underwent a colour change, being white in most of the surface and grey on the centre as shown in Figure 57. Approximately 20% of the total residue was ash and the remaining 80% was char.

Figure 57: Forward smouldering combustion type 2: Sample VF4 after test

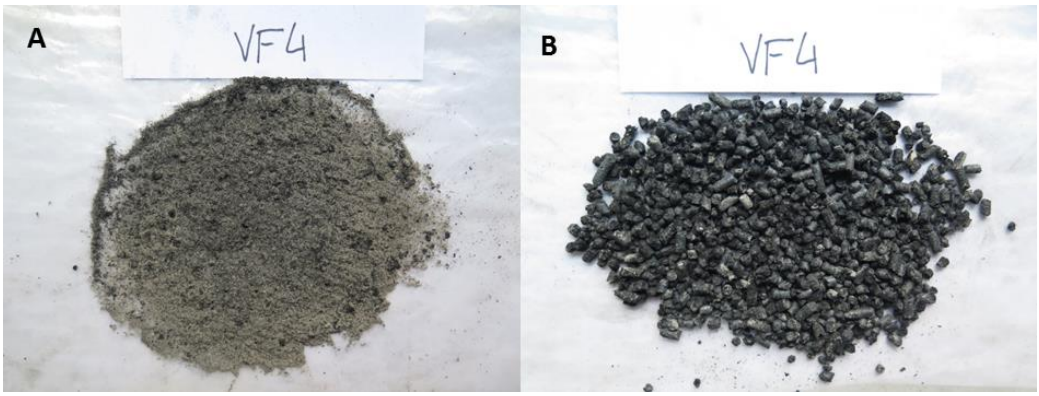

Figure 58: Sorted residue VF4. A) Ash (20,9 g); B) Black/char (114,7 g)

The flaming case looked similar to *forward smouldering type 2*, having white and grey ash all over the pipe surface. It was formed by 18 % of ash and 82 % of char as seen in Figures 59 and 60.

Figure 59: Forward smouldering combustion type 1: Sample VF1 after test

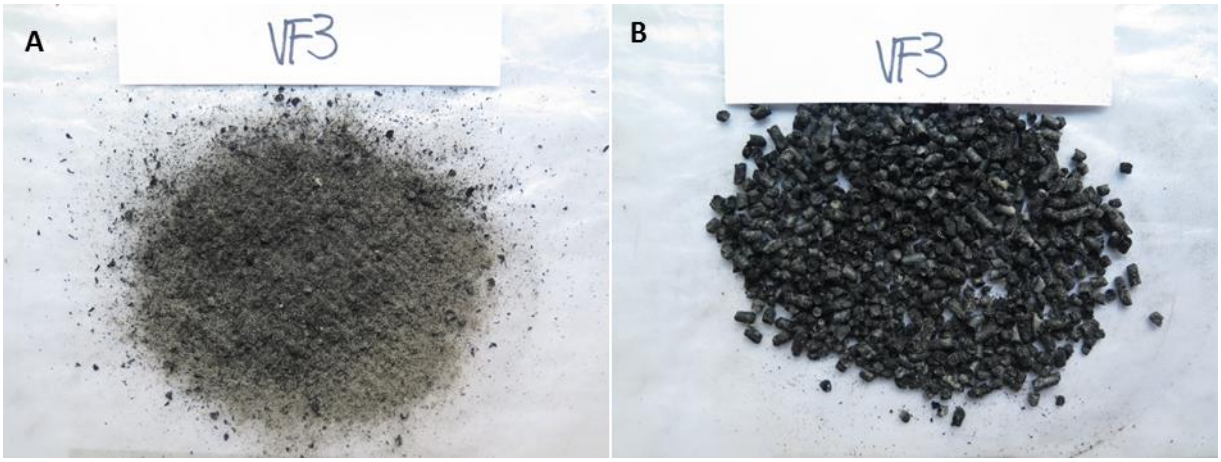

Figure 60: Sorted residue VF4. A) Ash (17,5 g); B) Black/char (78,4 g)

5. Discussion

In this section, the results got from testing will be discussed. This was done in order to study the different smouldering behaviour by changing the airflow.

There are consistent indications that can be used to affirm that the samples did undergo a self-sustained smouldering combustion. First, a high temperature peak well above the temperature provided by the external heating source. Second, a mass loss rate as the reaction was going forward, reaching its maximum at the same time as the maximum temperature peak. And thirdly, the development of a fluctuating smouldering period after the maximum temperature peak, produced when the heat released by oxidation was high enough to balance the heat required for the endothermic processes.

In this thesis, two different airflow configurations were studied: semi reverse and forward. In semi reverse propagation the oxygen supply flows first through the original fuel, and through the preheating and evaporation sub fronts before reaching the char where the oxidation front is. Then the hot, oxygen-depleted gases of combustion flow through the unreacted char and ash residues. This means that the heat is lost by convection in the opposite direction to the original fuel, reducing the drying and preheating which in turn results in a weaker smouldering process. In forward propagation higher temperatures were reached in less time, this can be explained since the oxygen supply is moving in the same spread direction of the smouldering flow. Consequently, forward smoulder is faster than reverse under the same fuel and oxidizer supply, and allows for a more complete combustion with the correspondent higher maximum temperature.

During the experiments both forward and semi reverse experienced a colour change as shown in Section 4.10. Samples that did undergo forward smouldering got more ash and less char than semi reverse smouldering, verifying that forward smouldering developed a more intense combustion.

The experiments showed three variations of smouldering combustion; temperature development was studied for each type. *Semi reverse smouldering* experiments showed a 20 hour steady temperature development (plateau) during the before intense

combustion period (BIC) because the proper conditions of pressure and temperature were not reached, even though this period was reach in oxygen. During this lapse, the heat was stored mostly in the middle of the pipe at approximately 250 ºC. In the middle of the pipe the heat losses were lower as the sample was not in direct contact with the pipe walls and the atmosphere. The maximum temperature peak of ~570 ºC was reached during the most intense combustion period (MIC). This temperature was found with the thermocouple placed on the top surface of the sample (10 cm height). Once the surface ignition took place, the smouldering front provided the majority of the heat to increase the temperature of the sample, enabling the development of the after intense combustion period (AIC). As the reaction was going forward, a fluctuation zone during the AIC period took place on the thermocouples placed at the 6, 4 and 2 cm placements, as there was still sample. The uppermost thermocouples, located at the 8 and 10 cm placements, underwent a drop on their temperature readings as they were on air due to mass consumption. Once the sample was turned into char and ash, in other words, when pyrolysis and oxidation processes were finished due to a lack of fuel and oxygen, the sample cooled down till ambient temperature. The total combustion time in this smouldering type was ~ 60 hours, becoming the longest combustion type.

Forward smouldering Type 1 showed a steady temperature development during the external heating period (H) at 6, 8 and 10 cm, the main reason for this outcome was due to heat conduction, as it takes more time to heat the upper part of the sample; it has also been considered the evaporation of moisture and volatiles. As well as *Semi reverse smouldering*, *Forward smouldering type 1* undergoes a before intense combustion period (BIC). The difference between these two types is that forward smouldering develops a more intense BIC, reaching higher temperatures in a shorter period of time (average of 470 ºC in 10 hours). During the most intense combustion period (MIC), the maximum temperature peak was reached at higher temperatures in less time than semi reverse smouldering, as the oxygen was also entering from below. The after intense combustion period (AIC) was less intense than semi reverse smouldering, it developed a slight self-sustained smouldering at 2 and 4 cm height showing that the sample has been consumed faster. After ~ 40 hours the sample cooled down till ambient temperature.

In *Forward smouldering behaviour Type 2* it was very noticeable how more intense forward smouldering is in comparison to semi reverse. In this case there is no before intense combustion period (BIC); the sample ignited before the external heating process was finished. The maximum temperature peak was reached in 5.5 hours at temperatures around 750 ºC, reaching higher temperatures than the ones set by Rein [9]. It is possible to affirm that it is a smouldering case, and not a flaming one, based on the temperature readings at 14 and 33 cm. In flaming combustion the heat release occurs on the gas phase around the fuel, and as the temperatures readings at these height reached low values (120 ºC) it is possible to affirm that the heat release occurs on the surface of the fuel. During the after intense combustion (AIC) a slight combustion zone was developed at the 2 and 4 cm placements until it end up cooling down at ambient temperature after ~ 20 hours.

During one of the forward tests a transition to flaming fire was produced due to equipment failure. It is possible to affirm that it is a flaming case based on the maximum temperature peak (910 ºC), which is way higher than the ones recorded in smouldering combustion, and the temperature readings at 14 and 33 cm, reaching 750 ºC. Also the total combustion time lasted less time than the smouldering cases, completing the combustion process in 14 hours.

Mass loss was studied in forward and reverse smouldering propagation; it was observed that semi reverse smouldering underwent a lower mass loss in comparison to forward, losing ~ 85% of its total mass in comparison to 90% for the forward case. On the other hand, forward smouldering type 1 and 2 do not defer considerably in mass loss terms, even though the combustion development was different. Both types lost around 90 % of its mass.

A gas measurement unit was incorporated to the setup with the aim of analysing the smoke composition. This study had its focus on finding any correlation between the smoke compounds and the smouldering periods.

As it was explained in Section 2.8 the major smouldering emissions were CO and CO_2, both products of pyrolysis and oxidation reactions. During the external heating period, CO and CO_2 values increased due to pyrolysis. When the oxidation reaction occurred, the concentrations of CO and CO_2 rapidly increase as shown during the MIC and AIC

periods. It was also observed that char oxidation releases predominantly CO_2 at relative lower temperatures. It should also be taken into consideration that it is difficult to separate the gases primarily produced by thermal degradation from the ones originated during the smouldering combustion, since both processes overlap. However, one indicates the presence of the other.

It was expected that the CO/CO_2 ratio would increase with the temperature. However, this ratio remains constant reaching lower values than the ones found in the literature [26], the results from combustion efficiency were not the ones expected either. Forward smouldering was expected to be more efficient as it developed a more intense combustion in less time than semi reverse smouldering, and in our results both efficiencies reached very similar values. Also the efficiency results were much higher than the ones found in [26], reaching 99.5 %. For this reasons, more tests are needed for a better understanding and comparison of the results.

It is important to notice that, in most studies concerning smouldering the propagation speed was studied for each test; in our case we cannot calculate this data due to the mass is collapsed at the bottom of the pipe. It is possible to have an approximately propagation speed seeing the difference on the sample height before and after test.

5.1 Discussion of hypotheses

Until now, the results from the testing have been discussed. In this section, the results will be summarized in order to see if they support or falsify the hypotheses.

1. Is forward propagation two times more intense than reverse? If so, are the highest temperatures reached in half the time?
   The results showed that forward propagation is more intense than semi reverse smouldering but not two times bigger. Maximum temperatures between forward and smouldering had 200ºC of difference.
   The maximum temperature peak was reached for semi reverse and forward configuration in 28 and 5 hours respectively; so forward reached the maximum temperature in less than the half of the time.

2. Is the total combustion time two times lesser than reverse propagation?
   No, semi reverse smouldering lasted for 60 hours while forward took 20 hours.

3. As forward smouldering is more intense, is the total mass loss significantly greater than reverse? Does the airflow readings in forward smouldering show more ups and downs in the air flow velocity than reverse?
   Mass loss is greater in forward than semi reverse smouldering, but not significantly bigger. In forward smouldering 91 % of the total mass was consumed during the combustion process while in reverse it was the 85 %.
   The airflow readings during forward tests showed more noticeable ups and downs as it undergoes a more intense smouldering reaction.

4. Does the maximum temperature peak match the highest mass loss rate in time?
   Yes, in the entire tests.

5. Is a higher air flow associated to greater amounts of CO_2 and lower CO?
   During the AIC period in semi reverse smouldering it is released more amounts of CO_2 and CO than in forward propagation, as the fluctuation zone is more reactive.

6. Conclusions

Smouldering is a different type of combustion than flaming fires, but as diverse and complex. As pellets are becoming more widely used as an alternative to oil-fired central heating in residential and industrial buildings, studying their smouldering properties is very important.

The influence of varying the airflow, using two different configurations of smouldering combustion was studied: semi reverse and forward propagation. Based on the experiments it is clear that the airflow configuration seems to influence smouldering both in terms of maximum temperatures, total combustion time, mass loss and combustion behaviour. Three different smouldering behaviours were observed in the test: *semi reverse smouldering, forward smouldering type 1 and forward smouldering type 2.*

The results indicate that forward smoulder propagates faster than reverse, as it develops a more intense combustion due to the oxygen supply moving in the same direction as the smouldering front. The total combustion time differs between one type and another; it was observed that semi reverse smouldering took around 60 hours to complete the whole process while forward smouldering lasted for approximately 20 hours. Because of this, the total mass loss in forward airflow propagation was higher than semi reverse smouldering, losing 91 % of its mass.

All the test samples were heated for 6 hours. Semi reverse smouldering and forward smouldering type 1 were the only models where a before intense combustion period (BIC) was developed; this zone is defined by an approximately constant temperature before reaching the maximum temperature peak. The BIC period for forward smouldering was 10 hours shorter than for semi reverse cases. On the other hand, forward smouldering Type 2 reached the maximum temperature peak before the external heating period was finished. Semi reverse smouldering developed a less intense and longer combustion than forward smouldering, reaching its maximum temperature of 580-560 ºC in ~27 hours while forward smouldering type 2 reached 690-781 ºC in ~5 hours and forward Type 1 650-690 ºC in ~18 hours.

References

[1] Rebaque V. *Smouldering fires in Wood pellets*. NTNU Norwegian University of Science and Technology, Specialization Project. 2016.

[2] Sieminski A. *International energy outlook*. Energy Information Administration (EIA). 2014.

[3] Zhang N, Lior N, Jin H. *The energy situation and its sustainable development strategy in China*. Energy. 2011. 3639-49.

[4] Petroleum British. *BP statistical review of world energy*. London: British Petroleum; 2012.

[5] Stupak I et al. *Sustainable utilisation of forest biomass for energy*. Biomass and Bioenergy. 2007;31(10):666-84.

[6] Perlack RD, Wright LL, Turhollow AF, Graham RL, Stokes BJ, Erbach DC. *Biomass as feedstock for a bioenergy and bioproducts industry: the technical feasibility of a billion-ton annual supply*. DTIC Document; 2005.

[7] Stelte W, Sanadi AR, Shang L, Holm JK, Ahrenfeldt J, Henriksen UB. *Recent developments in biomass pelletization–A review*. BioResources. 2012;7(3):4451-90.

[8] AEBIOM, EBA. *Annual Statistical Report on the Contribution of Biomass to the Energy System in the EU27*. 2011.

[9] Rein G. *Smouldering Combustion Phenomena in Science and Technology*. Int Rev Chem Eng. 2009;1:3–18.

[10] G. Rein, J.L. Torero, A.C. Fernandez-Pello, *Modeling the propagation of Forward and Opposed Smoldering Combustion*. Eurotherm 81, Reactive Heat Transfer in Porous Media, Albi, France. June 4-6, 2007.

[11] Rein G, et al., *Modeling of one-dimensional smoldering of polyurethane in microgravity conditions*. Proceedings of the Combustion Institute. 2005;30(2):2327-34.

[12] Drysdale D. *An Introduction to Fire Dynamics*. Third Edition. 3rd ed. Chichester, UK.: Wiley & Sons Ltd; 2011. Pages 211, 331-332.

[13] Shafizadeh F, Bradbury AGW. *Smoldering Combustion of Cellulosic Materials*. J Build Phys. 1979 Jan 1;2:141–52.

[14] Moussa NA, Toong TY, Garris CA. *Mechanism of smoldering of cellulosic materials*. Symp Int Combust. 1977 Jan 1;16(1):1447–57.

[15] Ohlemiller T. *Smoldering combustion propagation on solid wood*. Fire Safety Science. 1991;3:565-74.

[16] R Hadden, G Rein, *Burning and Suppression of Smouldering Coal Fires*, Chapter 18 in. Coal and Peat Fires: A Global Perspective, Volume 1, pp. 317–326, Stracher, Prakash and Sokol (editors), Elsevier Geoscience, 2011. ISBN 9780444528582.

[17] M. Tuomisaari, D. Baroudi, and R. Latva, *Extinguishing Smoldering Fires in Silos*, Publication 339, VTT Technical Research Centre of Finland, Espoo, Finland (1998).

[18] Jensen, U. E., *The Development of Smouldering Combustion in Combustible Building Insulation Materials*. Master's thesis. NTNU Trondheim, 2016.

[19] Hagen BC. *Onset of smoldering and transition to flaming fire*. 2013.

[20] Ohlemiller T. Smoldering combustion propagation on solid wood. Fire Safety Science. 1991;3:565-74.

[21] TJ. Ohlemiller, *Modeling of Smoldering Combustion Propagation*, Progress in Energy and Combustion Science, 11, p. 277 (1985)

[22] A. Bar Ilan, Rein G, Fernandez Pello AC, Torero JL, Urban DL (2004a) *Forced forward smouldering experiments in microgravity*. Exper Thermal and Fluid Science 28 (7):743–751.

[23] A. Bar Ilan, Rein G, Walther DC, Fernandez Pello AC, Torero JL, Urban DL (2004b) *The effect of buoyancy on opposed smoldering.* Combust Sci Technol 176(12):2027–2055.

[24] LEE, Taehyoung, et al. *Chemical smoke marker emissions during flaming and smoldering phases of laboratory open burning of wildland fuels*. Aerosol Science and Technology, 20 10, vol. 44, no 9, p. i-v.

[25] ISO 19706 International Standard. *Guidelines for assessing the fire threat to people*.

[26] ASTM E871 - 82(2013) *Standard Test Method for Moisture Analysis of Particulate Wood Fuels.*

[27] Kollie, T. G., et al. *Temperature measurement errors with type K (Chromel vs Alumel) thermocouples due to short-ranged ordering in Chromel*. Review of Scientific Instruments 46.11 (1975): 1447-1461.

[28] McCaffrey, B. J., and G. Heskestad. *A robust bidirectional low-velocity probe for flame and fire application*. *Combustion and Flame* 26 (1976): 125-127.

[29] Weigel, Ralf, et al. *Thermodynamic correction of particle concentrations measured by underwing probes on fast-flying aircraft*. Atmospheric Measurement Techniques 9.10 (2016): 5135.

[30] FIGARO ENGINEERING INC. Product information. CDM4160-Pre-calibrated module for carbon dioxide.

[31] FIGARO USA INC. Product information. TGS 5342 - for the detection of Carbon Monoxide.

[32] FIGARO GROUP. Technical Information for Figaro Oxygen Sensor SK-25F.

[33] FIGARO USA INC. Product information. TGS 823 - for the detection of Organic Solvent Vapors.

Appendices

A) Semi reverse smouldering charts

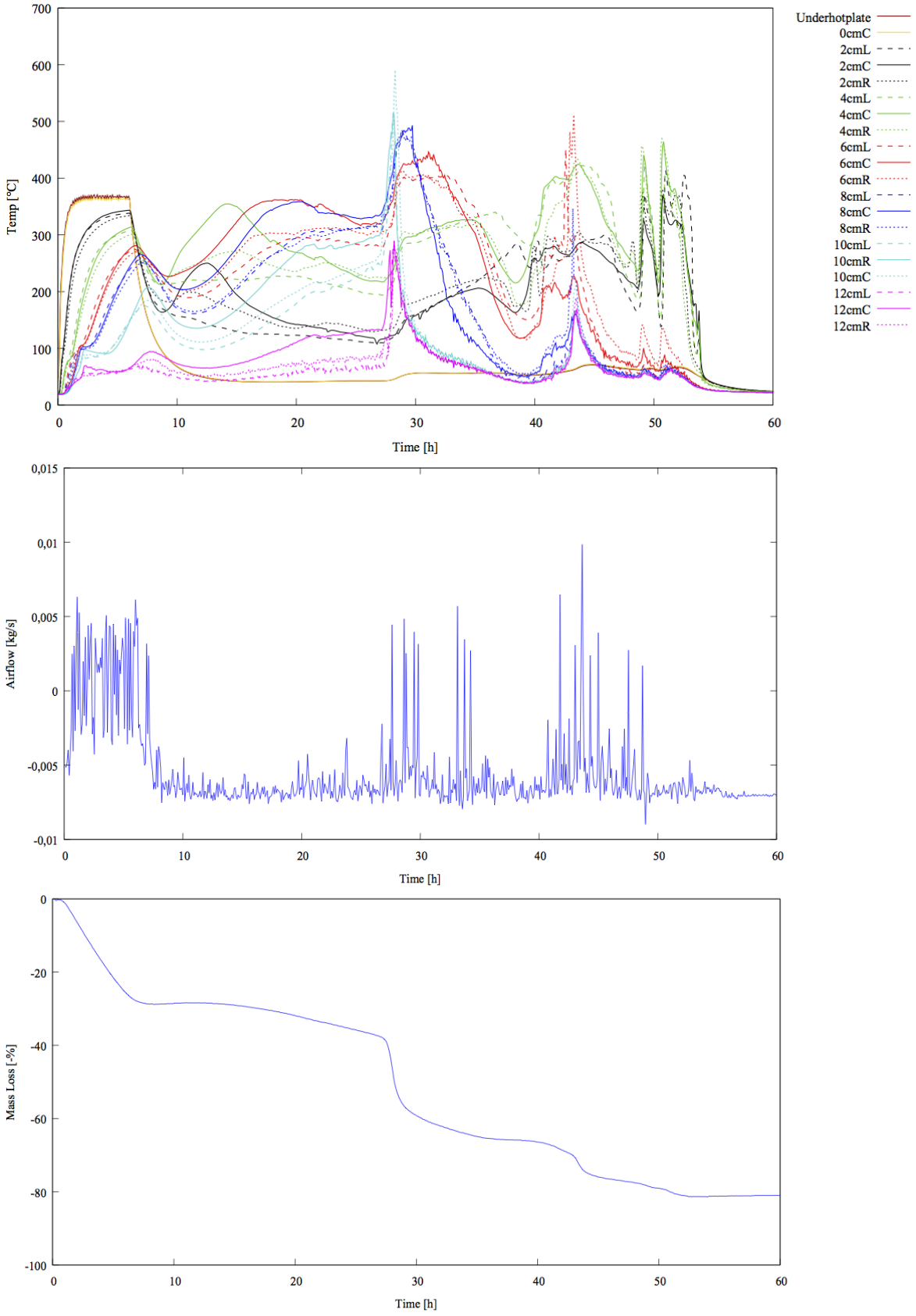

Figures A-1: VR1 test. Temperature development within the sample vs time (top graph), airflow measurement vs time (middle graph), mass change (%) vs time (bottom graph).

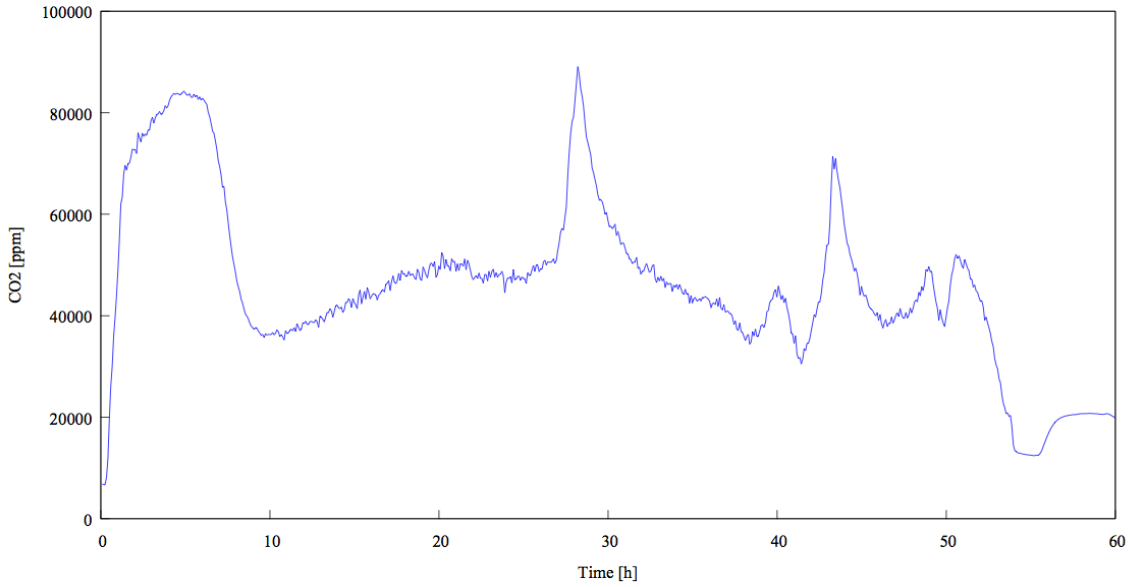

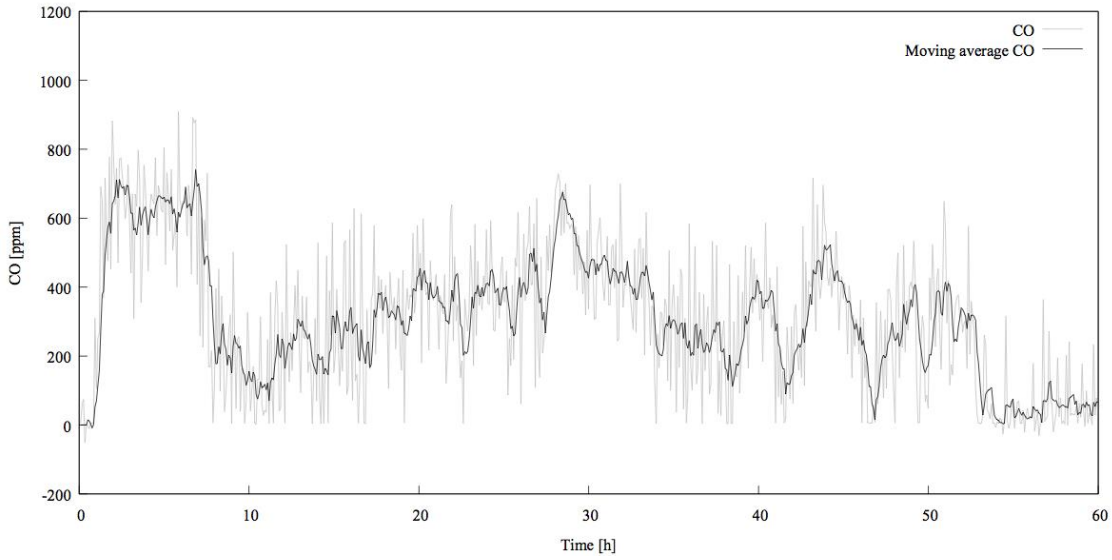

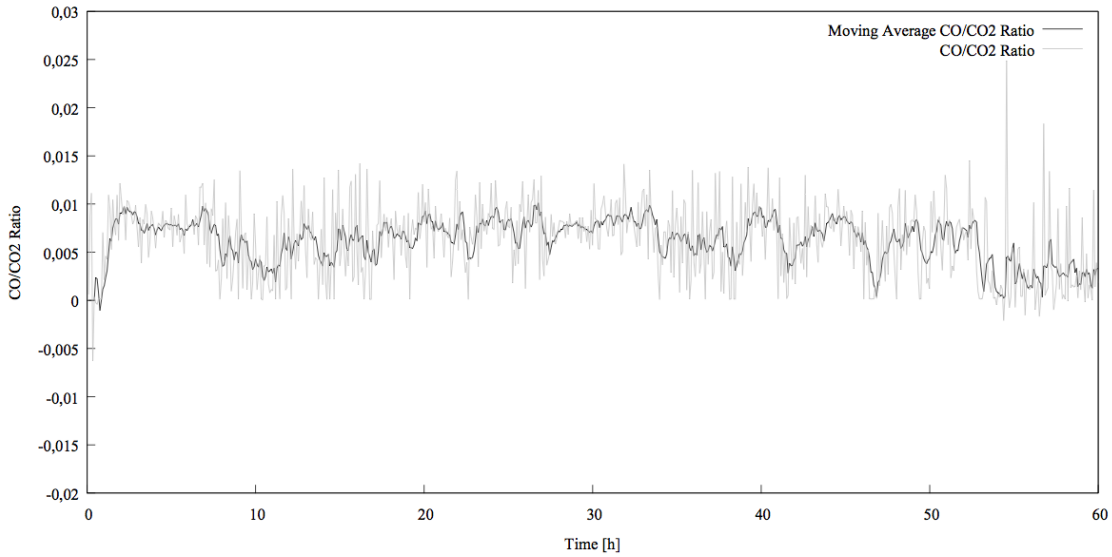

Figures A-2: VR1 test. CO2 readings [ppm] vs time (top graph), CO and CO moving average (6 times period) vs time [ppm] (middle graph), CO/CO2 ratio and moving average (6 times period) vs time (bottom graph).

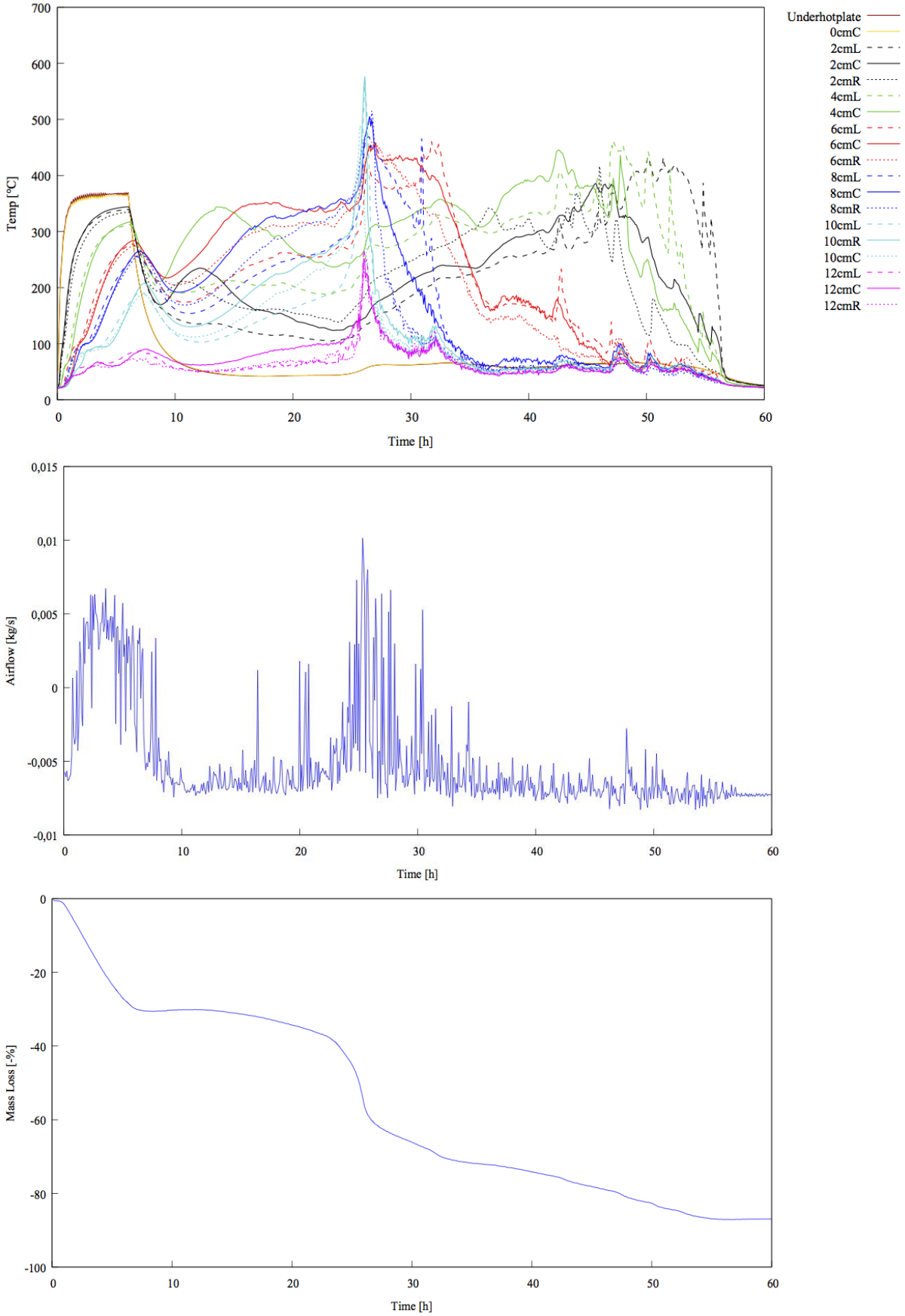

Figures A-3: VR2 test. Temperature development within the sample vs time (top graph), airflow measurement vs time (middle graph), mass change (%) vs time (bottom graph).

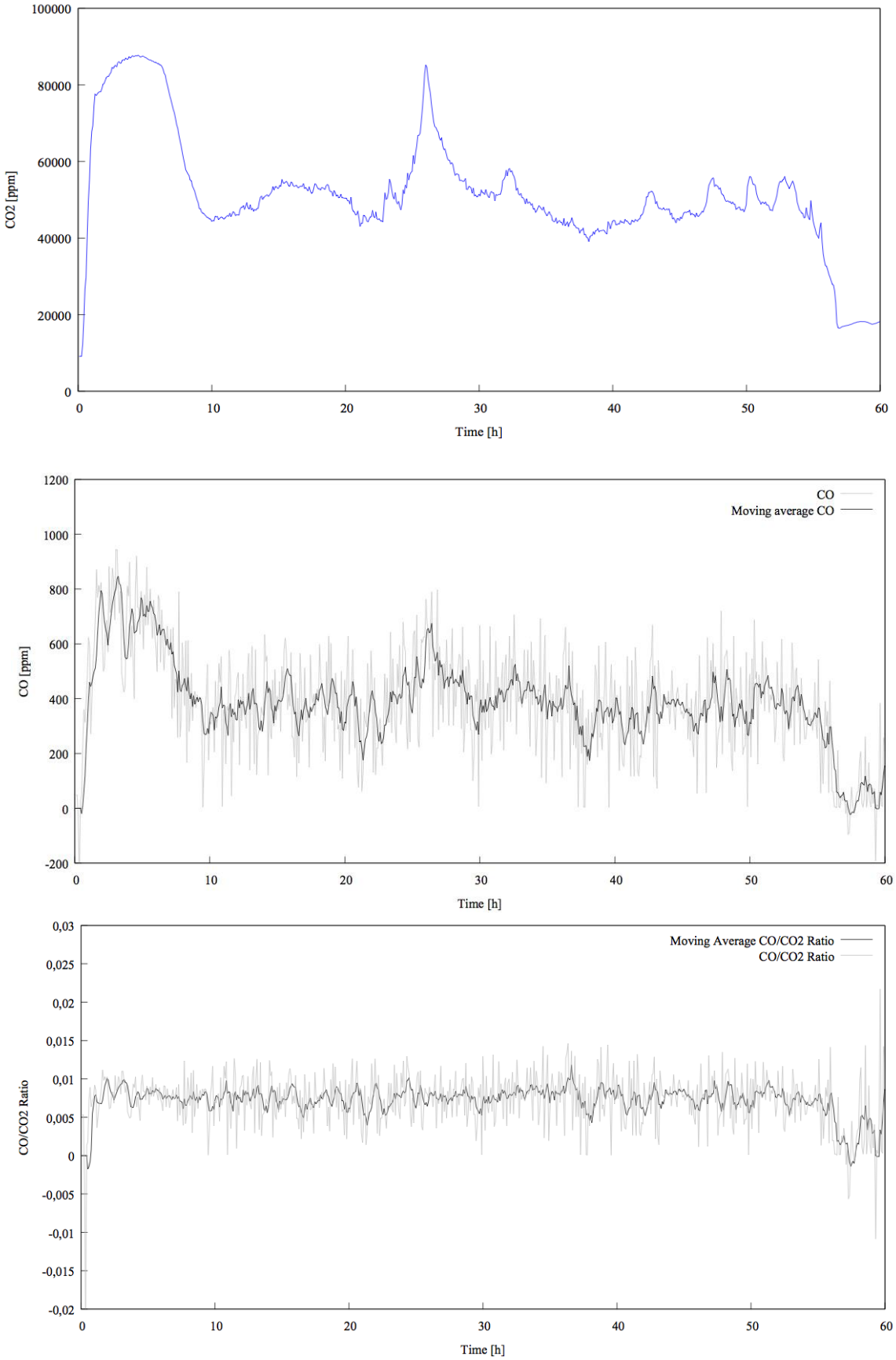

Figures A-4: VR2 test. CO_2 readings [ppm] vs time (top graph), CO and CO moving average (6 times period) vs time [ppm] (middle graph), CO/CO_2 ratio and moving average (6 times period) vs time (bottom graph).

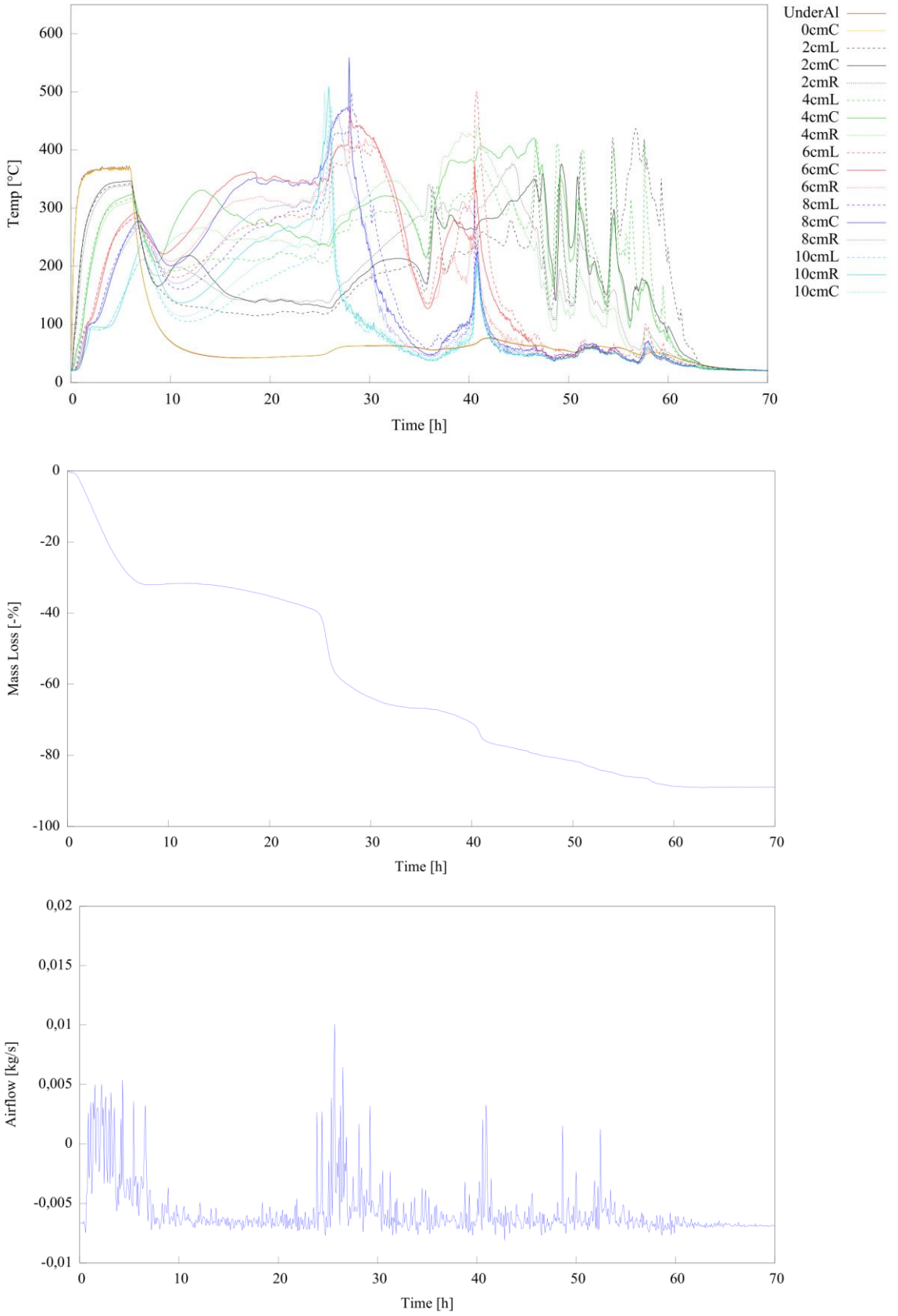

Figures A-5: VR3 test. Temperature development within the sample vs time (top graph), airflow measurement vs time (middle graph), mass change (%) vs time (bottom graph).

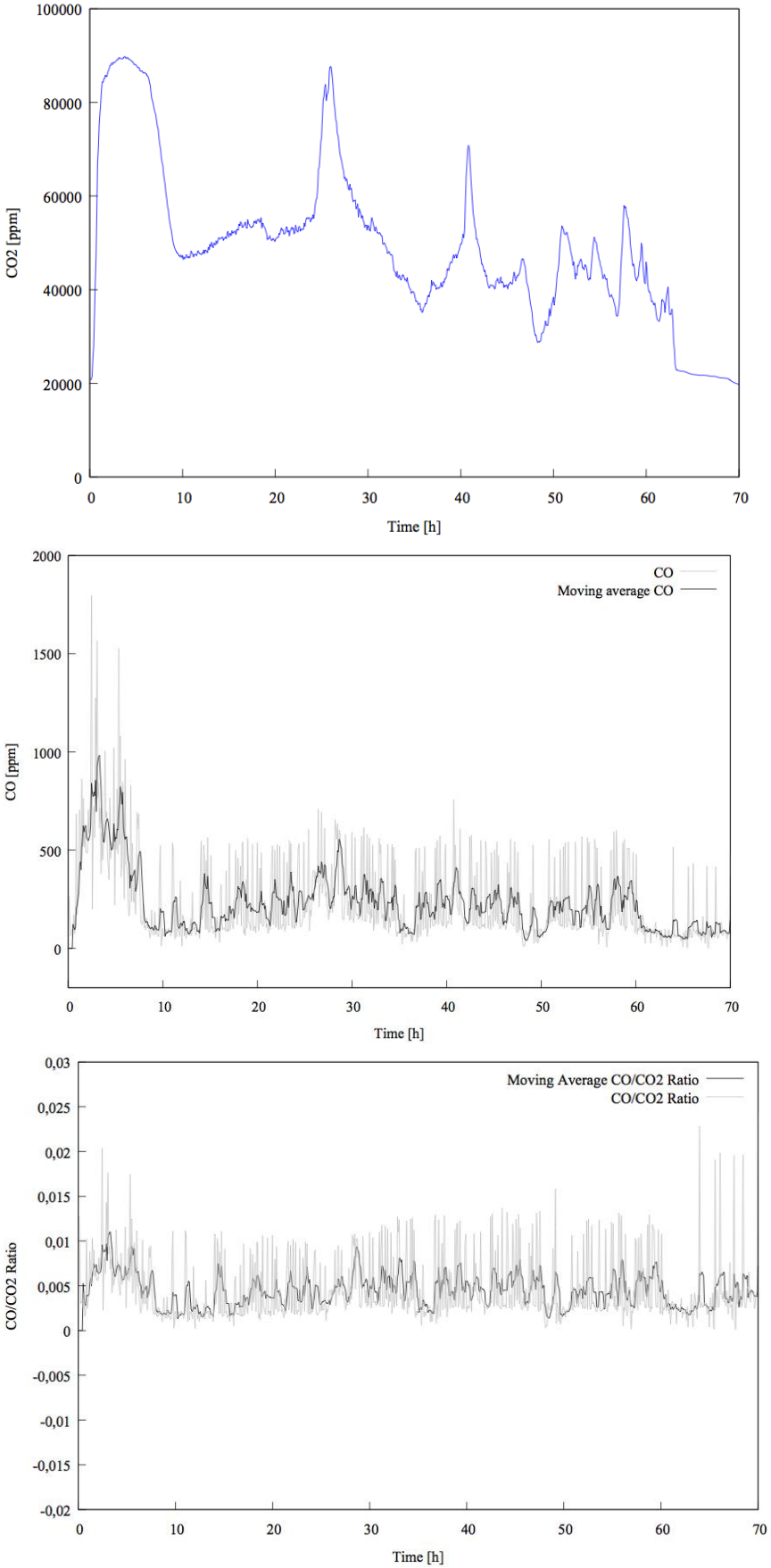

Figures A-6: VR3 test. CO_2 readings [ppm] vs time (top graph), CO and CO moving average (6 times period) vs time [ppm] (middle graph), CO/CO_2 ratio and moving average (6 times period) vs time (bottom graph).

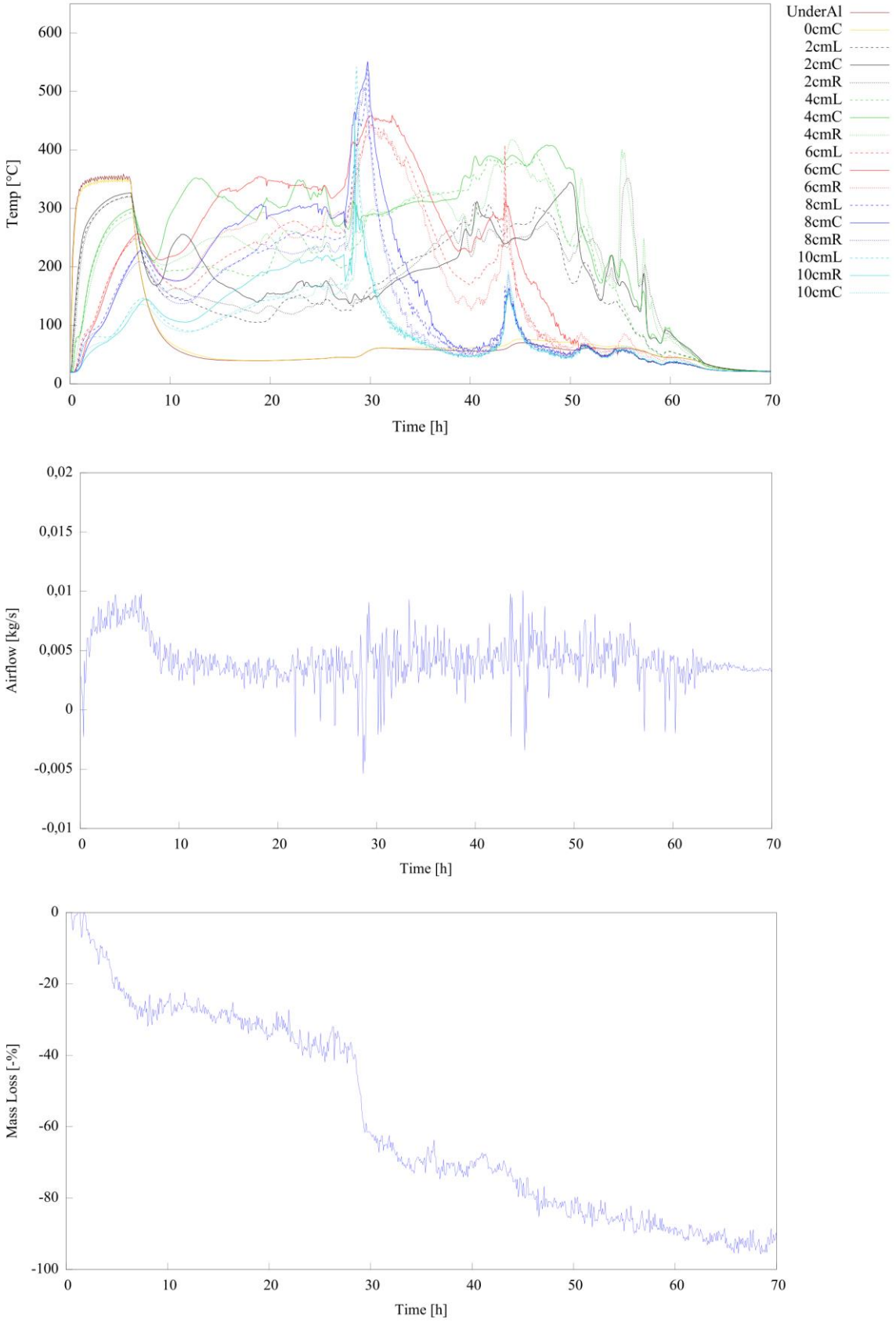

Figures A-7: VR6 test. Temperature development within the sample vs time (top graph), airflow measurement vs time (middle graph), mass change (%) vs time (bottom graph).

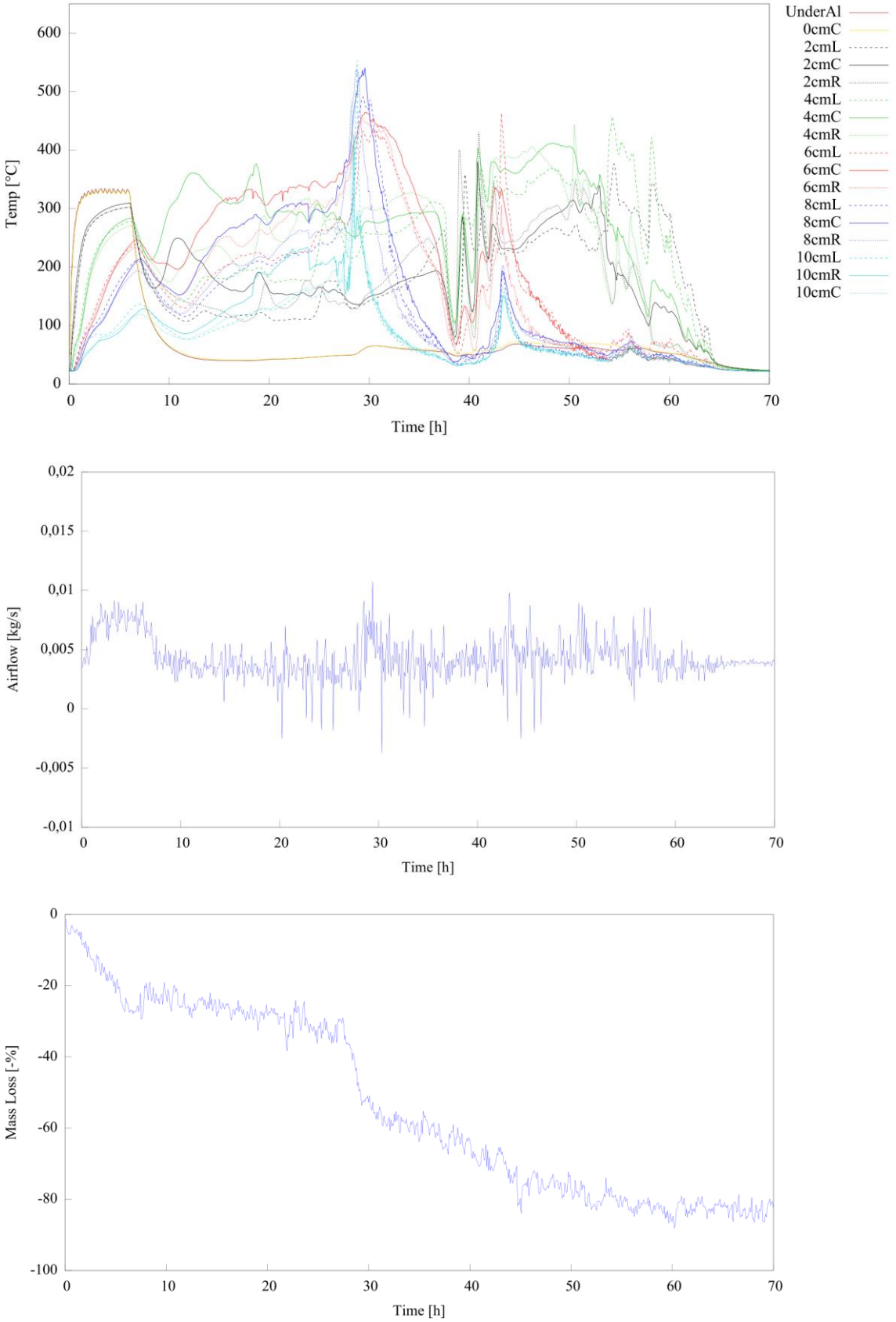

Figures A-8: VR7 test. Temperature development within the sample vs time (top graph), airflow measurement vs time (middle graph), mass change (%) vs time (bottom graph).

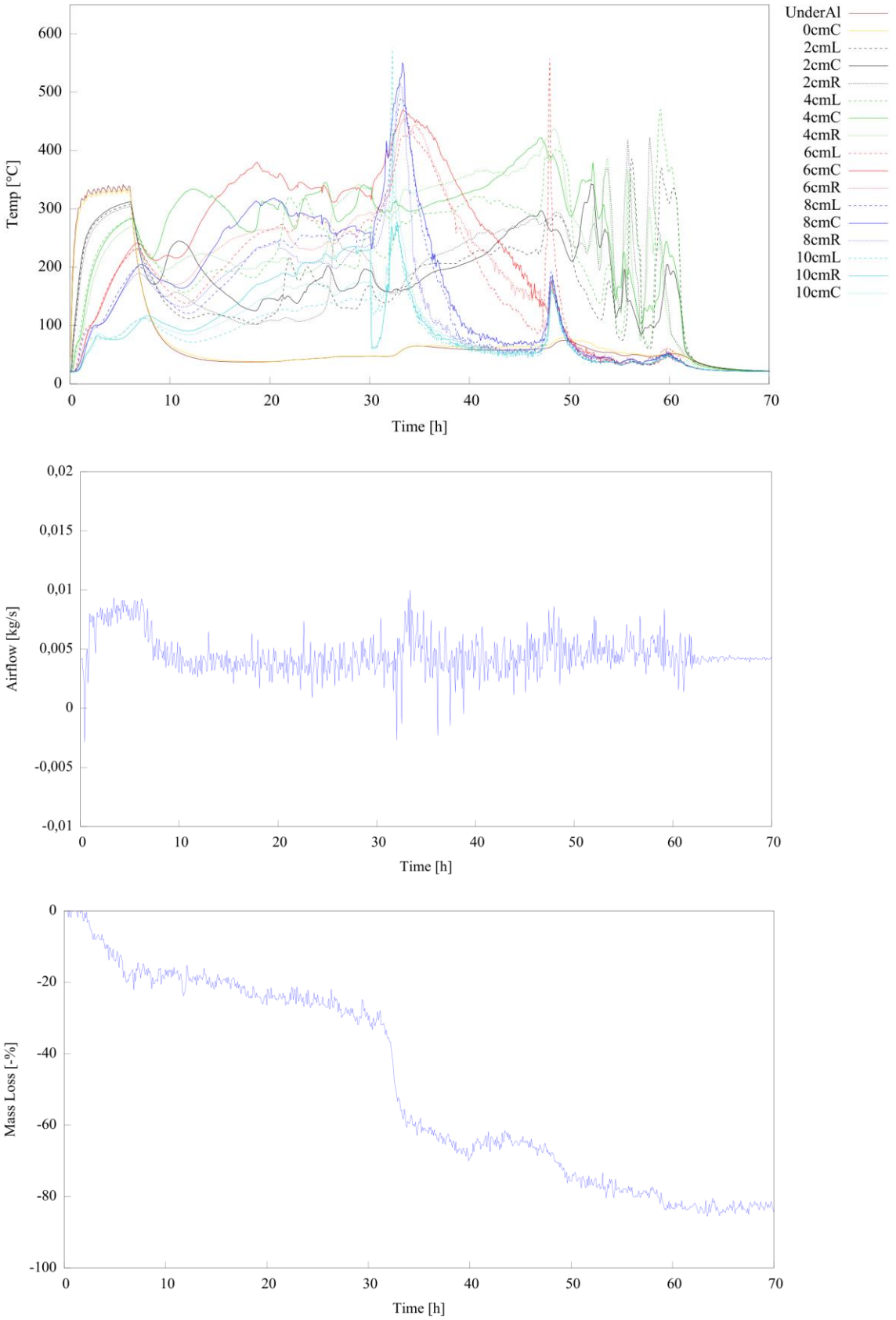

Figures A-9: VR8 test. Temperature development within the sample vs time (top graph), airflow measurement vs time (middle graph), mass change (%) vs time (bottom graph).

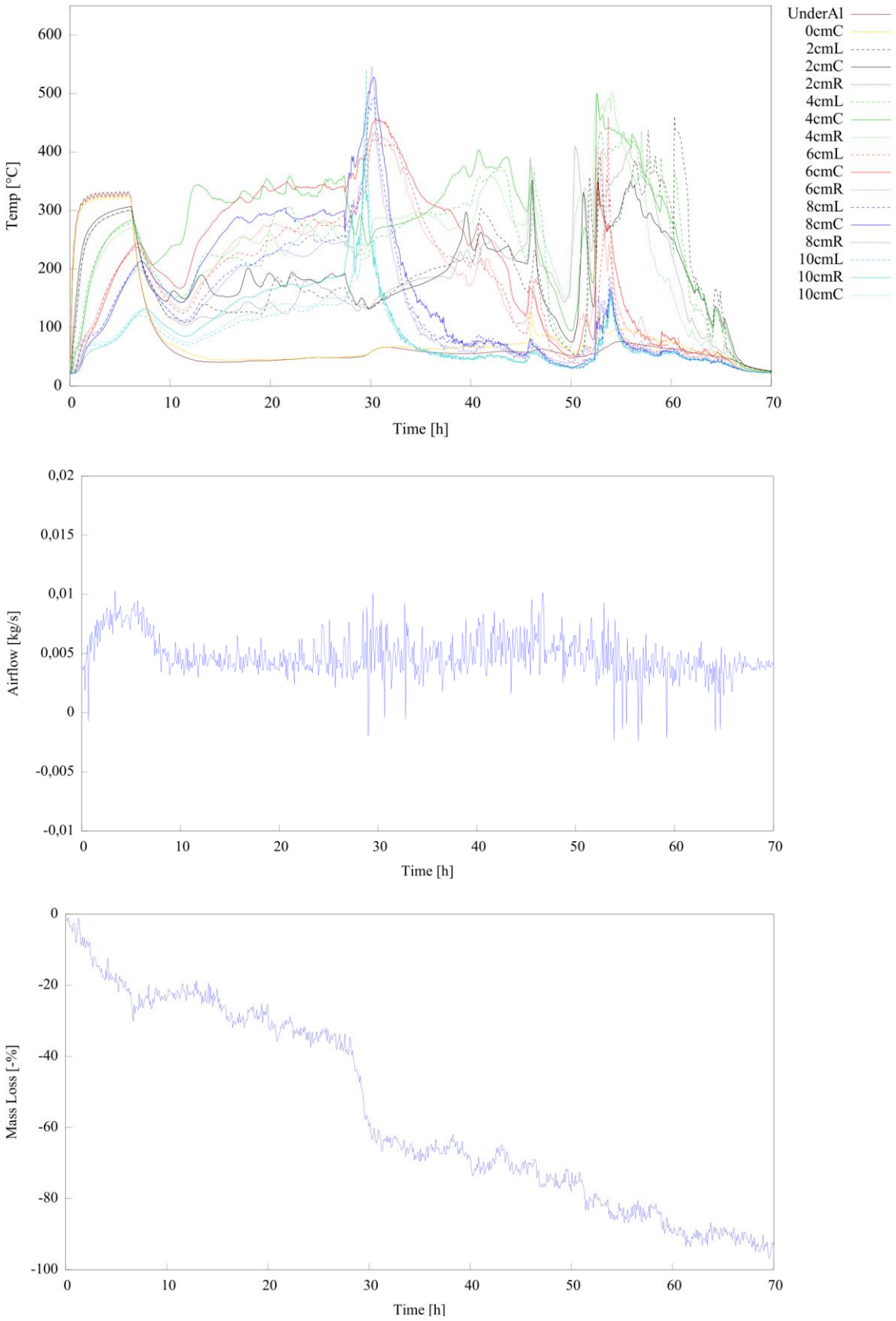

Figures A-10: VR9 test. Temperature development within the sample vs time (top graph), airflow measurement vs time (middle graph), mass change (%) vs time (bottom graph).

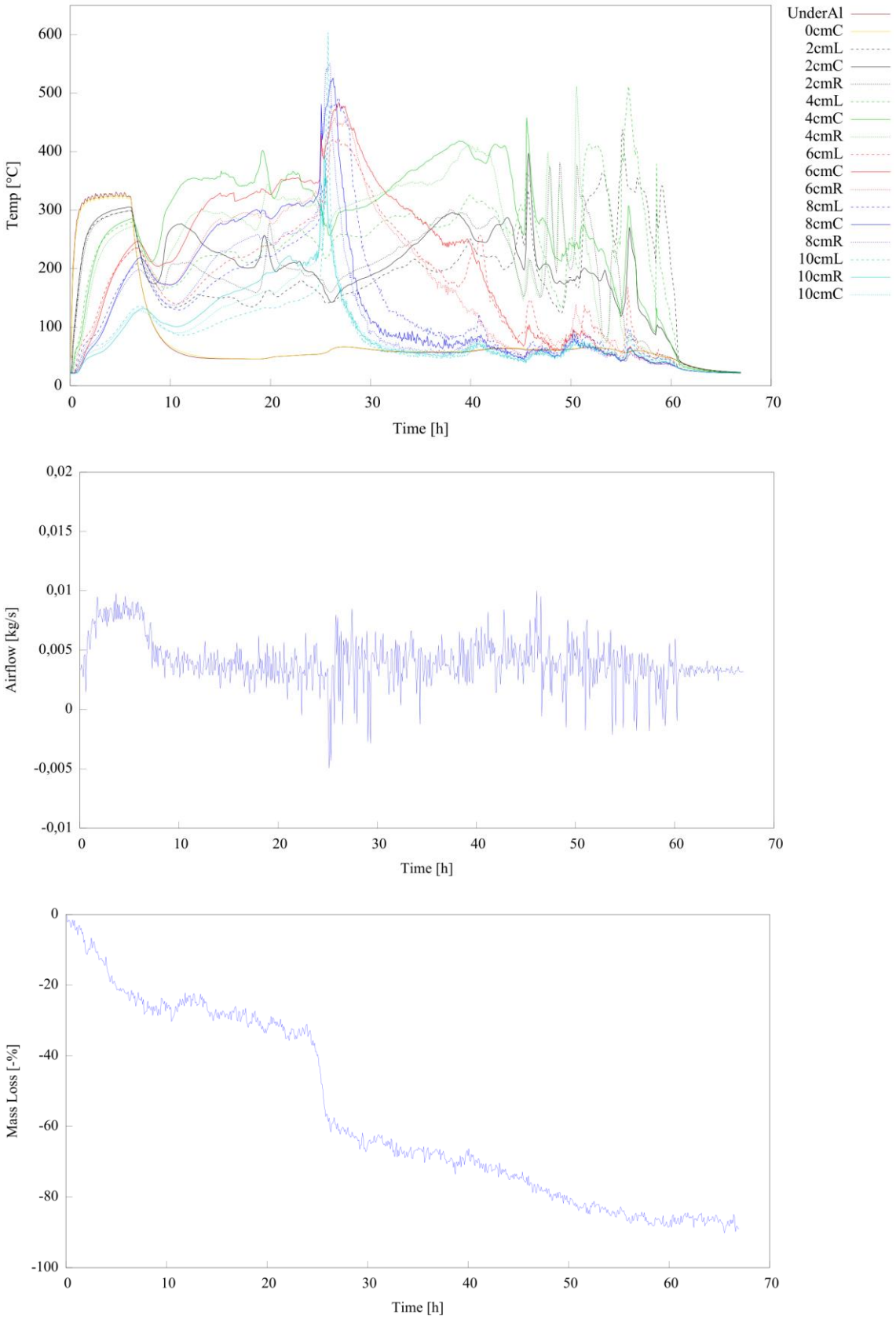

Figures A-11: VR10 test. Temperature development within the sample vs time (top graph), airflow measurement vs time (middle graph), mass change (%) vs time (bottom graph).

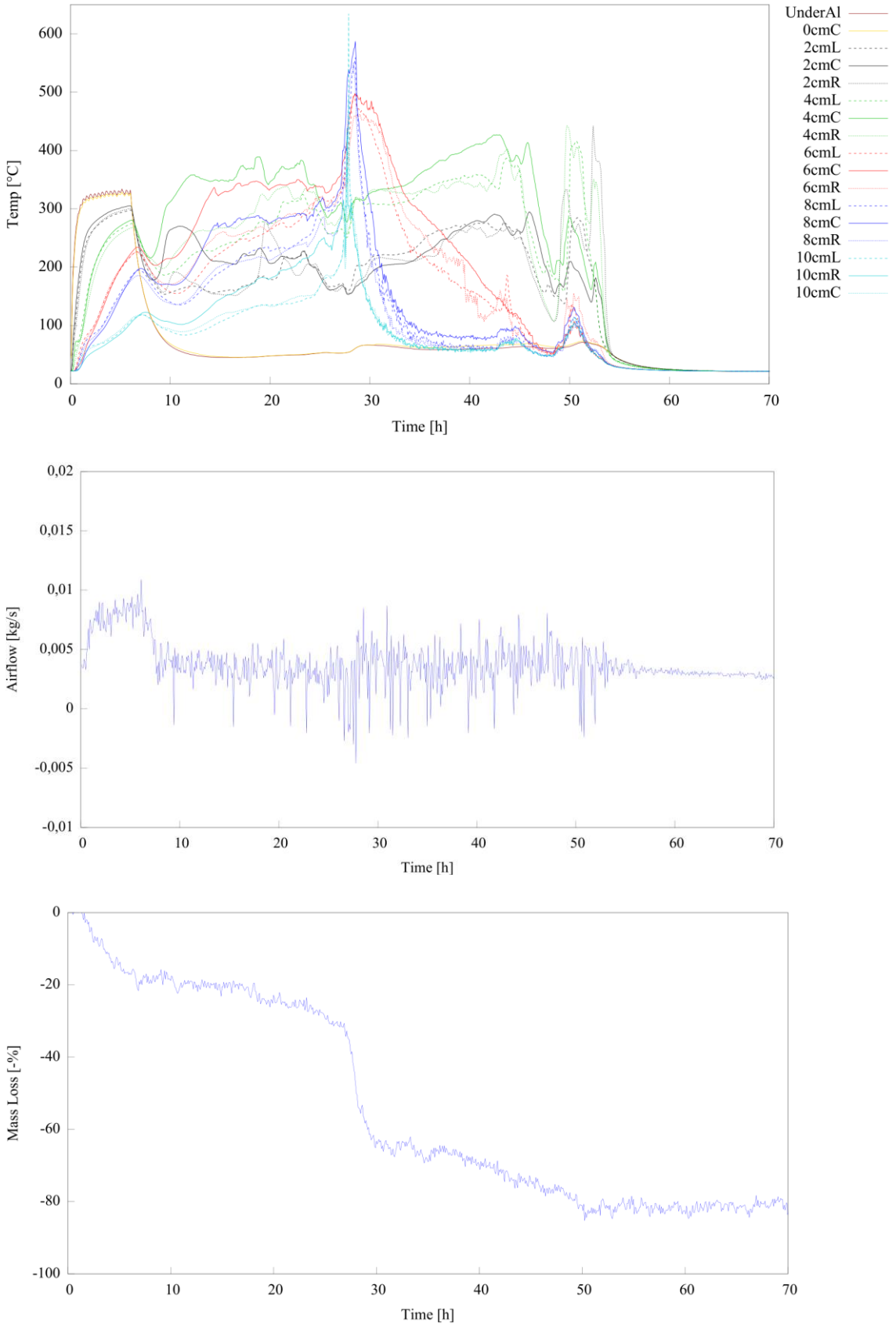

Figures A-12: VR11 test. Temperature development within the sample vs time (top graph), airflow measurement vs time (middle graph), mass change (%) vs time (bottom graph).

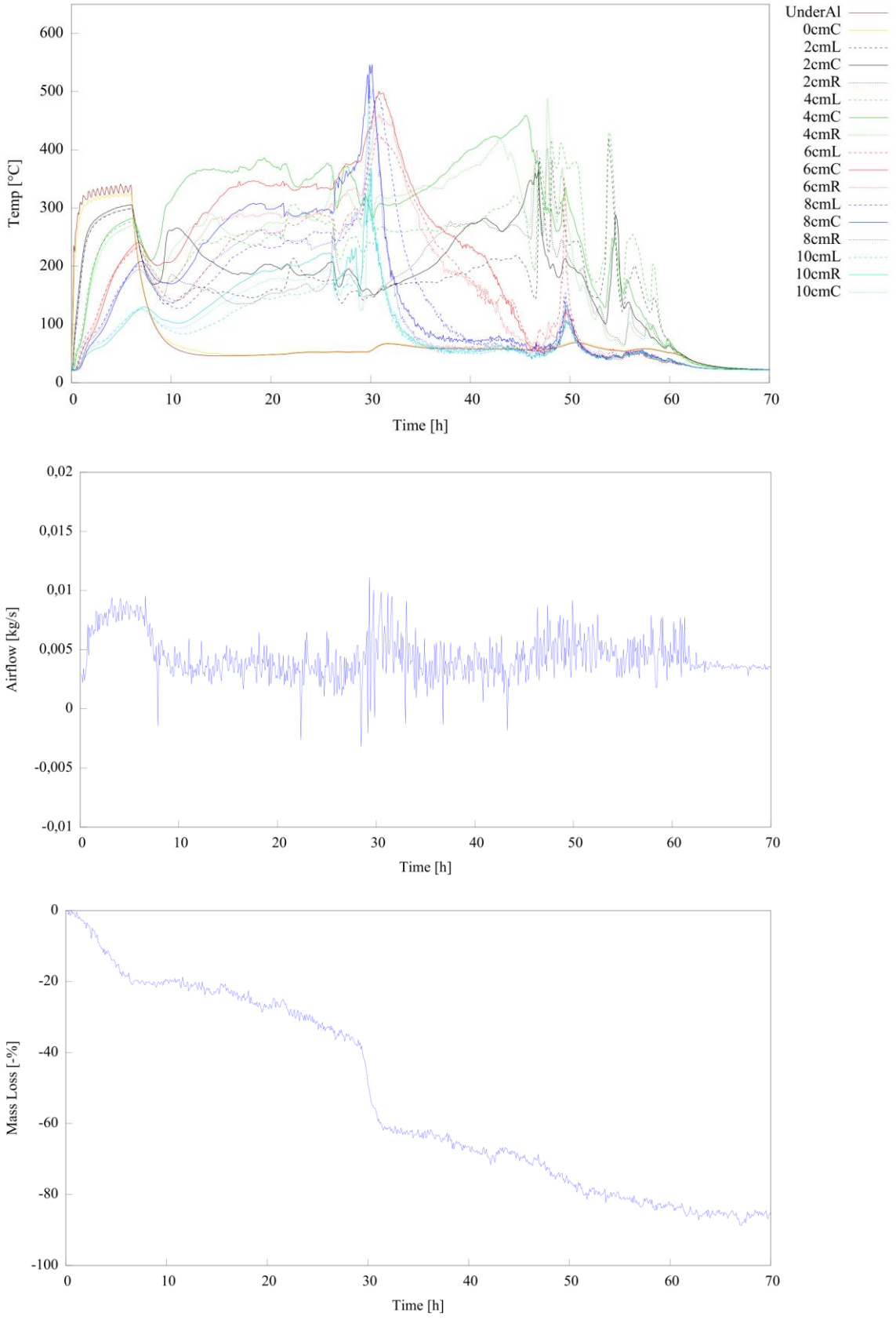

Figures A-13: VR12 test. Temperature development within the sample vs time (top graph), airflow measurement vs time (middle graph), mass change (%) vs time (bottom graph).

B) Forward smouldering charts

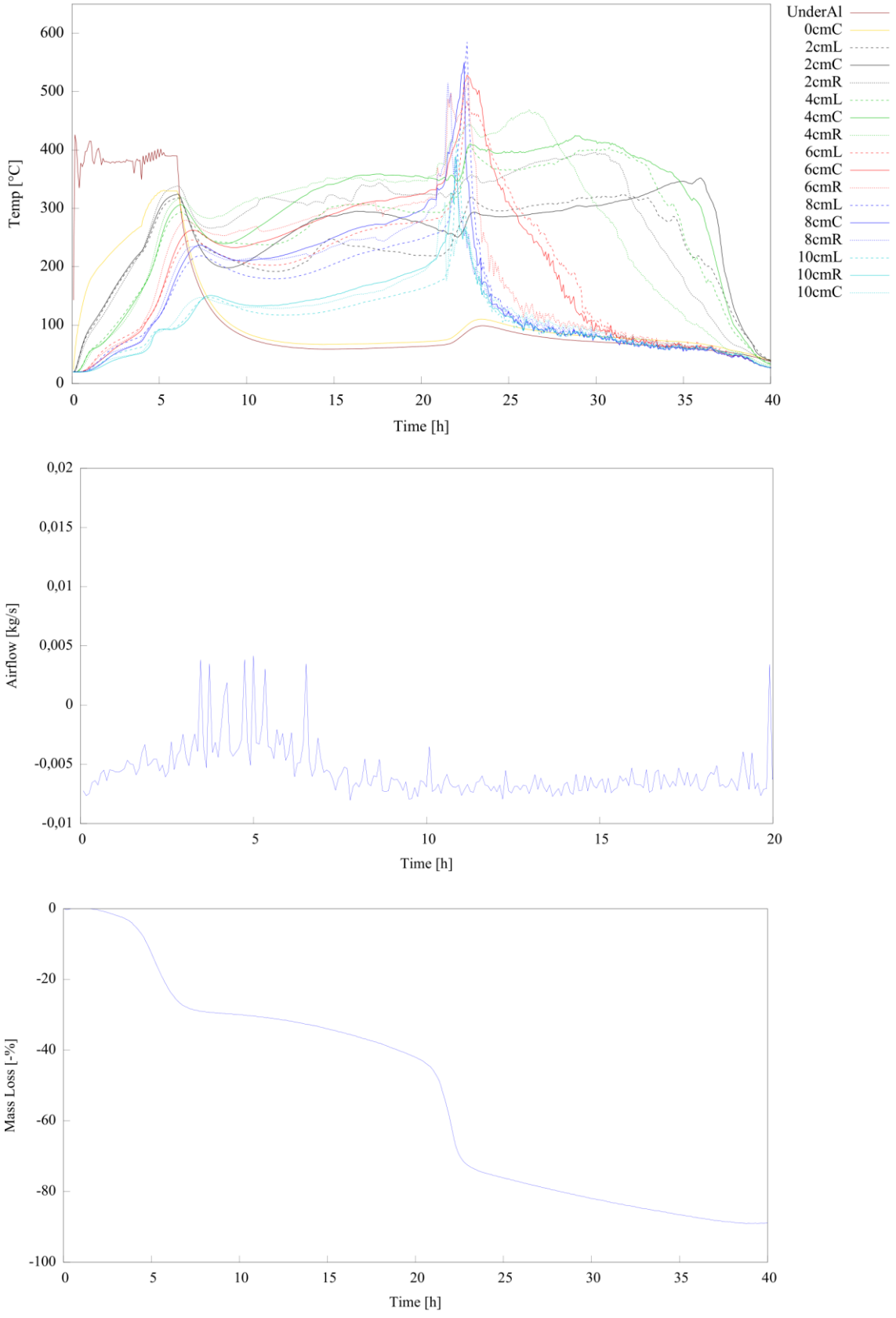

Figures B-1: VF1 test. Temperature development within the sample vs time (top graph), airflow measurement vs time (middle graph), mass change (%) vs time (bottom graph).

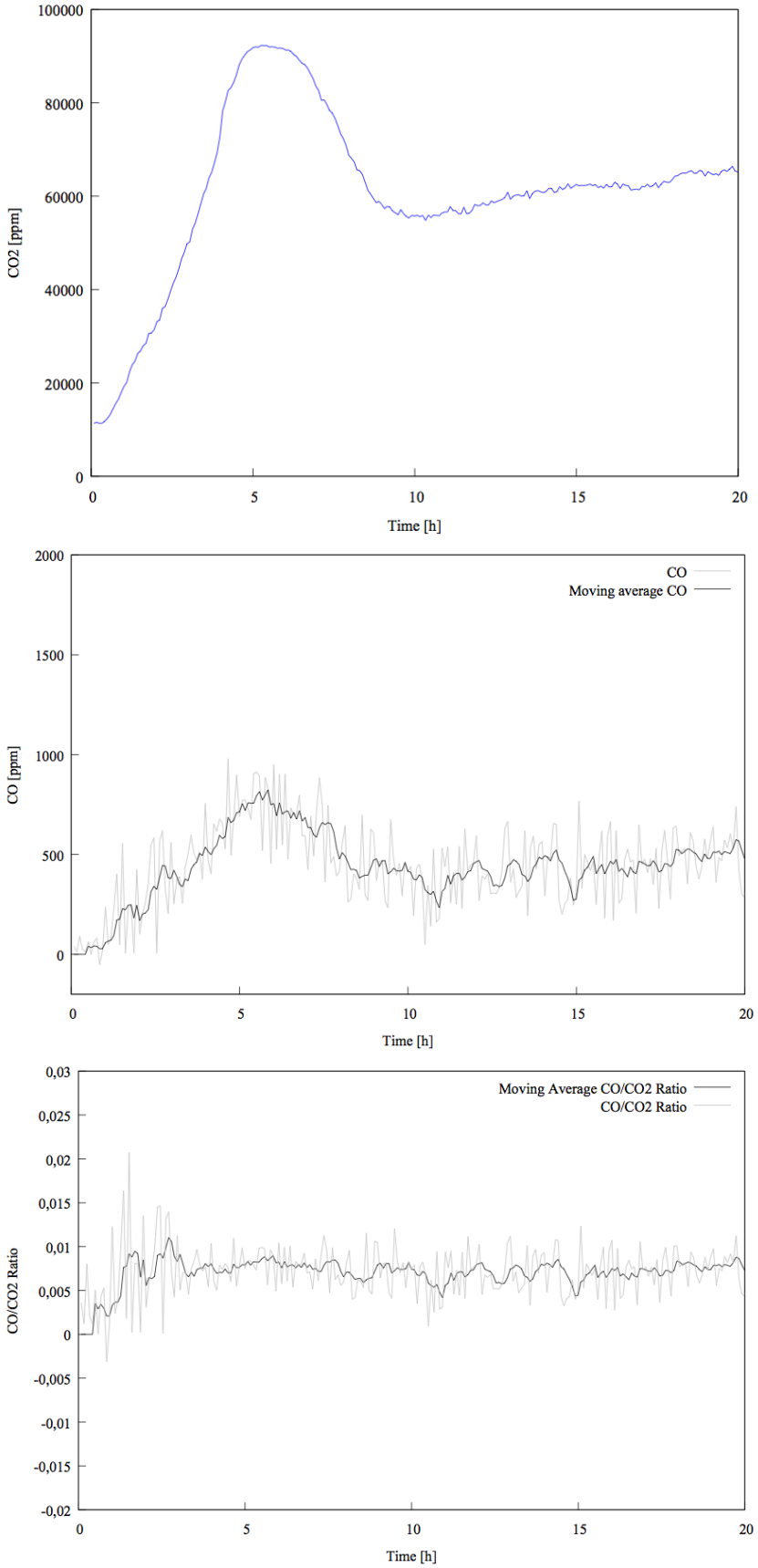

Figures B-2: VF1 test. CO_2 readings [ppm] vs time (top graph), CO and CO moving average (6 times period) vs time [ppm] (middle graph), CO/CO_2 ratio and moving average (6 times period) vs time (bottom graph).

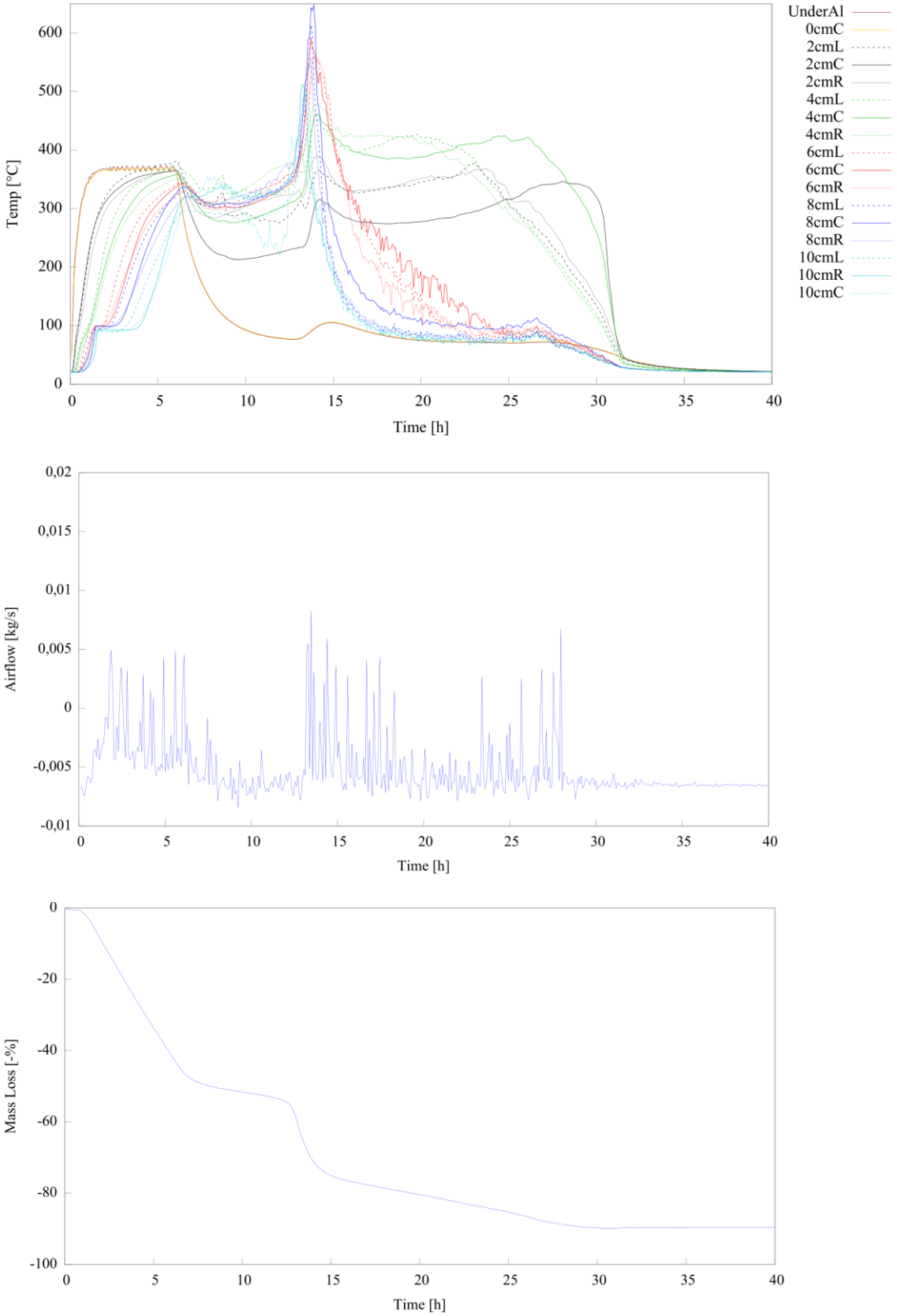

Figures B-3: VF2 test. Temperature development within the sample vs time (top graph), airflow measurement vs time (middle graph), mass change (%) vs time (bottom graph).

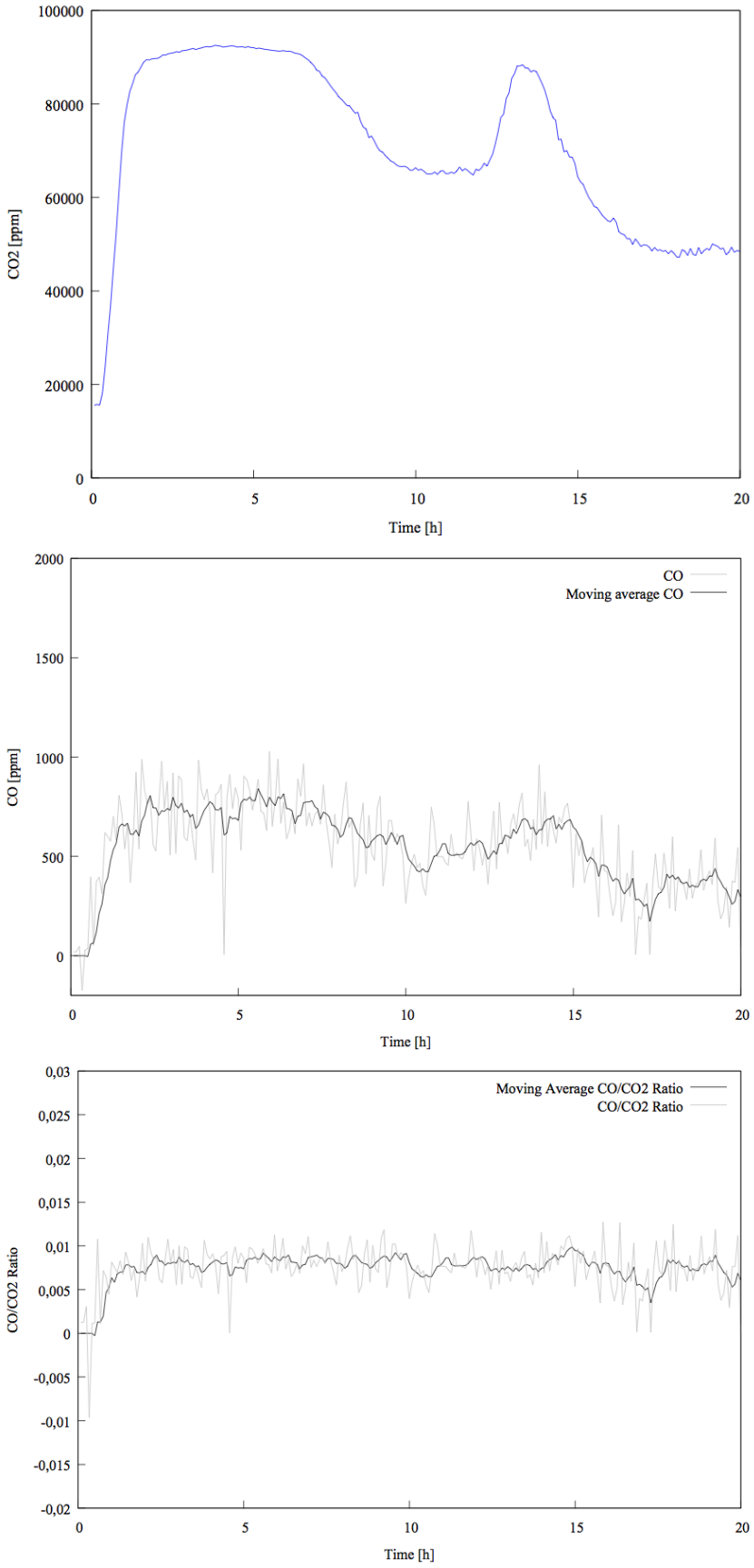

Figures B-4: VF2 test. CO_2 readings [ppm] vs time (top graph), CO and CO moving average (6 times period) vs time [ppm] (middle graph), CO/CO_2 ratio and moving average (6 times period) vs time (bottom graph).

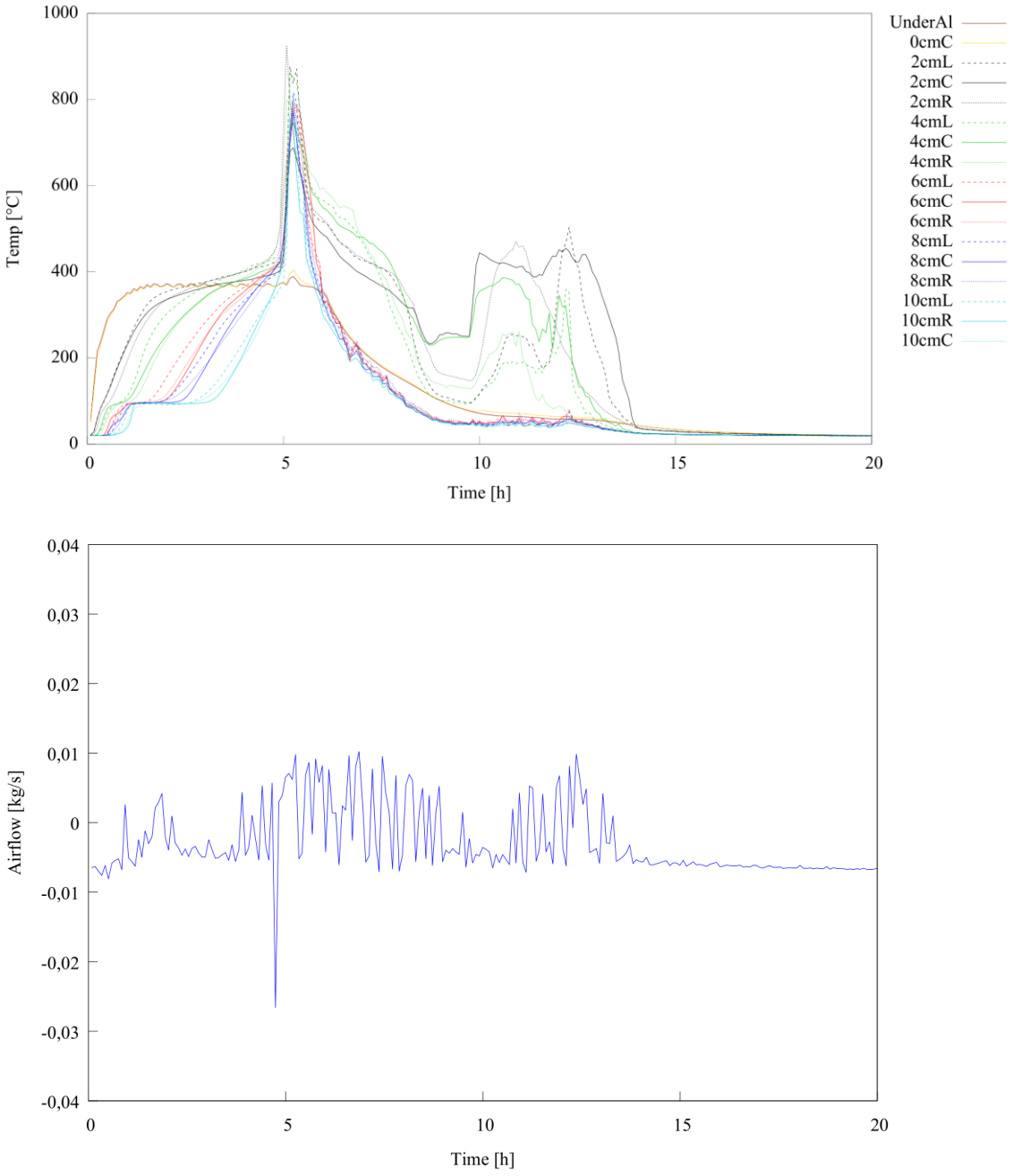

Figures B-5: VF3 test. Temperature development within the sample vs time (top graph), airflow measurement vs time (bottom graph),there is no mass change (%)chart due to defect in the equipment.

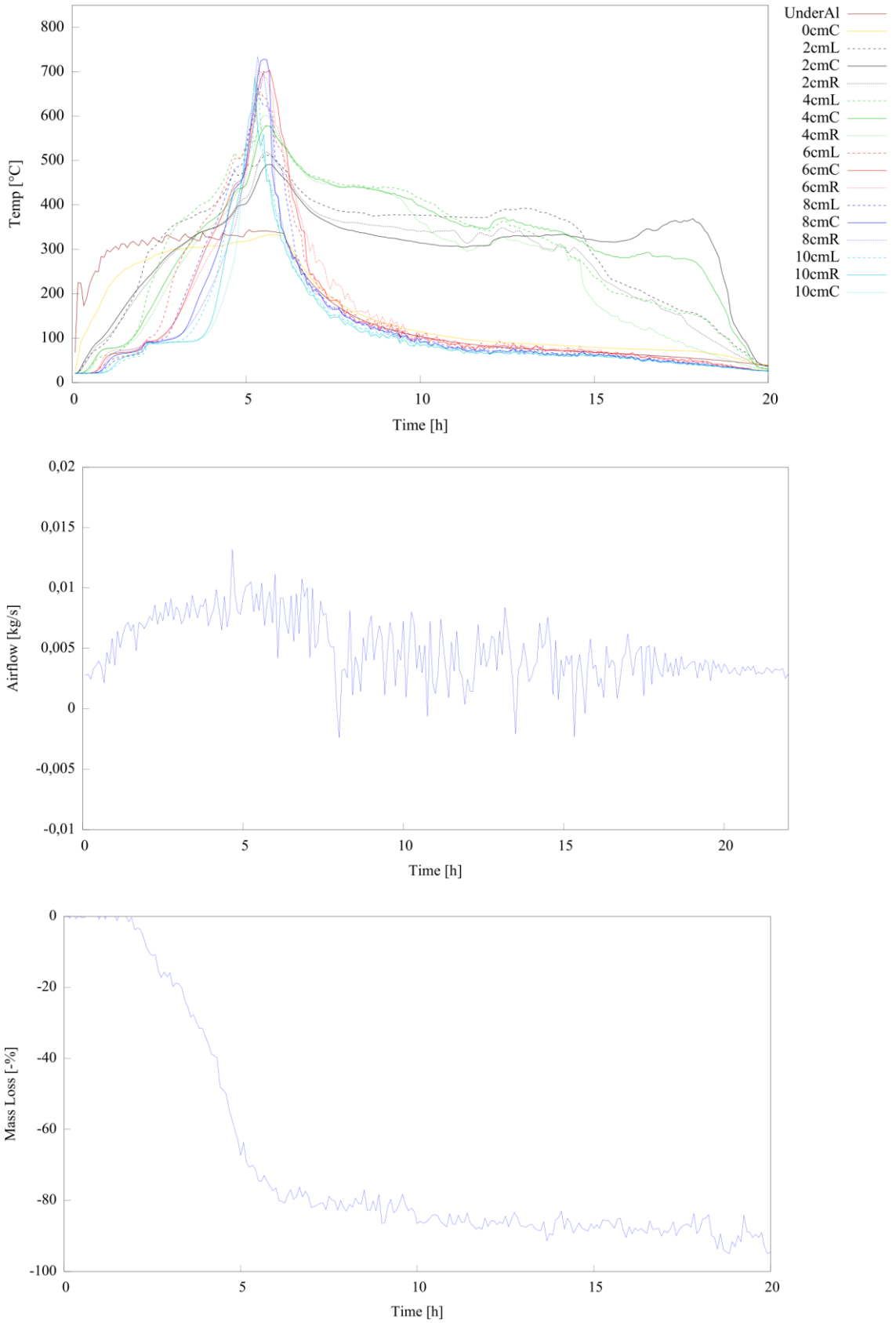

Figures B-6: VF4 test. Temperature development within the sample vs time (top graph), airflow measurement vs time (middle graph), mass change (%) vs time (bottom graph).

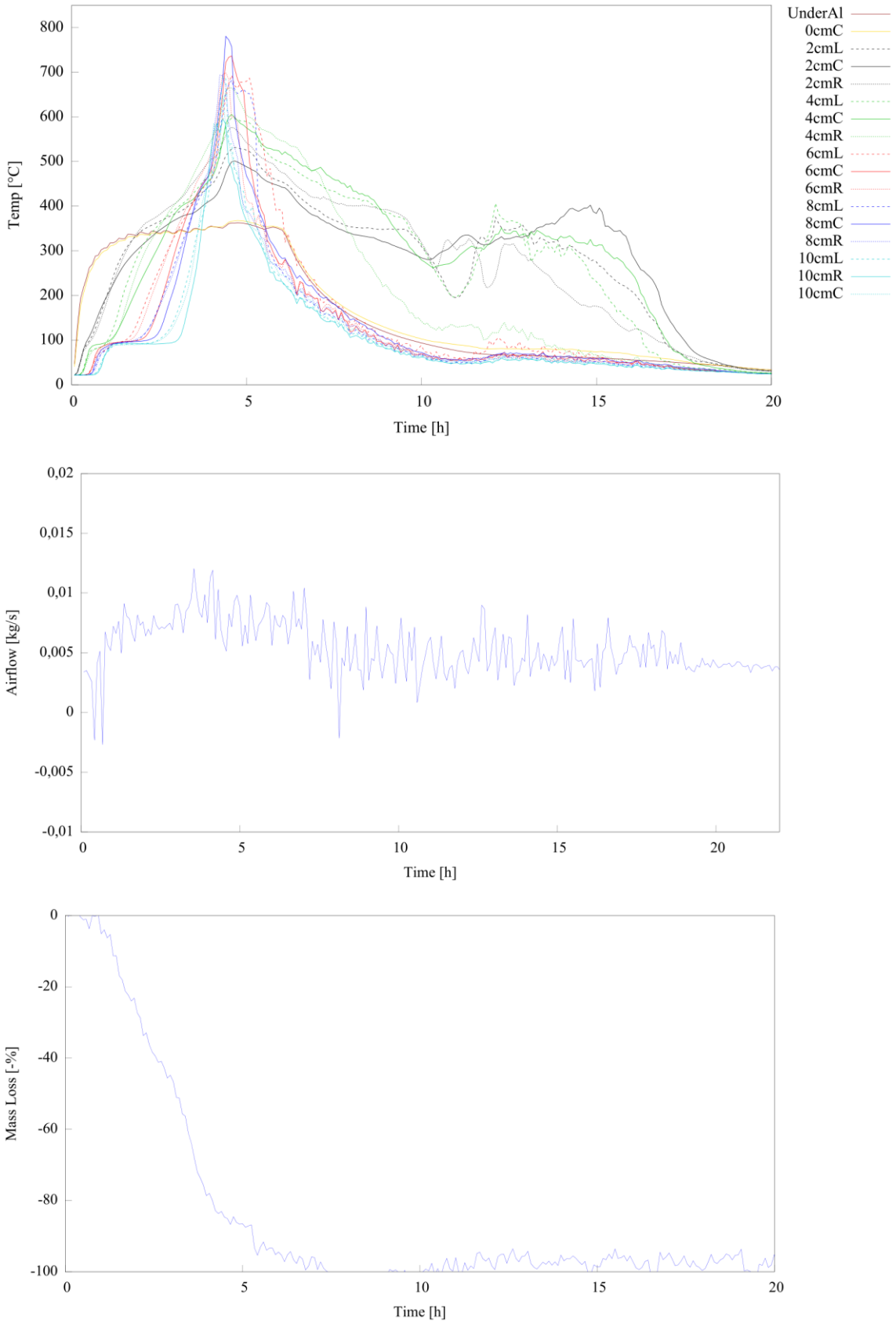

Figures B-7: VF5 test. Temperature development within the sample vs time (top graph), airflow measurement vs time (middle graph), mass change (%) vs time (bottom graph).

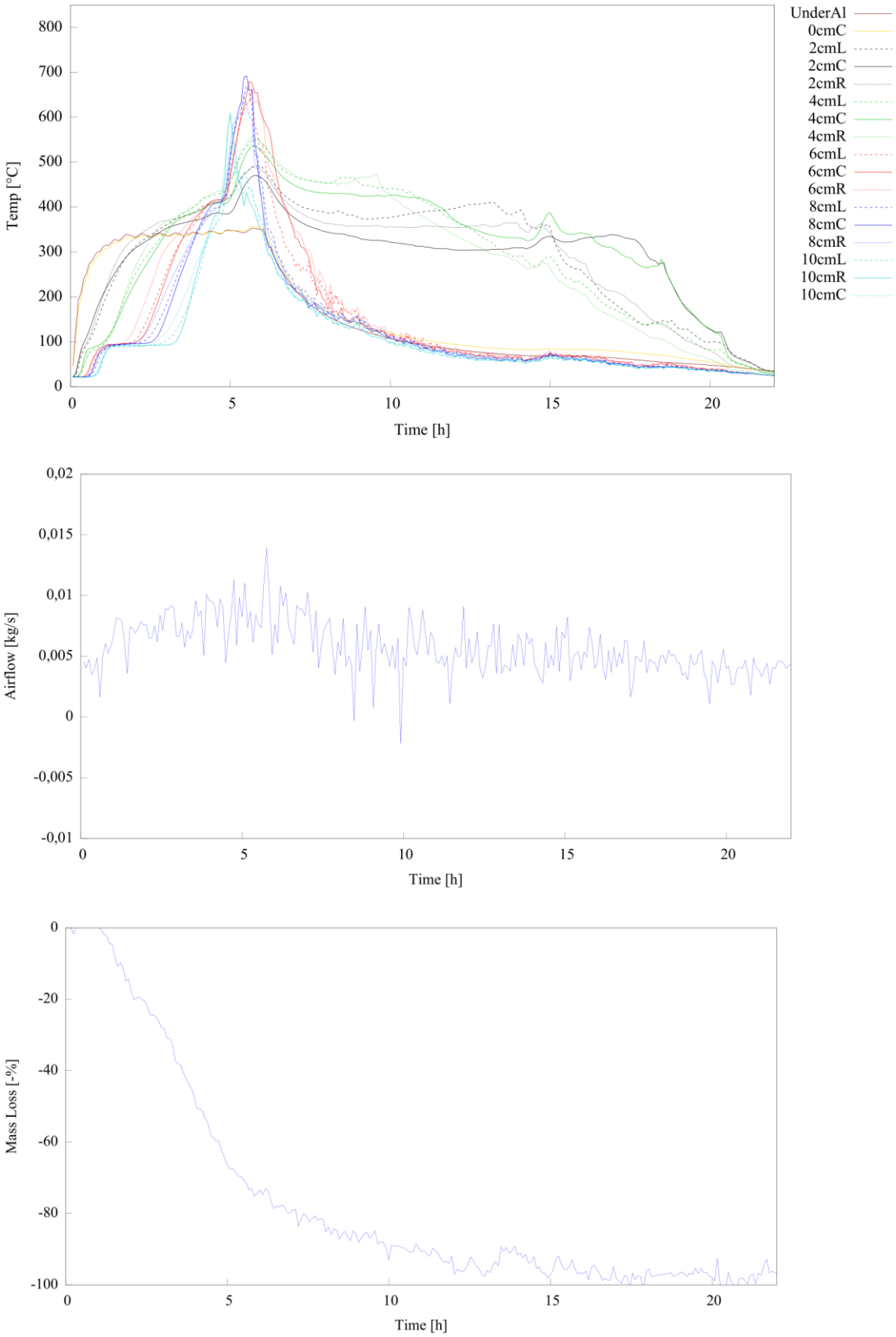

Figures B-8: VF6 test. Temperature development within the sample vs time (top graph), airflow measurement vs time (middle graph), mass change (%) vs time (bottom graph).

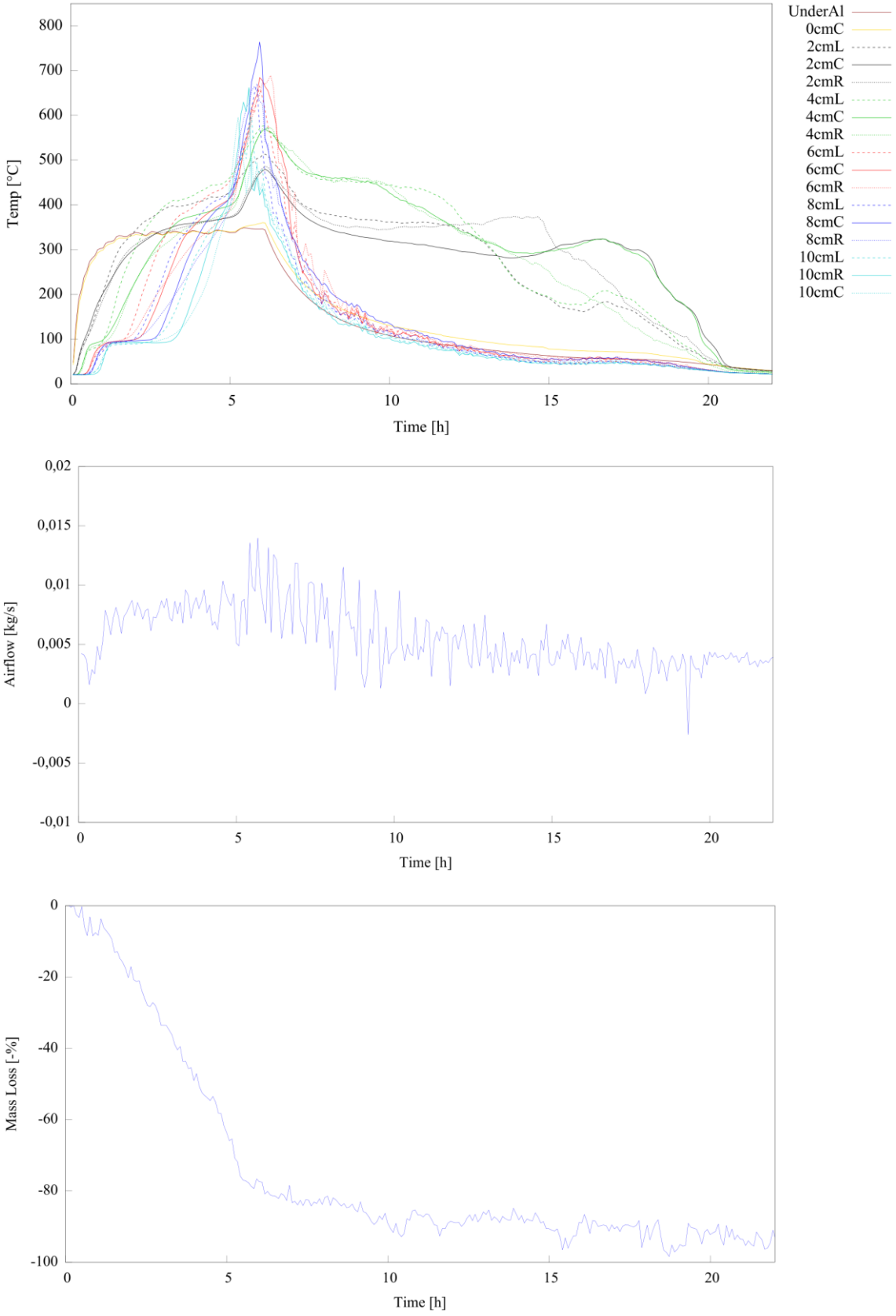

Figures B-9: VF7 test. Temperature development within the sample vs time (top graph), airflow measurement vs time (middle graph), mass change (%) vs time (bottom graph).

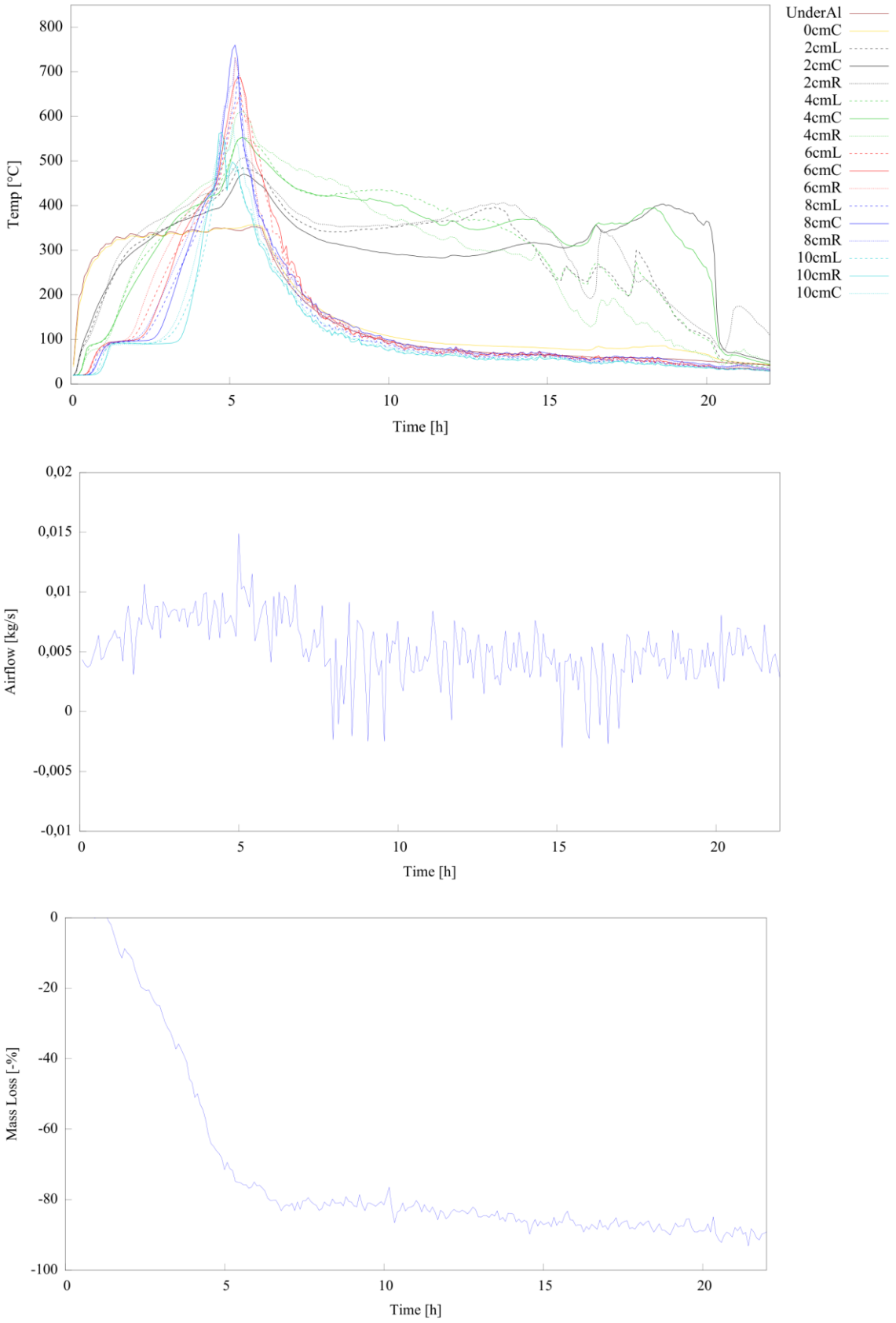

Figures B-10: VF8 test. Temperature development within the sample vs time (top graph), airflow measurement vs time (middle graph), mass change (%) vs time (bottom graph).

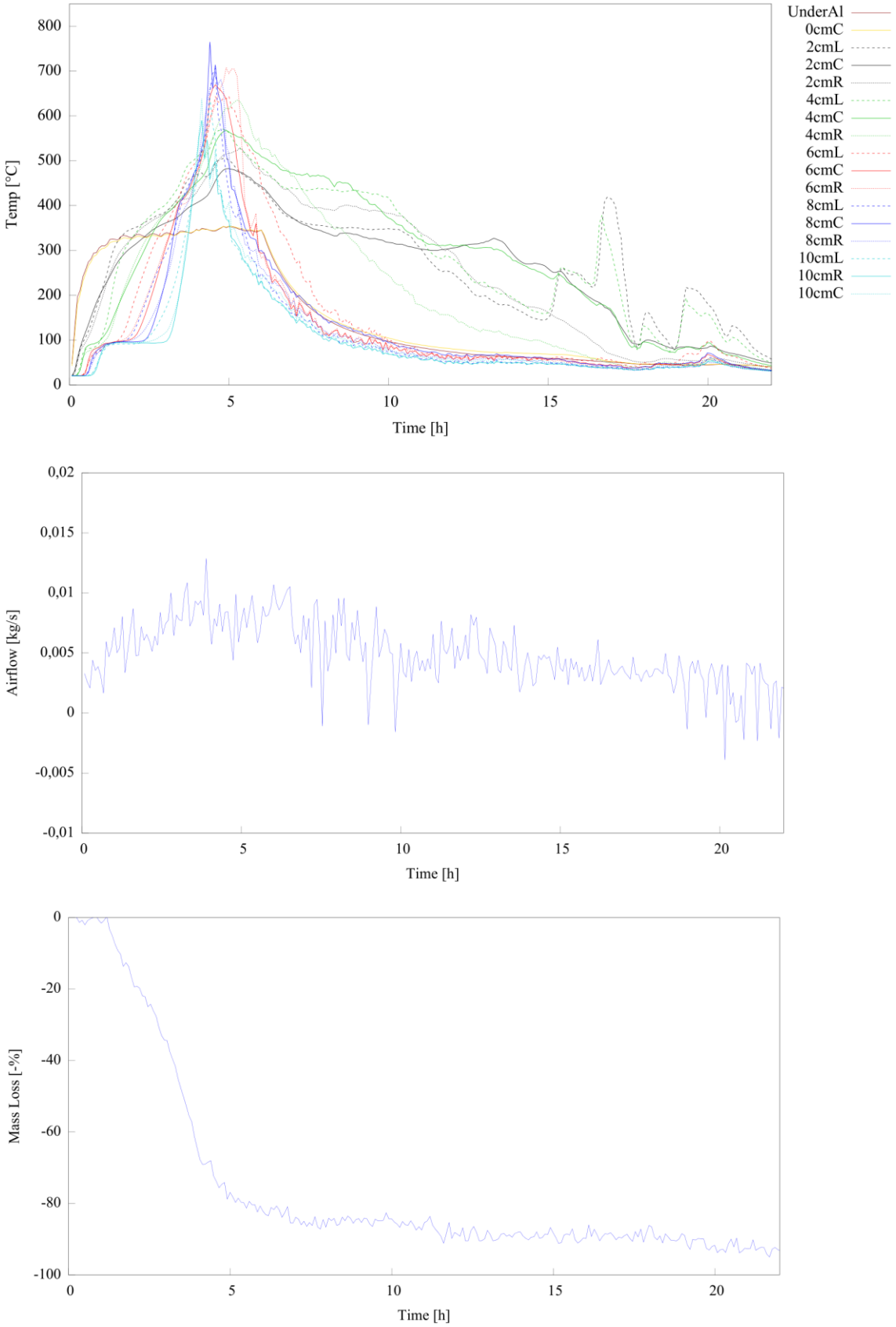

Figures B-11: VF9 test. Temperature development within the sample vs time (top graph), airflow measurement vs time (middle graph), mass change (%) vs time (bottom graph).

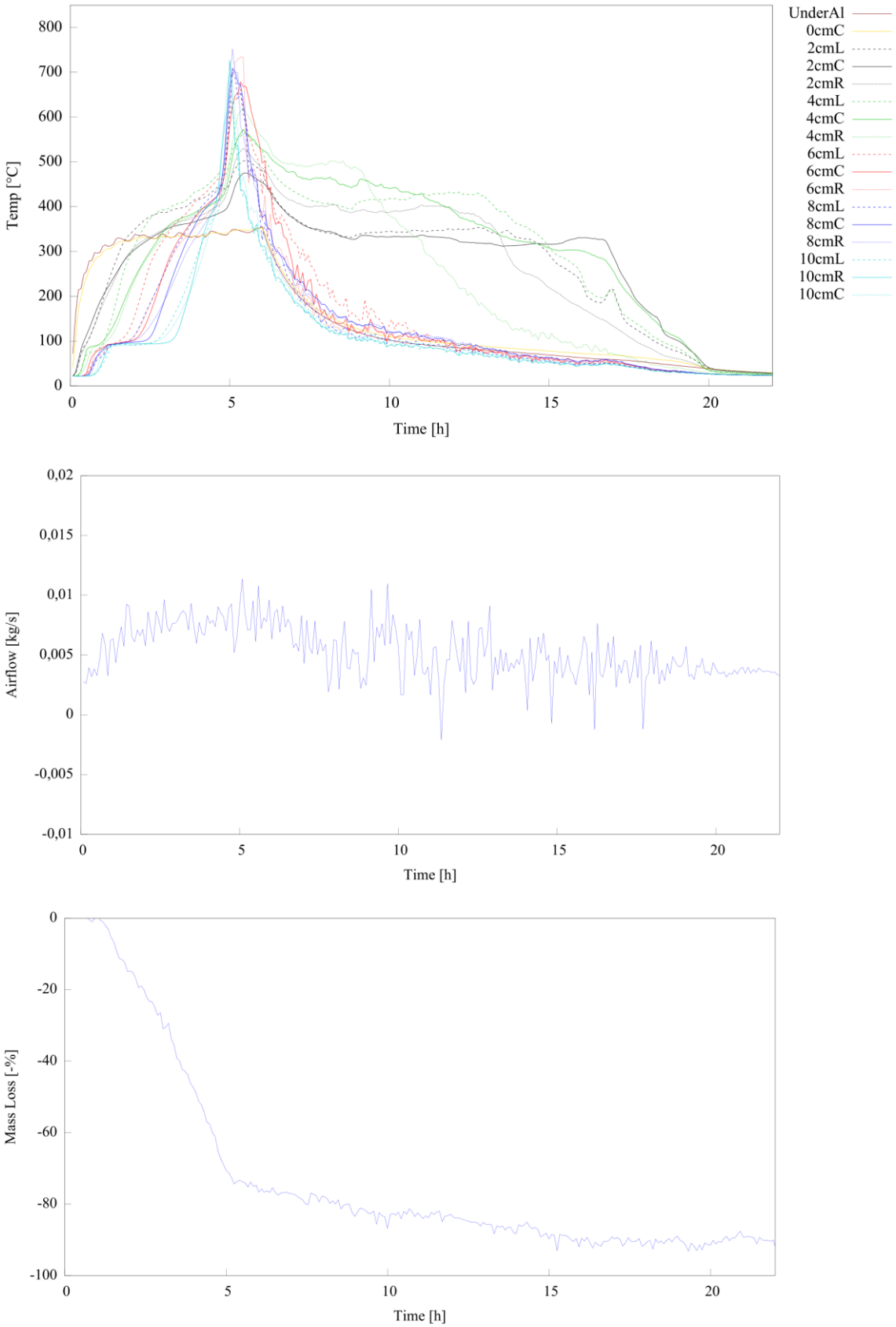

Figures B-12: VF10 test. Temperature development within the sample vs time (top graph), airflow measurement vs time (middle graph), mass change (%) vs time (bottom graph).

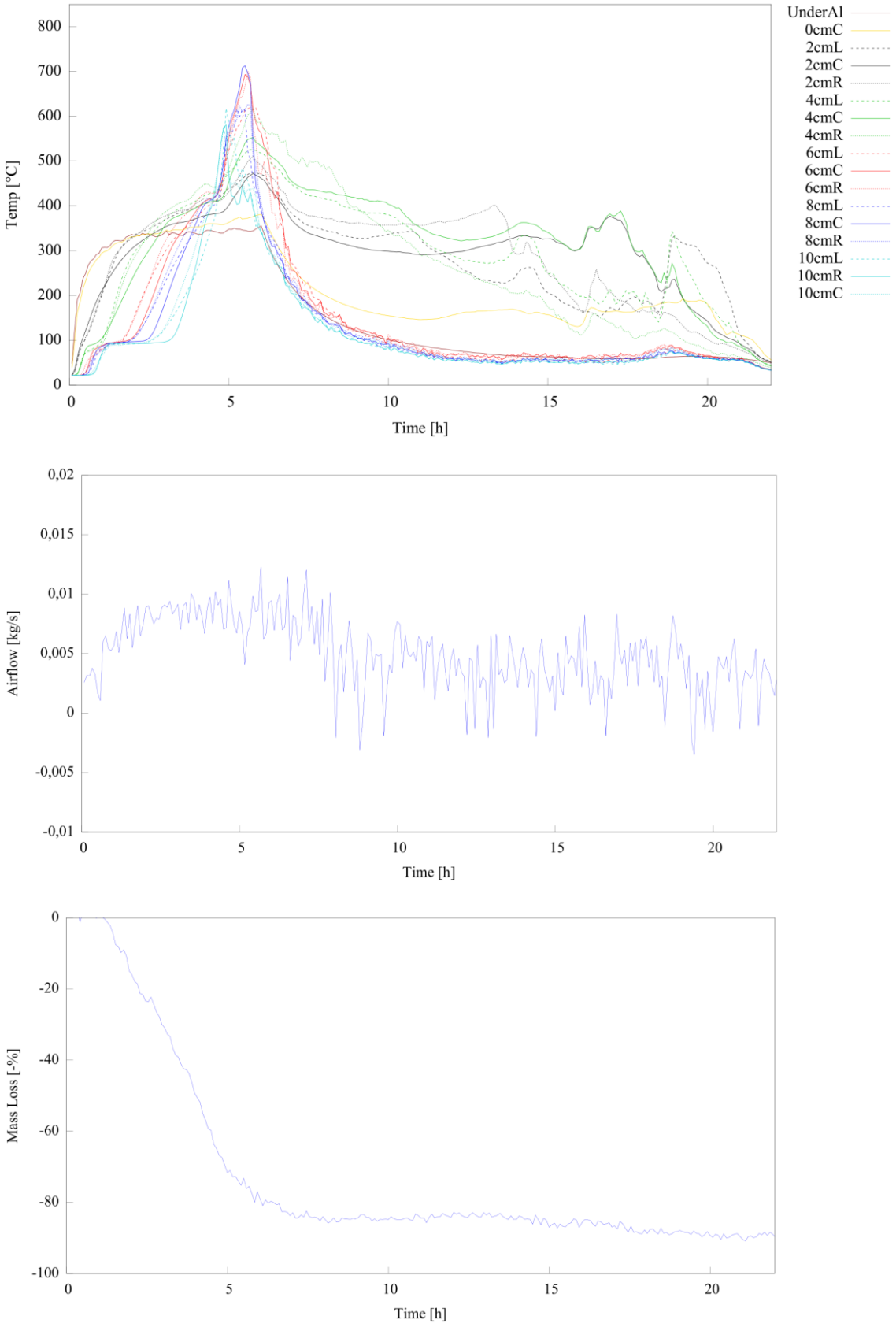

Figures B-13: VF11 test. Temperature development within the sample vs time (top graph), airflow measurement vs time (middle graph), mass change (%) vs time (bottom graph).